UNIVERSITY OF CALIFORNIA,
IRVINE

Isolation and Reactivity of Reduced Rare-Earth Metal Homoleptic and Heteroleptic Complexes Featuring Cyclopentadienyl Ligands

DISSERTATION

submitted in partial satisfaction of the requirements for the degree of

DOCTOR OF PHILOSOPHY

in Chemistry

by

Tener F. Jenkins

Dissertation Committee:
Distinguished Professor William J. Evans, Chair
Professor A. S. Borovik
Associate Professor Jenny Y. Yang

2021

DEDICATION

To

my parents, Robert and Nancy,

my brothers and sisters, Taylor, Jake, Andrew, Mary Kate, and Ray,

and to my partner, Melina,

in recognition of your love and support.

inspiration

To see a World in a Grain of Sand
And a Heaven in a Wild Flower
Hold Infinity in the palm of your hand
And Eternity in an hour

William Blake
Auguries of Innocence

and a golden rule

Do unto others 20% better than you would expect them to do unto you,
to correct for subjective error

Linus Pauling

TABLE OF CONTENTS

LIST OF FIGURES

LIST OF TABLES

ACKNOWLEDGEMENTS

To my advisor, Professor Bill Evans, I would like to thank you for so much. As a new graduate student in a long distance relationship, you were the only professor that made me feel that I could work on my Ph.D. and maintain my relationship. Throughout my graduate school experience, you have always helped me be accountable to myself and the group. Writing this, I am truly grateful that you had the tough conversations with me that you did. Every day, I look back on that fateful day as a new beginning and I will always remember our meetings and conversations. I hope to garner some of your wisdom and work ethic into my own career!

To Professor Andy Borovik, thank you for being the chair on my candidacy committee and being part of my defense committee. Your advice and feedback have been instrumental in shaping my thoughts and opinions in graduate school.

To Professor Jenny Yang, thank you for taking part in my candidacy exam and being on my defense committee. Your feedback has been really helpful, and I would not be where I am today without your help.

To everyone mentioned above as well as Professors Alan Heyduk, Mike Green, Ann Marie Carlton, and Melanie Cocco, thank you for participating in my 2nd year examination and my candidacy exam. Your time and efforts helped me become the individual I am today!

To Professor Filipp Furche, Luke Nambi Mohanam, and Samuel Bekoe, thank you for your help collaborating. Our collaborations helped understand the important characteristics and properties of my work, and without all of you, I would not be as knowledgeable as I am!

To Dr. Joe Ziller, as well as X-ray facility assistants, Dr. Mikey Wojnar, Dr. Austin Ryan, Dr. Dan Huh, and Chen Sun, thank you for your help with mounting crystals and solving structures. To Dr. Victoria Oswald, Justin Lee, and Megan Goulet, thank you for your assistance with EPR spectroscopy. To Dr. Phil Dennison and Dr. Dima Fishman, thank you for maintaining the facilities that you do, I cannot express my gratitude for your help and assistance these past 5 years.

To Dr. David Woen, thank you for being my mentor. I know that I was your 5th mentee, but you help set me up for success in the Evans Lab. I would also like to thank Dr. Nick Rightmire, Dr. Chad Palumbo, Dr. Megan Dumas. Dr. Daniel Huh, Dr. Samuel Moehring, and Dr. Austin Ryan, who helped and advise me when I was a new graduate student. To all previous and current Evans group members, including those mentioned above, and Mitch Nascimento, Monica Boshart, Mary Angadol, Justin Wedal, Jessica White, Sierra Ciccone, Amanda Chung, Lauren Anderson-Sanchez, Will Moore, Joseph Nguyen, Kito Gilbert-Bass, and Michael Trinh, I will remember all of our interactions and laughs together. Without all of you, my graduate school experience would not be the same!

To Professor Robert Luttrell, thank you for showing me how research is done! As a junior at Salisbury University, I remember talking to you about your research and feeling lucky enough to take part in it. Since leaving SU, the conversations that we had have left an indelible mark on my thinking and I owe that to you. Thank you for letting me join your group; I do not think I would have gone to graduate school otherwise!

To my older siblings, Taylor, and Jake, thank you for your love and support. I am lucky to have family out in California, and even in the limited time we shared together, I am very happy that we shared it. You will mean more to me than I can express, and I could not have finished without your support.

To my younger siblings, Andrew, Mary Kate, and Ray, thank you for your love and support. These 5 years have not been easy, but I would not have made it without your support. As we all get older, I cannot believe the amazing people you are growing up to be!

To my parents, Robert, and Nancy, thank you for everything. Since I was a toddler, conducting my "water research" you have shaped me into the scientist I am today. I appreciate how you always answered my "Why?" questions and pushed me to excel. I would not be as motivated as I am today without your guidance.

To my partner, Melina, I cannot express how much you mean to me. Our relationship started before I came to graduate school, and you have been my rock for these past 5 years! I am excited to start the next chapter of our life together, we have earned it! Without you, I would not have the perseverance to finish my degree and I will always appreciate the time and energy you put in to help me succeed!

CURRICULUM VITA

Tener Fredric Jenkins

EDUCATION

PhD, Chemistry May 2021
University of California, Irvine | Irvine, CA
Advisor: Professor William J. Evans
Thesis Title: "Isolation and Reactivity of Reduced Rare-Earth Metal Homoleptic and Heteroleptic Complexes Featuring Cyclopentadienyl Ligands"

Bachelor of Science May 2016
Salisbury University | Salisbury, MD
Major: Chemistry (American Chemical Society Certified) **Minor:** Mathematics
Overall GPA: 3.788/4.000 (Summa Cum Laude)

RESEARCH EXPERIENCE

Graduate Assistant, (Ph.D. Candidate) University of California, Irvine Fall 2016-Spring 2021

- Advisor: Professor William J. Evans
- Synthesized and characterized highly air-sensitive rare-earth metal complexes
- Performed techniques involving NMR, IR, and EPR spectroscopy as well as electrochemistry and X-ray diffraction
- Utilized thermodynamic and kinetic principles for the design of reduced mixed ligand rare-earth metal complexes
- Purchased lab equipment & chemicals

Undergraduate Researcher, Salisbury University Fall 2015-Spring 2016

- Advisor: Professor Robert Luttrell
- Developed advanced data fusion techniques involving least-squares regression
- Utilized C++ code to implement and evaluate the accuracy of new data analysis techniques

WORK EXPERIENCE

Teaching Assistant (TA), University of California, Irvine Fall 2016-Spring 2021

- Led undergraduate students through lab courses including general chemistry, organic chemistry, and inorganic chemistry
- Instructed upper division labs involving air-free chemical synthesis and characterization of inorganic and organometallic complexes
- Led discussion sections for undergraduate students for general chemistry and radiochemistry courses

Supplemental Instruction (SI), Salisbury University Fall 2013-Spring 2016

- Dedicating 9 hours per week to attending classes, holding office hours, and leading study sessions.
- Selected to instruct CHEM 221 (Organic Chemistry), CHEM 121 (General Chemistry I) and MATH 202 (Calculus II).

PUBLICATIONS

- "Tetramethylcyclopentadienyl Ligands Allow Isolation of Ln(II) Ions across the Lanthanide Series in [K(2.2.2-cryptand)][$(C_5Me_4H)_3Ln$] Complexes," Tener F. Jenkins, David H. Woen; Luke Nambi Mohanam, Joesph W. Ziller, Filipp Furche, William J. Evans *Organometallics*. **2018**, *37*(21), 3863-3873. DOI: 10.1021/acs.organomet.8b00557
- "Synthesis of a 2-Isocyanophenolate Ligand, $[2\text{-}CNC_6H_4O]^{1-}$, by Ring-Opening of Benzoxazole with Rare-Earth Metal Complexes," Megan T. Dumas, Tener F. Jenkins, Justin C. Wedal, Joseph W. Ziller, Fillip Furche, and William J. Evans *Organometallics*. **2021**, *40*(6), 735-741. DOI: 10.1021/acs.organomet.1c00002
- "Synthesis of Heteroleptic Bis(cyclopentadienyl) Amide Yttrium(II) Complexes, [K(2.2.2-cryptand)][$Cp^X_2Ln(NR_2)$], and Their C–H Bond Activated Y(III) Derivatives (Cp^X = C_5Me_5, C_5Me_4H)," Tener F. Jenkins, Samuel Bekoe, Joesph W. Ziller, Filipp Furche, William J. Evans. *Submitted*
- "Isolation and Characterization of a Californium Metallocene," Goodwin, C. A. P.; Su, J.; Stevens, L. M.; White, F. D.; Albrecht-Schönzart, T. E.; Batista, E. R.; Cross, J. N.; Evans, W. J.; Gaiser, A. N.; Gaunt, A. J.; Janicke, M. T.; Jenkins, T. F.; Kozimor, S. A.; May, I.; Scott, B. L.; Sperling, J. M.; Windorff, C. J.; Yang, P.; Ziller, J. W. *Submitted*

PRESENTATIONS

- Jenkins, T. F.; Luttrell, R.; Advanced Data Fusion: Optimized Stacked Moving Window Regression Analysis of Complex Infrared Spectra. Salisbury University Undergraduate Research Conference, Salisbury, MD, 2016.

AWARDS & AFFILIATIONS

American Chemical Society 2020-
Allen R. Dudley Award for Excellence in Chemistry 2016 Academic Year
International Mentor Training Program Level 1 Certification by College Reading and Language Association 2016 Academic Year
Awardee, Goldwater Fellowship 2015 Academic Year

- 1 of 8 Honorable Mentions for the state of Maryland

Awardee, ACS Undergraduate Award in Analytical Chemistry 2015 Academic Year

- Awarded for academic excellence in Analytical Chemistry & Instrumental Analysis

Initiate, Phi Kappa Phi 2015 Academic Year
Must be in Top 10% of class to get initiated
Awardee, Dean's List: maintain GPA above 3.5 Fall 2012-Spring 2016

Awardee, 2 scholarships

- Wallace Q. French Scholarship: $2000 per year, awarded by Tidewater Environmental Health Association for future scientists
- SU Achieve Scholarship, $1000 per year, awarded by Salisbury University for maintaining a GPA of 3.75

ABSTRACT OF THE DISSERTATION

Isolation and Reactivity of Reduced Rare-Earth Metal Homoleptic and Heteroleptic Complexes Featuring Cyclopentadienyl Ligands

by

Tener F. Jenkins

Doctor of Philosophy in Chemistry

University of California, Irvine, 2021

Professor William J. Evans, Chair

This dissertation focuses on the expansion of ligand sets available to isolate new +2 ions of the rare earth metals, i.e., Sc, Y, and the lanthanides. In addition to their isolation, their reactivity and physical properties have also been investigated. Chapter 1 describes the basis of this dissertation research, i.e., the initial isolation of new Ln(II) ions using the $(C_5H_4SiMe_3)_3^{3-}$ ligand set and the characterization of these new Ln^{2+} ions. Chapter 2 describes the use of the $(C_5Me_4H)_3^{3-}$ ligand set to isolate a new series of Ln^{2+} complexes and compares their properties to the $(C_5H_4SiMe_3)_3^{3-}$ complexes. In the $(C_5H_4SiMe_3)_3^{3-}$ ligand set, Dy adopts a $4f^9 5d^1$ electron configuration while in the $(C_5Me_4H)_3^{3-}$ ligand set, Dy adopts a $4f^{10}$ electron configuration. Chapter 3 describes efforts to isolate the first C_5Me_5 complex of a new Ln^{2+} ion in heteroleptic Y^{2+} complexes of the form, $[Cp^X_2Y(NR_2)]^{1-}$, where Cp^X = C_5Me_5 and C_5Me_4H, and study their properties. Chapter 4 describes the reactivity and reductive chemistry of rare earth metal allyl

complexes with benzoxazole. Appendix A describes the reactivity of the $[(C_5Me_4H)_3Ln]^{1-}$ complexes for Ln = La and Ce with *tert*-butyl isocyanide including EPR spectroscopy. Appendix B describes efforts to synthesize and reduce other heteroleptic rare earth metal complexes by investigating the dynamic between ligand choice and the identity of the rare earth metal.

CHAPTER 1

Introduction

Chemical reactions can be complex and varied; however, most can be categorized into two groups: acid/base reactions and reduction/oxidation reactions. Reduction/oxidation reactions, or redox reactions, involve the transfer of electrons between compounds. The number of electrons an atom gains or loses in comparison to its neutral form is referred to as its oxidation state. Consequently, redox processes involve changes in oxidation states and are critical to understanding the properties of compounds. In this dissertation, the redox chemistry, specifically the reduction chemistry, of the rare-earth metals is presented along with investigations into new oxidation states for these metals.

The rare earth metals (abbreviated Ln) refer to the group of elements Sc, Y, La, Ce, Pr, Nd, Pm, Sm, Eu, Gd, Tb, Dy, Ho, Er, Tm, Yb, and Lu. Despite their name, as a group the rare earth elements are not scarce. On the contrary, their abundances are comparable to Sn, Pb, and Co.[1] Rare earth metals are ubiquitous in a wide range of technology including a. digital displays and energy efficient lighting due to the emissive properties of Eu(III), Ce(III), and Tb(III), b. cell phones, MRI technology, and strong permanent magnets as result of the electronic structure of Nd(III), Sm(III), and Gd(III), and c. catalytic converters.[2-7] These applications highlight the industrial significance of this unique group of metals.

The lanthanides are unusual because the valence 4*f* subshell does not extend very far from the nucleus.[8] Consequently, the valence electrons added from La through Lu are placed close to the nucleus. This renders the electronic structure, and thus magnetic moments and optical transitions, of rare earth ions insensitive to their environment and uniquely suited for the

applications described above.[9] Since these 4f electrons behave like core electrons, these metals have many similar properties. For instance, the 15 rare earth metals all prefer to adopt the +3 oxidation state and exhibit bonding that is ionic in character.[10] One notable difference between these metals is their atomic radii which differ sequentially by ~ 0.012 Å for La – Lu.[11] As a consequence of their similar properties, the rare earth metals are typically found together in Nature.[1]

This dissertation expands the known examples of the +2 oxidation state for these metals. Until 2008, Nd, Sm, Eu, Dy, Tm, and Yb were the only rare earth metals with examples of the +2 oxidation state in crystallographically-characterized molecular complexes.[12-15] Upon reduction of a $4f^n$ Ln^{3+} ion, these Ln^{2+} ions adopted electron configurations with the electron added to the 4*f* subshell i.e., $4f^{n+1}$. Structural analysis of these Ln^{2+} complexes displayed characteristic changes in bond distances that followed the ionic radii of these ions. Specifically, the bond distances in Ln^{2+} complexes increased by 0.16 Å – 0.19 Å upon reduction.[16] These Ln^{2+} ions also feature strong absorptions in the UV-visible region compared to the weakly absorbing and colorless Ln^{3+} ions. Solid state studies[13,14] and reduction potentials, for the $4f^n + e^- \rightarrow 4f^{n+1}$ reduction process, extrapolated from spectroscopic data[17] suggested that the other rare earth metals had reduction potentials that were too negative to isolate, Table 1.1.

Table 1.1. Estimated $Ln^{3+/2+}$ ($4f^n + e^{1-} \rightarrow 4f^{n+1}$) Reduction Potentials (± 0.2 V vs. SHE) of Yttrium and the Lanthanides Based on Experimental and Spectroscopic Data. [17]

Ln	Potential	Ln	Potential
Eu	−0.35	**Pr**	−2.7
Yb	−1.15	**Y**	−2.8
Sm	−1.55	**Ho**	−2.9
Tm	−2.3	**Er**	−3.1
Dy	−2.5	**La**	−3.1
Nd	−2.6	**Ce**	−3.2
Pm	−2.6	**Tb**	−3.7
Lu	−2.72	**Gd**	−3.9

Evidence of the +2 oxidation state for the other rare earth metals in molecular complexes was first reported in 1997.[18] Reduction of Cp''_3La [$Cp'' = (C_5H_3(SiMe_3)_2)^{1-}$] with K in dimethoxyethane generated a solution which featured an EPR spectrum with an eight-line hyperfine pattern, consistent with ^{135}La ($I = 7/2$), but the only isolable product was $[Cp''_2La(\mu\text{-}OMe)]_2$. However, in 2008 the first crystallographically-characterized Ln^{2+} complex, beyond the six "traditional" ions discussed above, was isolated via reduction of Cp''_3La.[19] It was found that using THF or Et_2O as a solvent and a chelate such as 18-crown-6 (crown) or 2.2.2-cryptand (crypt) enhanced the stability of the La^{2+} complex to allow crystallographic identification.

The next advancement in Ln^{2+} chemistry was in 2011, when the Evans group reported an EPR spectrum from the reduction of $Y(NR_2)_3$ ($R = SiMe_3$) with KC_8.[20] This spectrum contained a two-line hyperfine pattern consistent with ^{89}Y ($I = 1/2$), but the EPR active species was too unstable to isolate. Subsequently, reduction of Cp'_3Y [$Cp' = (C_5H_4SiMe_3)^{1-}$] with KC_8 and crown in THF was investigated. Upon reduction, a dark colored solution was generated which contained

an EPR active species that was later identified as the first isolable crystallographically-characterizable molecular example of Y^{2+}.[21]

The reduction of Cp'_3Ln (Ln = Ho, Er) with KC_8 and crown in THF was studied next and although the EPR data collected were not interpretable, UV-visible spectra were collected and the first crystallographically characterized examples of Ho^{2+} and Er^{2+} were isolated.[22] Using crypt rather than crown, Y^{2+}, Ho^{2+}, and Er^{2+} were crystallographically-characterized and the first Ln^{2+} examples were later crystallographically-characterized for the other members of the series Pr, Gd, Tb, and Lu (Pm was not studied due to its radioactivity).[23] Consequently, the +2 oxidation state had been isolated and crystallographically-characterized for Y and the entire lanthanide series, eq. 1.1.

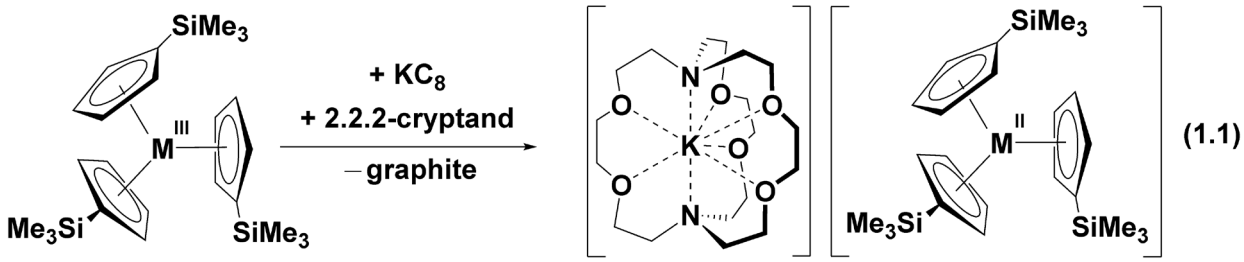

(1.1)

R = H; M = Y, La, Ce, Pr, Nd, Sm, Gd, Tb, Dy, Ho, Er, Tm, Lu

These new rare earth ions in the +2 oxidation state were unusual in comparison to the known traditional Ln^{2+} ions and were labelled "non-traditional."[16] The new non-traditional Ln^{2+} ions were compared with the known traditional Ln^{2+} ions on the basis of structural changes as well as UV-visible spectroscopy, corroborated by TDDFT analyses.[24] The non-traditional $[K(crypt)][Cp'_3Ln^{II}]$ complexes featured much smaller increases in metal–ring centroid distances (0.027 Å – 0.031 Å) compared to their Ln^{3+} precursors which differed from the large differences observed with the traditional Ln^{2+} ions (0.1 Å – 0.2 Å). UV-visible spectroscopy revealed that the new non-traditional ions display ε values > 1000 $M^{1-}cm^{1-}$, while the traditional ions featured molar

absorptivities below 1000 $M^{1-}cm^{1-}$. TDDFT analysis showed that these new non-traditional ions adopted electron configurations that disobeyed the Aufbau principle i.e., they formed $4f^n5d^1$ configurations, while Y^{2+} adopted a $4d^1$ configuration. [24]

For Nd and Dy, despite being previously known to adopt $4f^{n+1}$ configurations, TDDFT analysis revealed that their $(Cp'_3Ln)^{1-}$ complexes featured non-traditional, $4f^n5d^1$, electron configurations.[24] Structural analysis of these $(Cp'_3Ln)^{1-}$ complexes for Nd and Dy revealed that the change in metal–ring centroid distance was not in the range of the other traditional Ln^{2+} $(Cp'_3Ln)^{1-}$ complexes (0.123 Å – 0.156 Å), but was much smaller, 0.030 Å and 0.036 Å, respectively. Similarly, UV-visible spectra of the Nd and Dy $(Cp'_3Ln)^{1-}$ complexes showed absorptions similar in intensity to the new $4f^n5d^1$ configurations rather than $4f^{n+1}$ configurations. Consequently, Nd and Dy have been grouped together as "configurational crossover" ions since both traditional $4f^{n+1}$ and non-traditional $4f^n5d^1$ configurations have been isolated and crystallographically characterized. [24]

Dissertation Outline. The research presented in this dissertation focuses on the reduction and isolation of non-traditional Ln^{2+} ions using new ligand sets and heteroleptic ligand systems to expand the isolable examples and understand the reactivity of these new electron configurations. Chapter 2 describes the synthesis and characterization of a new series of Ln^{2+} compounds with the homoleptic $(C_5Me_4H)_3^{3-}$ ligand system. These complexes were characterized by EPR spectroscopy, UV-visible spectroscopy, and crystallography. Analysis showed that the $[(C_5Me_4H)_3Dy]^{1-}$ complex featured a traditional, $4f^{10}$, configuration while $[(C_5Me_4H)_3Nd]^{1-}$ featured a non-traditional, $4f^35d^1$, configuration. Chapter 3 describes efforts to investigate if a C_5Me_5 complex of Y(II) could be isolated and to examine the synthetic accessibility of heteroleptic Y(II) complexes. The reduction of $(C_5Me_5)_2Y(NR_2)$ ($R = SiMe_3$) with potassium graphite in THF

in the presence of 2.2.2-cryptand (crypt) was examined. An intensely dark colored solution is formed that has EPR spectra indicative of a $4d^1$ Y(II) complex, but single crystals of the products contained a mixture of an Y(II) complex $[K(crypt)][(C_5Me_5)_2Y(NR_2)]$, and an Y(III) cyclometalated derivative resulting from C–H bond activation of a methyl group of the Me_3Si substituent of the amide ligand. Chapter 4 describes investigations into the reductive chemistry of a new type of rare earth complex formed by reaction of rare-earth metal allyl complexes, $(C_5Me_5)_2Ln(\eta^3\text{-}C_3H_5)$ (Ln = Y, Tb, Dy) with benzoxazole. This reaction proceeds by deprotonation and ring-opening to form 2-isocyanophenolate-bridged bimetallic species, $[(C_5Me_5)_2Ln(\mu\text{-}2\text{-}CNC_6H_4O\text{-}\kappa C\text{:}\kappa O)]_2$. These bimetallic complexes contain two lanthanide centers bound to the carbon of one isocyanophenolate ligand and the oxygen of another to form a 12-membered $(Ln–O–C–C–N–C)_2$ ring which is coplanar to within 0.024 Å. The reductive chemistry of this ring system is also described. Appendix A describes the Ln^{2+} reactivity of the $[K(crypt)][(C_5Me_4H)_3Ln]$ (Ln = La, Ce) complexes with ^{t}Bu–NC. No Ln-containing crystals were isolated, but unusual EPR spectra were collected. Appendix B describes efforts to isolate examples of other heteroleptic Ln^{2+} complexes. These efforts include investigating the reduction of $(C_5Me_5)_2Ln(NR_2)$ for Ln = Ce, Nd, and Lu as well as other heteroleptic Y complexes, $(C_5Me_5)_2YA$ ($A = BH_4$, $OAr^{tBu,tBu,Me}$).

References

(1) Haskin, L. A.; Frey, F. A. *Science* **1966,** *152*, 299-314.

(2) Van Loy, S.; Binnemans, K.; Van Gerven, T. *J. Clean. Prod.* **2017,** *156*, 226-234.

(3) Ronda, C. R.; Jüstel, T.; Nikol, H. *J. Alloys Compd.* **1998,** *275-277*, 669-676.

(4) Emeleus, H. J.; Sharpe, A. G. *Modern Aspects of Inorganic Chemistry,* 4th ed.; Wiley: New York, 1973.

(5) Bunzli, J.-C. G.; Choppin, G.R. *Lanthanide Probes in Life, Chemical, and Earth Sciences: Theory and Practice;* Elsevier: Amsterdam, 1989.

(6) Dieke, G. H. *Spectra and Energy Levels of Rare Earth Ions in Crystals;* Crosswhite, H. M., Crosswhite, H., Eds.; John Wiley & Sons Inc.: New York, 1968

(7) Kramer, M.J.; McCallum, R. W.; Anderson, I. A.; Constantinides, S. *J. Miner. Met. Mater. Soc.* **2012**, *64* (7), 752-763.

(8) Freeman, A. J.; Watson, R. E. *Physical Review* **1962,** *127*, 2058-2075.

(9) Johnson, K. E.; Sandoe, J. N. *J. Chem. Soc. A* **1969**, 1694-1697.

(10) Connick, R. E. *J. Chem. Soc.* **1949**, S235-S241.

(11) Shannon, R. D. *Acta Crystallogr. Sect. A: Found. Crystallogr.* **1976,** *32*, 751-767.

(12) Bochkarev, M. N. *Coord. Chem. Rev.* **2004,** *248*, 835-851.

(13) Meyer, G. *Chem. Rev.* **1988,** *88*, 93-107.

(14) Meyer, G., *The Rare Earth Elements: Fundamentals and Applications*; Atwood, D., Ed. John Wiley & Sons: Chichester, UK, 2012; p 161-173.

(15) Nief, F., *Handbook on the Physics and Chemistry of Rare Earths*; Jr., K. A. G.; Bünzli, J.-C. G.; Pecharsky, V. K., Eds.; Elsevier: Amsterdam, 2010; p 241-300.

(16) Evans, W. J. *Organometallics* **2016,** *35*, 3088-3100.

(17) Morss, L. R. *Chem. Rev.* **1976,** *76*, 827-841.

(18) Cassani, M. C.; Duncalf, D. J.; Lappert, M. F. *J. Am. Chem. Soc.* **1998,** *120*, 12958-12959.

(19) Hitchcock, P. B.; Lappert, M. F.; Maron, L.; Protchenko, A. V. *Angew. Chem. Int. Ed.* **2008,** *47*, 1488-1491.

(20) Fang, M.; Lee, D. S.; Ziller, J. W.; Doedens, R. J.; Bates, J. E.; Furche, F.; Evans, W. J. *J. Am. Chem. Soc.* **2011,** *133*, 3784-3787.

(21) MacDonald, M. R.; Ziller, J. W.; Evans, W. J. *J. Am. Chem. Soc.* **2011,** *133*, 15914-15917.

(22) MacDonald, M. R.; Bates, J. E.; Fieser, M. E.; Ziller, J. W.; Furche, F.; Evans, W. J. *J. Am. Chem. Soc.* **2012,** *134*, 8420-8423.

(23) MacDonald, M. R.; Bates, J. E.; Ziller, J. W.; Furche, F.; Evans, W. J. *J. Am. Chem. Soc.* **2013,** *135*, 9857-9868.

(24) Fieser, M. E.; MacDonald, M. R.; Krull, B. T.; Bates, J. E.; Ziller, J. W.; Furche, F.; Evans, W. J. *J. Am. Chem. Soc.* **2015,** *137*, 369-382.

CHAPTER 2

Tetramethylcyclopentadienyl Ligands Allow Isolation of Ln(II) Ions Across the Lanthanide Series in [K(2.2.2-cryptand)][$(C_5Me_4H)_3Ln$] Complexes*

Introduction

As described in the Introduction, the range of oxidation states accessible to the rare-earth metals in crystallographically-characterizable molecular complexes available for reactivity in solution has greatly expanded.[1, 2] Prior to 2008, it was thought that only six lanthanides could form crystallographically-characterizable molecular complexes of Ln(II) ions in solution: Eu, Yb, Sm, Tm, Dy, and Nd.[3-6] The synthesis of these complexes often involved reduction of $4f^n$ Ln(III) precursors which formed Ln(II) ions with $4f^{n+1}$ electron configurations as expected by the Aufbau principle.

However, it is now known that scandium, yttrium and all of the lanthanides (except Pm which was not studied due to its radioactivity) can form isolable molecular complexes of Ln(II) ions if reductions are done in the proper coordination environment.[7-12] Specifically, it has been demonstrated that reduction of tris(cyclopentadienyl) complexes with silyl-substituted ligands $C_5H_3(SiMe_3)_2$ (Cp'')[7, 8] and $C_5H_4SiMe_3$ (Cp')[9-12] could provide access to Ln(II) ions across the series as shown in eq 2.1.[1, 2] This was also extended to the actinides, Th,[13] U,[14, 15] Pu,[16] and Np.[17]

Examples of complexes with these Ln(II) ions have been characterized with the *tert*-butyl-substituted cyclopentadienyl ligands $C_5H_3(CMe_3)_2$ (Cp^{tt}),[18, 19] $C_5H_2(CMe_3)_3$ (Cp^{ttt}),[20, 21] and the tris(aryloxide) mesitylene ligand, $[(^{Ad,Me}ArO)_3mes]^{3-}$.[22, 23]

---

*Portions of this chapter have been published: Jenkins, T.F.; Woen, D.H.; Mohanam, L.N.; Ziller, J.W.; Furche, F.; Evans, W.J. *Organometallics*. **2018**, *37*(21), 3863-3873. DOI:10.1021/acs.organomet.8b00557

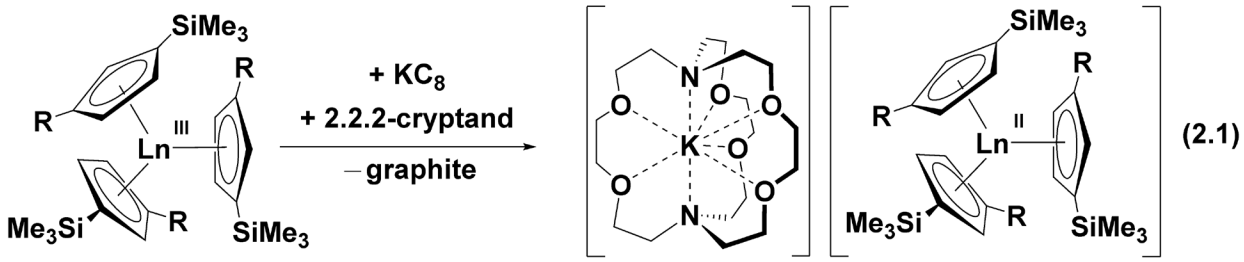

(2.1)

R = H; M = Y, La, Ce, Pr, Nd, Sm, Gd, Tb, Dy, Ho, Er, Tm, Lu, U
R = $SiMe_3$; M = La, Ce, Pr, Nd, Th, U, Pu, Np

Extensive crystallographic, spectroscopic, magnetic, and density functional theory (DFT) studies showed that the new Ln(II) ions in the tris(cyclopentadienyl) environments adopted $4f^n5d^1$ electron configurations.[1, 7-12, 23-26] This could be rationalized by the crystal field splitting in a tris(cyclopentadienyl) coordination environment, which allows an effectively non-bonding $5d_z^2$ orbital to be comparable in energy to the 4f subshell.[27-32]

A comparison of the rare-earth metals in the [K(crypt)][Cp'_3Ln], series (crypt = 2.2.2-cryptand) revealed that the electronic configuration of Ln(II) ions are trichotomous.[10] Sm, Eu, Tm, and Yb form complexes of traditional Ln(II) ions with $4f^{n+1}$ electron configurations. For Ln = Nd and Dy, the [K(crypt)][Cp'_3Ln] complexes have $4f^n5d^1$ configurations, but in other ligand environments the metals form $4f^{n+1}$ Ln(II) ions. These are designated as configurational crossover ions. The third category contains the rest of the lanthanide metals which have $4f^n5d^1$ configurations and Y(II) which is a $4d^1$ ion.

Soon after the first Y(II) complex, $(Cp'_3Y)^{1-}$, was isolated,[11] the Evans group examined the importance of the ligand system by investigating the reductions of $Cp_3Y(THF)$ ($Cp = C_5H_5$), $Cp^{Me}{}_3Y(THF)$ ($Cp^{Me} = C_5H_4Me$), and Cp''_3Y.[25] In each case, the reduction product was examined in solution by EPR spectroscopy.[9, 11] However, none of these ligand systems gave isolable Y(II) complexes as found in the reduction of Cp'_3Y. Comparison of the hyperfine coupling constants of

these tris(cyclopentadienyl) complexes along with that of the solution reduction product of $Y(NR_2)_3$ (R = $SiMe_3$), a system that had not yielded an isolable Y(II) complex at the time,[33] suggested an correlation of the observed results: The more unstable complexes had larger hyperfine coupling constants. The instability of Cp''_3Y was attributed to the steric crowding in this complex with the large ligand and the small metal.[34, 35]

The larger hyperfine coupling constants observed in the reductions of $Y(NR_2)_3$, Cp^{Me}_3Y, and Cp_3Y compared to Cp'_3Y suggested that the NR_2, Cp^{Me}, and Cp ligands were more electron donating than Cp′ in this yttrium system and made the Y(II) complex too electron-rich to be isolated. These results were consistent with data obtained on electrochemical analysis of $(C_5R_5)_2ZrCl_2$ complexes,[36] as well as studies by Lappert that showed that it was more difficult to reduce $[C_5H_3(CMe_3)_2]_3La$ than $[C_5H_3(SiMe_3)_2]_3La$.[19]

However, the isolation of Ln(II) ions in complexes of NR_2 (R = $SiMe_3$) ligands, suggested that strongly donating ligands could also provide these new ions. Specifically, amide ligands were used to isolate the first crystallographically-characterizable complex of a +2 ion of the smallest rare-earth metal, scandium, and the lanthanides, Ln = Nd, Gd, Tb, Dy, Ho, and Er, in the compounds $[M(chelate)][Ln(NR_2)_3]$ (M = K, Rb; chelate = 18-crown-6 and crypt; R = $SiMe_3$), and this was later extended to yttrium.[37-39] Consequently, the Evans group examined reduction of Cp^{tet}_3Ln complexes (Cp^{tet} = C_5Me_4H). These complexes were not examined earlier on the basis that the Cp^{tet} ligand was too electron donating to form stable complexes. [25]

Dr. David Woen investigated the reduction of Cp^{tet}_3Ln (Ln = Y, Nd) with KC_8 in the presence of 2.2.2-cryptand (crypt). While only EPR evidence was collected for the reduction product of Cp^{tet}_3Y due to poor thermal stability, crystals of $[K(crypt)][Cp^{tet}_3Nd]$ were obtained but no further characterization was done. I report here that the $(Cp^{tet}_3)^{3-}$ ligand set provides an entire

new *series* of Ln(II) complexes that allows for further evaluation of the trichotomous electron configurations observed in the [K(crypt)][Cp′$_3$Ln] complexes.

Results

Synthesis of [K(crypt)][Cp$^{tet}_3$Ln] Complexes. Reduction of Cp$^{tet}_3$Ln, **1-Ln** (Ln = La, Ce, Pr, Sm, Gd, Tb, Dy) at −35 °C with KC_8 in the presence of 2.2.2-cryptand (crypt) yielded dark blue solutions stable enough to crystallize. Layering a THF solution with Et_2O at −35 °C, yielded crystals of [K(crypt)][Cp$^{tet}_3$Ln], **2-Ln**, after several days, eq 2.2. Crystallographic data were collected on all six of these samples which provided a new series of Ln(II) ions in a single coordination environment for comparison with the [K(crypt)][Cp′$_3$Ln] series.[8-11]

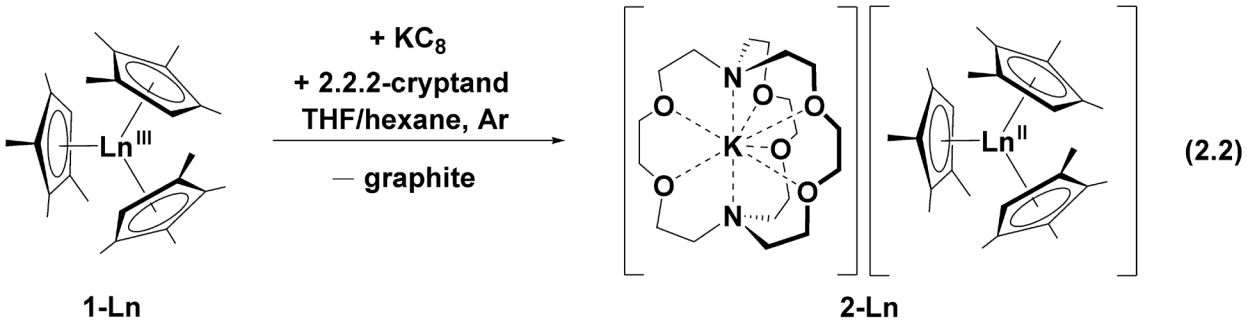

(2.2)

The compounds crystallize in three different space groups. Complexes of the largest metals**, 2-La** and **2-Ce**, are isomorphous, crystallizing in $P2_12_12_1$. Complexes of the non-traditional middle lanthanides, **2-Pr**, **2-Nd**, **2-Gd**, and **2-Tb**, are isomorphous and crystallize in $P2_1/c$. However, **2-Sm**, a known traditional ion, crystallizes in a different space group, $C2/c$. The **2-Dy** complex crystallizes in a different space group, $R\bar{3}c$. The Dy structure in Figure 2.1 is representative of these complexes and spectroscopic data are presented later. It should be noted that mixed ether solvent occupancy was found in the lattice for Pr, Nd, Sm, Gd, Tb, and Dy, but no solvents were found in the crystal lattice of the complexes of largest metals, La and Ce.

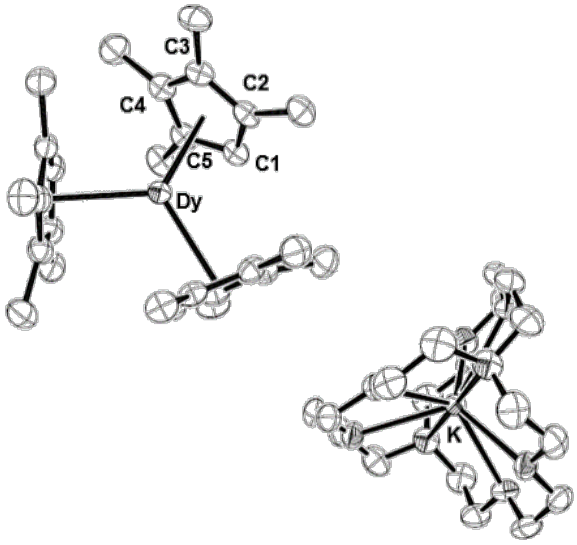

Figure 2.1. Thermal ellipsoid plots of [K(crypt)][Cp^{tet}_3Dy], **2-Dy** drawn at the 50% probability level.

Ho and Er. Attempts to make the Ho and Er analogs also gave dark solutions, but they did not persist for more than a few hours even at −35 °C and were not pursued further. This instability was consistent with that of the similarly-sized yttrium complex.

EPR Spectroscopy. The EPR spectra of [K(crypt)][Cp^{tet}_3La], **2-La**, and [K(crypt)][Cp^{tet}_3Gd], **2-Gd**, are shown in Figure 2.2. The eight-line hyperfine pattern of **2-La** is as expected for La(II) since the 99.9% naturally abundant ^{139}La has an I = 7/2 nuclear spin. The data are best modelled with g_{iso} = 1.98 and A_{avg} = 291. The average hyperfine coupling constant for **2-La** is larger than the values found for **3-La**,[10] 154 G, and [K(crypt)][Cp″$_3$La],[7] 133.5 G, as well as the reduction product of Cp^{Me}_3La,[40] 195 G, as expected for the more electron donating Cp^{tet} ligand. The spectrum of **2-Gd** is similar to that of crystallographically-characterized **3-Gd**,[9] as well as the reduction products of Cp″$_3$Gd, Cp″$_2$GdCp, and Cp″$_2$GdCp^{Me}.[25]

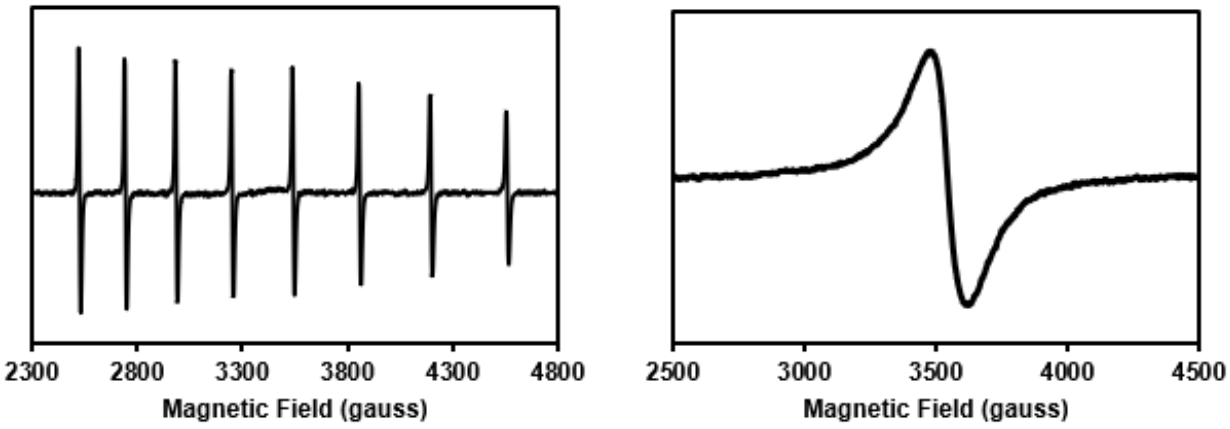

Figure 2.2. Room temperature EPR spectra of [K(crypt)][Cp^{tet}_3La] (left; mode: perpendicular; g_{iso} = 1.97; A_{iso} = 291 G; v = 9.8175 GHz; P = 2.021; modulation amplitude = 1 mT) and [K(crypt)][Cp^{tet}_3Gd] (right; mode: perpendicular; g_{iso} = 1.9786; v = 9.8182 GHz; P = 2.026; modulation amplitude = 1.464 mT).

Structural Analysis. Metrical parameters on the [K(crypt)][Cp^{tet}_3Ln], **2-Ln**, series are presented in Table 2.1, along with data on the analogous [K(crypt)][Cp'_3Ln], **3-Ln**,[9-12] and [K(crypt)][Cp''_3Ln][7, 8] complexes when available. The Ln–(C_5Me_4H ring centroid) distances (Ln–Cnt) for six of the eight **2-Ln** complexes with Ln = La, Ce, Pr, Nd, Gd, and Tb are consistent with Ln ionic radii, decreasing with increasing atomic number, following the lanthanide contraction. For each of these six metals, the Ln–Cnt distance also decreases in the order of the size of the ligands: $Cp^{tet} \gg Cp'' > Cp'$. This suggests that the $(Cp^{tet}_3)^{3-}$ environment occupies more space than $(Cp''_3)^{3-}$ which is surprising given that $(Cp'')^{1-}$ was investigated as a ligand for being sterically similar to $(C_5Me_5)^{1-}$.[41]

Table 2.1. Comparison of Ln–(cyclopentadienyl ring centroid) distances (Ln–Cnt) for [K(crypt)][Cp^X_3Ln] with Cp^X = Cp^{tet}, Cp′, and Cp″.

	Ln–Cnt Range (Å)	$Ln–Cnt_{Ave}$ (Å)	Δ[Ln(II) vs Ln(III)][a]
$(Cp^{tet}_3La)^{1-}$	2.626-2.642	2.633	0.058[42]
$(Cp''_3La)^{1-}$	2.606-2.642	2.620	0.018[7, 43]
$(Cp'_3La)^{1-}$	2.581-2.595	2.586	0.026[10, 35]
$(Cp^{tet}_3Ce)^{1-}$	2.594-2.612	2.603	0.051[44]
$(Cp''_3Ce)^{1-}$	2.574-2.609	2.587	0.022[8, 45]
$(Cp'_3Ce)^{1-}$	2.553-2.567	2.558	0.029[10, 45]
$(Cp^{tet}_3Pr)^{1-}$	2.572-2.583	2.578	0.046[44]
$(Cp''_3Pr)^{1-}$	2.552-2.588	2.566	--[b]
$(Cp'_3Pr)^{1-}$	2.530-2.544	2.535	0.026[9, 46]
$(Cp^{tet}_3Nd)^{1-}$	2.555-2.568	2.563	0.045[47]
$(Cp''_3Nd)^{1-}$	2.530-2.559	2.544	0.019[8, 43]
$(Cp'_3Nd)^{1-}$	2.514-2.528	2.519	0.031[10, 46]
$(Cp^{tet}_3Sm)^{1-}$	2.623-2.640	2.630	0.147[42]
$(Cp'_3Sm)^{1-}$	2.603-2.615	2.608	0.148[10]
$(Cp^{tet}_3Gd)^{1-}$	2.511-2.519	2.516	0.047
$(Cp'_3Gd)^{1-}$	2.463-2.475	2.468	0.031[9]
$(Cp^{tet}_3Tb)^{1-}$	2.498-2.505	2.502	0.054[42]
$(Cp'_3Tb)^{1-}$	2.448-2.461	2.454	0.032[9]
$(Cp^{tet}_3Dy)^{1-}$	2.543-2.543	2.543	0.099
$(Cp'_3Dy)^{1-}$	2.434-2.450	2.443	0.036[10]

[a] Δ[Ln(II) vs Ln(III)] = the difference in Ln–Cnt distances of $[Cp^x_3Ln^{II}]^{1-}$ vs $Cp^x_3Ln^{III}$ (Å). The references are to the structures of the $Cp^x_3Ln^{III}$ complexes.

[b] The structure of Cp''_3Pr has not been reported for comparison.[8]

The differences in Ln–Cnt distances between the Ln(III) $(C_5R_5)_3Ln$ precursor and the reduced Ln(II) product for La, Ce, Pr, Nd, Gd, and Tb are 0.045-0.058 Å for the Cp^{tet} series versus 0.018-0.022 Å for the Cp″ complexes and 0.026-0.031 Å for the Cp′ compounds. All these differences are much smaller than the 0.1-0.2 Å differences found for $4f^{n+1}$ Ln(II) versus $4f^n$ Ln(III) complexes of the traditional Ln(II) ions of Eu, Yb, Sm, and Tm. This is structural evidence consistent with $4f^n5d^1$ configurations for these six metals based on previous structural, spectroscopic, and DFT analysis of the **3-Ln** complexes.[9-12]

Sm and Dy. The metrical parameters of the samarium and dysprosium complexes, **2-Sm** and **2-Dy**, differ from those of the six metals above. The difference in Ln–Cnt distances between the Ln(II) complexes and their Ln(III) precursors are 0.147 and 0.099 Å for **2-Sm** and **2-Dy**, respectively. This is substantially larger than the 0.045-0.058 Å differences for the six other metals in the series. These larger distances suggest that **2-Sm** and **2-Dy** contain $4f^6$ and $4f^{10}$ ions, respectively, and not $4f^n5d^1$ species. These metrical parameters and $4f^{n+1}$ electronic configuration assignments are consistent with the UV-vis spectra reported below since Sm is known as a traditional Ln(II) ion and Dy is known as a configurational crossover ion.[10] The difference in these two structures is shown graphically in Figure 2.3 which plots Ln–Cnt distances as a function of atomic number. In addition, the Evans method[48-50] measured magnetic moment of **2-Dy** is 10.8 μ_B. This is close to the 10.6 μ_B theoretical value for a $4f^{10}$ complex and is smaller than the 11.3-11.7 μ_B values observed for $4f^95d^1$ complexes.[24]

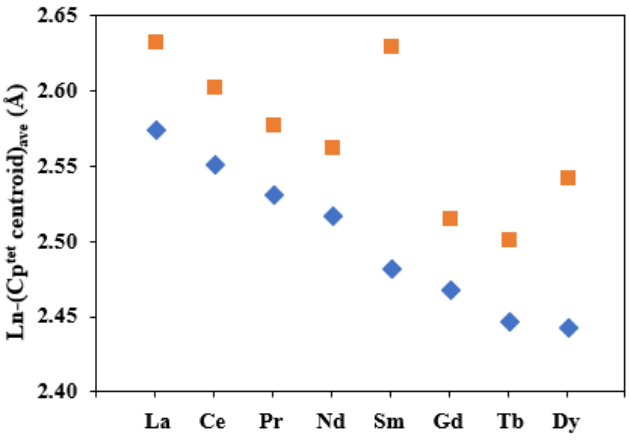

Figure 2.3. Plot of average Ln–(Cp^{tet} centroid) distances in Cp^{tet}_3Ln, **1-Ln** (blue diamonds) and in **2-Ln** (orange squares).

UV-vis Spectroscopy. The UV-vis spectra of **2-Ln** are shown in Figure 2.4 and the absorbance maxima and extinction coefficients are compared with those of **3-Ln** in Table 2.2. The spectra of **2-Ln** for Ln = La, Ce, Pr, Nd, Gd, and Tb show the strongest absorptions in the near-infrared region with λ_{max} values in the range of 745-874 nm with a molar extinction coefficient, ε, of 1700-5600 $M^{-1}cm^{-1}$, Figure 4. In comparison, the previously reported spectra of **3-Ln** complexes of these metals have the largest absorptions from 420-635 nm in the visible region with ε = 4400-6500 $M^{-1}cm^{-1}$.[1, 2, 9-12]

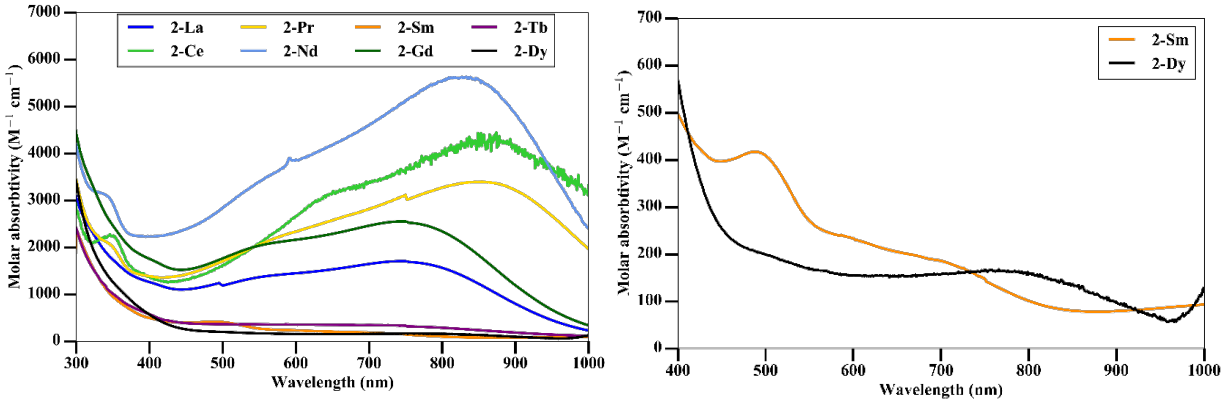

Figure 2.4. UV-vis spectra of **2-Ln** (Ln = La, Ce, Pr, Nd, Sm, Gd, Tb, Dy) collected at 5.0 mM concentration in THF at room temperature on the left, and expanded scale spectra of **2-Dy** and **2-Sm** on the right.

In contrast to the UV-vis spectra of La, Ce, Pr, Nd, Gd, and Tb, the spectra of **2-Dy** and **2-Sm** have weaker absorptions. These are shown with a different scale in Figure 4 (right). Less intense absorptions were previously observed for the **3-Ln** complexes for the metals with $4f^{n+1}$ electron configurations, *i.e.,* Eu, Yb, Sm, and Tm.[10] Hence, the λ_{max} = 466 nm with ε = 203 $M^{-1}cm^{-1}$ for **2-Sm** is consistent with a $4f^6$ electron configuration for this complex. The weaker absorption for **2-Dy** with λ_{max} = 766 nm and ε = 200 $M^{-1}cm^{-1}$ is also consistent with a $4f^{n+1}$ configuration and this matches the structural data above which suggested that **2-Dy** had a $4f^{10}$ configuration.

Table 2.2. Comparison of UV-Vis absorption maxima of [K(crypt)][Cp^{tet}_3Ln], **2-Ln**, and [K(crypt)][Cp'_3Ln], **3-Ln**.

	λ_{max} (nm)	ε ($M^{-1}cm^{-1}$)		λ_{max} (nm)	ε ($M^{-1}cm^{-1}$)
2-La	745	1700	**2-Sm**	466	200
3-La[10]	554	6500	**3-Sm**[10]	360	700
2-Ce	874	4100	**2-Gd**	745	2500
3-Ce[10]	635	4700	**3-Gd**[9]	430	4400
2-Pr	854	4500	**2-Tb**	784	650
3-Pr[9]	518	4500	**3-Tb**[9]	464	4800
2-Nd	833	5600	**2-Dy**	766	200
3-Nd[10]	420	4700	**3-Dy**[10]	483	3400

Theoretical Analysis. The structures of the Cp^{tet}_3Ln precursors and the $(Cp^{tet}_3Ln)^{1-}$ anions in the **2-Ln** complexes were optimized with density functional theory (DFT) by Luke Nambi Mohanam from the research group of Professor Filipp Furche**.** For the La, Ce, Pr, Nd, Gd, and Tb anions in **2-Ln**, the computed change in Ln–Cnt distances between the Ln(III) precursor Cp^{tet}_3Ln and the reduced Ln(II) product, **2-Ln**, matches the X-ray data within 0.02 Å when $[4f^n]5d^1$ configurations for the anions are assumed. The highest occupied molecular orbital of **2-La** is shown in Figure 2.5. The d_z^2 nature of this SOMO matches those found for **3-Ln**. However, the calculated differences in Ln−ring centroid distances for Sm and Dy, 0.200 and 0.199 Å respectively, were much larger than those of the $4f^n5d^1$ ions described above. The experimentally observed Ln(II) vs Ln(III) differences for Sm and Dy, 0.147 and 0.099 Å, are not as large as the

calculated differences, but the data support the presence of $4f^{n+1}$ configurations for the ions in $(Cp^{tet}_3Sm)^{1-}$ and $(Cp^{tet}_3Dy)^{1-}$.

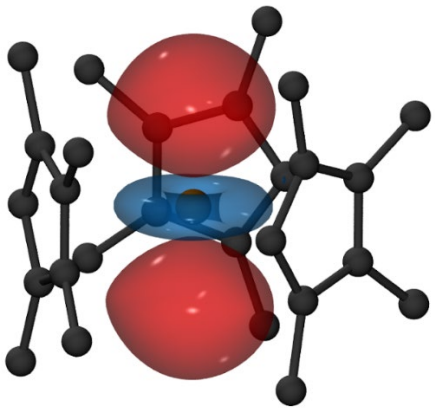

Figure 2.5. Highest singly occupied molecular orbital of **2-La** (contour value 0.04 a.u.), obtained using DFT.

Time-dependent density functional theory (TDDFT) simulations qualitatively reproduce the much stronger visible absorption of the $4f^n5d^1$ La, Ce, Pr, Nd, Gd, and Tb compounds compared to the $4f^{n+1}$ Sm and Dy compounds, see Figure 2.6. Analysis of TDDFT simulations for the $(Cp^{tet}_3Ln)^{1-}$ (Ln = La, Ce, Pr, Nd, Gd, and Tb) compounds reveals that in addition to the MLCT absorptions found previously in the **3-Ln** series, there are strongly dipole-allowed Ln 5d→6p and 5d→π* lower energy transitions. MLCT transitions are still present in **2-Ln** (Ln = La, Ce, Pr, Nd, Gd, and Tb), but they are much weaker than these 5d→6p transitions. It should also be noted that 5d→6p absorptions are also present in **3-Ln** but are weaker in those complexes.

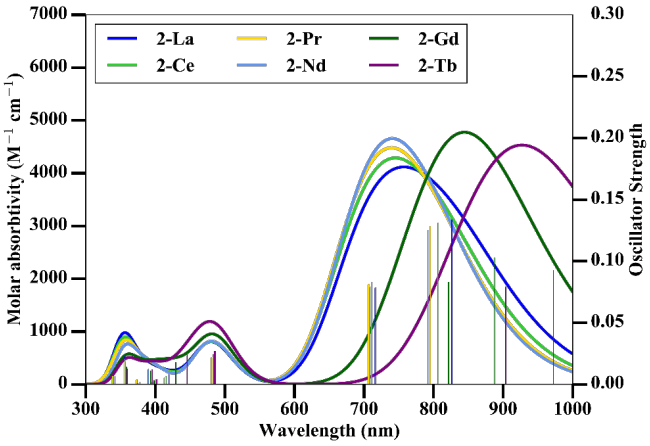

Figure 2.6. Predicted UV-Vis spectra of **2-Ln** from TDDFT.

Thermal Stability. The stability of the **2-Ln** complexes of the larger metals, Ln = La, Ce, Pr, Nd, Sm, and Gd, is greater than that of Ln = Tb, Dy, Ho, Er, and Y. For the larger metal ions, the dark blue/ black solutions obtained by reduction with KC_8 in THF, followed by Et_2O layer diffusion at room temperature are stable for at least 48 h. However, for Dy, the reduction must be done at −35°C to isolate a dark-colored product. For Ho, Er, and Y, reductions, even at −35°C yield, unstable black solutions that do not persist longer than 12 h at −35°C. Only the dark colored solutions of **3-La**, **3-Ce**, and **3-Nd** exhibit thermal stability comparable to the larger members of the **2-Ln** series, Ln = La-Gd. Hence, it appears that the **2-Ln** complexes of the larger lanthanides are more stable than the **3-Ln** analogs.

The thermal decomposition of **2-Tb** was examined in a manner analogous to previous studies on **3-Ln** and [K(crypt)][Cp″$_3$Ln][8, 9] complexes by monitoring the decrease in the maximum absorbance in the UV-vis spectrum, in this case at λ_{max} = 784 nm. The data on **2-Tb** was best modeled with second order kinetics, which is consistent with previous Ln(II) decomposition studies.[8, 9] The observed second order rate constant of 5.4(7) x 10^{-2} M^{-1} cm^{-1} is an order of magnitude larger than the second order rate constant, 4.25(5) x 10^{-3} M^{-1} cm^{-1}, observed for **3-Tb**

at a concentration of 3 mM.[9] Hence, for this smaller metal, the **2-Tb** complex is less stable than the **3-Tb**.

Discussion

Although Cp^{tet} was originally considered to be an unlikely ligand to stabilize $4f^n5d^1$ Ln(II) ions because it is so electron donating, it has provided crystallographically-characterizable tris(cyclopentadienyl) Ln(II) complexes for La, Ce, Pr, Nd, Gd, and Tb, as well as the traditional Sm(II) and configurational crossover Dy(II). The EPR data on [K(crypt)][Cp^{tet}_3La], **2-La**, show larger hyperfine coupling values than the Cp′ and Cp″ analogues consistent with more electron density on La. Given the isolation of these **2-Ln** complexes, cyclopentadienyl ligands with alkyl substituents are not too electron donating to form Ln(II) complexes of this type.

There are two major differences between [K(crypt)][Cp^{tet}_3Ln], **2-Ln**, and the previously reported [K(crypt)][Cp'_3Ln], **3-Ln**, series. One notable difference for the six $4f^n5d^1$ ions of La, Ce, Pr, Nd, Gd, and Tb is that the Ln–Cnt distances for the Ln(II) Cp^{tet} complexes, **2-Ln**, are 0.043 to 0.048 Å longer than those of the analogous Ln(II) Cp′ complexes, **3-Ln**. Hence, although the Cp^{tet} ligands may be more electron donating, they are further away from the metal. This may mitigate their greater electron donating ability which renders the isolation of Ln(II) complexes for these metals feasible. Concomitantly, the Cp^{tet} ligands may also provide more steric bulk around the metal ion with their four substituents compared to the mono-substituted Cp′. The importance of steric saturation to the stability of Ln(III) complexes is well established. It is interesting to note that the difference in Ln–Cnt distances between **2-Ln** and **3-Ln** for the traditional Sm(II) complexes is only 0.022, whereas the difference for the configurational crossover Dy(II) complex is 0.10 Å. Hence, these $4f^{n+1}$ systems do not show regularity in the difference in metal–ring centroid distances between Cp^{tet} and Cp′ ligand systems.

Another notable difference between **2-Ln**, and **3-Ln** are the UV-vis spectra. The absorptions with the largest λ_{max} values are at lower energies compared to the most intense absorptions of **3-Ln** for Ln = La, Ce, Pr, Nd, Gd, and Tb. TDDFT studies indicate that the maximum absorbances for the two series do not arise from analogous transitions. For **2-Ln**, the most intense absorptions arise from Ln 5d→6p transitions; for **3-Ln** the largest absorptions are attributed to MLCT. While both transitions are present in both complexes, the MLCT transitions are more intense for **3-Ln** and the metal-metal transitions are more intense for **2-Ln**. It is likely that the longer metal–ligand distances in **2-Ln** weaken the MLCT and enhance the 5d→6p transitions. The difference in intensities of the two series could also occur due to the difference in the geometry of the complexes. In addition to the changes in metal-ligand distance, the higher molecular symmetry of the **2-Ln** complexes could cause greater metal p-character in lower energy unoccupied MOs, which could strengthen oscillator strength due to a large 5d→6p transition dipole moment.

In the [K(crypt)][Cp^{tet}_3Ln], **2-Ln**, series both the crystallographic data and the UV-vis data suggest that $4f^n5d^1$ ions are present for La Ce, Pr, Nd, Gd, and Tb and $4f^{n+1}$ ions for Sm and Dy. This is supported by the DFT calculations. This differs from the [K(crypt)][Cp'_3Ln], **3-Ln**, series where the Dy complex was assigned a $4f^n5d^1$ electron configuration. The dichotomy exhibited by Dy is consistent with the realization that the ligand field can affect configurations involving the 5d orbitals demonstrates that changing the substitution on the cyclopentadienyl rings can delineate between $4f^n5d^1$ and $4f^{n+1}$ configurations. This is shown graphically in Figure 2.7 where the differences in Ln–Cnt distances for Ln(II) and Ln(III) analogs are plotted versus the $4f^{n+1}$ to $4f^n5d^1$ promotion energy determined from gas phase atomic spectra of +2 ions.[51] The dotted line border between traditional and non-traditional electron configurations has changed for Cp^{tet} compared to

Cp′. It is interesting to note that attempts to make **2-Ho** and **2-Er** in this study led to solutions too reactive to isolate. According to Figure 7, if it can be quantitatively interpreted, **2-Ho** and **2-Er** should be $4f^{n+1}$ ions in the $(Cp^{tet}_3)^{3-}$ coordination environment. Calculations of $4f^n$ Ln(III) to $4f^{n+1}$ Ln(II) reduction potentials for Ho and Er are -2.9 and -3.1 V vs. SHE, respectively, i.e., they could be more reactive and thus difficult to isolate than the non-traditional $4f^n5d^1$ Ho(II) and Er(II) ions in the **3-Ln** complexes which have reduction potentials less negative than -2.9 V.

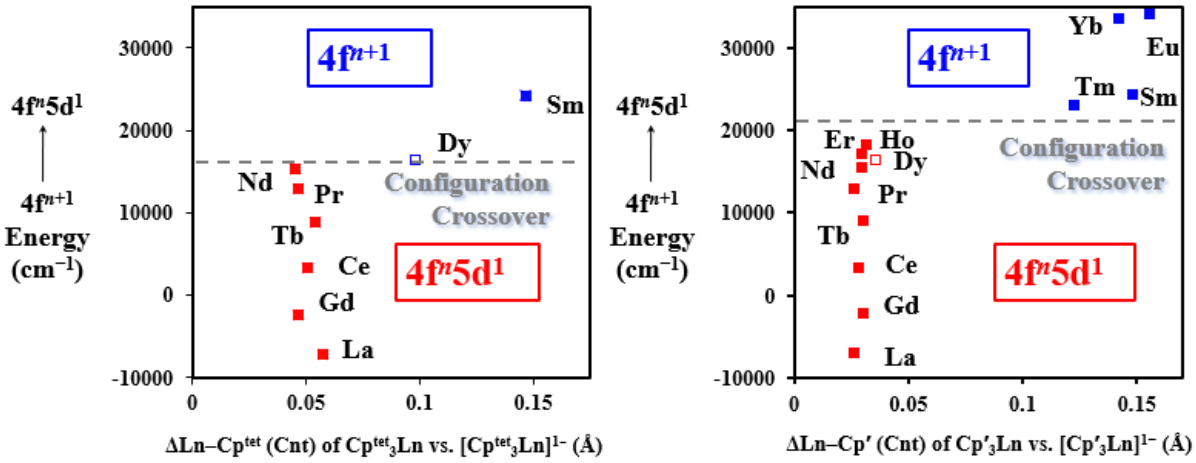

Figure 2.7. Plot of the $4f^{n+1}$ to $4f^n5d^1$ promotion energy compared to the change in distance upon reduction of Cp^x_3Ln to $(Cp^x_3Ln)^{1-}$ for $Cp^x = Cp^{tet}$ (left) and $Cp^x = Cp'$ (right).

Conclusion

The isolation of $(Cp^{tet}_3Ln)^{1-}$ complexes for Ln = La, Ce, Pr, Nd, Gd, and Tb, indicates that the prior assumption that electron rich cyclopentadienyl ligands cannot be used to isolate $4f^n5d^1$ Ln(II) complexes is incorrect. More generally, this suggests that the new mixed configuration Ln(II) ions are likely to be accessible with a variety of ligand systems. This will allow a broader investigation of both their physical properties and their reactivity. In addition, the results show

the importance of the ligand in determining which configuration, $4f^{n+1}$ or $4f^n5d^1$ is adopted by Ln(II) ions in tris(cyclopentadienyl) coordination environments. The crossover point between the two configurations is variable depending on the ligands. Thus, judicious choice of the ligand environment may profoundly affect the chemical, optical, and magnetic properties of divalent lanthanides which can be significantly different for $4f^{n+1}$ vs $4f^n5d^1$ configurations.

Experimental Details

All manipulations and syntheses described below were conducted with rigorous exclusion of air and water using standard Schlenk line and glovebox techniques under an argon atmosphere. Solvents were sparged with UHP argon (Airgas) and dried by passage through columns containing Q-5 and molecular sieves prior to use. THF-d_8 (Cambridge Isotope Laboratories) was dried over NaK alloy, degassed by three freeze-pump-thaw cycles, and vacuum transferred before use. KC_8[52] was prepared as previously described. KCp^{tet} ($Cp^{tet} = C_5Me_4H$), and Cp^{tet}_3Ln (Ln= Y[53], La[42], Ce[44], Pr[44], Nd[47], Sm[42], Tb[42]), **1-Ln**, were synthesized using modified literature procedures described below. 2.2.2-Cryptand (4,7,13,16,21,24-hexaoxa-1,10-diazabicyclo[8,8,8]hexacosane, VWR), was held under vacuum (1 mTorr) for 12 h prior to use. Evans method magnetic susceptibility[48-50] was obtained on a CRYO500 MHz spectrometer at 298 K unless otherwise stated and referenced internally to residual protio-solvent resonances. UV-vis measurements were conducted at 298 K in THF with a Jasco 670 UV-vis-NIR Spectrophotometer. IR samples were prepared as KBr pellets on a Jasco FT/IR-4700 spectrometer. Elemental analyses were conducted on a Perkin-Elmer 2400 Series II CHNS elemental analyzer.

Synthesis of $(C_5Me_4H)_3Gd$, 1-Gd. After $GdCl_3$ (110 mg, 0.418 mmol) was stirred in THF (10 mL) for 2 h, KCp^{tet} (201 mg, 1.26 mmol) was added, and the mixture was stirred for 12 h. The solvent was removed, toluene (10 mL) was added, and the mixture has heated to reflux in a sealed

flask under a slight vacuum (~85 °C) for 12 h. The mixture was centrifuged, and the supernatant was filtered to give a pale-yellow solution. Removal of the solvent (in vacuo) followed by trituration with hexane produced a pale-yellow solid, **1-Gd** (0.111 g, 51%). Orange single crystals suitable for X-ray diffraction were obtained from a concentrated solution of toluene. IR (cm^{-1}): 3113m, 2962vs, 2905vs, 2885vs, 2722s, 2499w, 2046w, 1645w, 1580s, 1544s, 1484s, 1436vs, 1381vs, 1371vs, 1329s, 1173s, 1133m, 1107m, 1018s, 971s, 776vs, 699m, 610s. Anal. Calcd for $C_{27}H_{39}Gd$: C, 62.26; H, 7.55. Found: C, 59.87; H, 7.36. The results give a formula of $C_{27}H_{39.6}$. Obtaining satisfactory analysis on the new members of the known **1-Ln** series[42, 44, 47, 54, 55] as well as the **2-Ln** series has been unexpectedly challenging, although problems with elemental analyses of organolanthanides are well documented.[7, 56-58]

Synthesis of $(C_5Me_4H)_3Dy$, 1-Dy. Similarly, to **1-Gd**, KCp^{tet} (190 mg, 1.19 mmol) was added stepwise to a solution of $DyCl_3$ (100 mg, 0.372 mmol) in THF (10 mL). After reflux and collection of the resulting supernatant, a pale orange solid was obtained, **1-Dy** (101 mg, 95%). Orange single crystals suitable for X-ray diffraction were obtained from a concentrated solution of toluene. IR (cm^{-1}): 3117w, 2965s, 2901vs, 2856vs, 2723m, 1653m, 1436s, 1382s, 1327m, 1173m, 1141m, 1019s, 971s, 781vs, 668m, 608m. Anal. Calcd for $C_{27}H_{39}Dy$: C, 61.64; H, 7.47. Found: C, 57.54; H, 7.23. The low values suggest incomplete sample combustion. The results give a formula of $C_{27}H_{40.4}$.

Synthesis of [K(crypt)][$(C_5Me_4H)_3La$], 2-La. 1-La (28 mg, 0.056 mmol) and crypt (21 mg, 0.057 mmol) were dissolved in THF (2 mL). The solution was cooled to ⁻35 °C prior to addition of KC_8 (12 mg, 0.085 mmol). The solution was immediately filtered, layered using chilled hexane and left at –35 °C. A dark blue crystalline solid, identified as [K(crypt)][$(C_5Me_4H)_3La$], **2-La**, by X-ray diffraction, was obtained after 3 days (46 mg, 89%). Single dark blue crystals of **2-**

La suitable for X-ray diffraction were obtained by diffusion of the concentrated THF solution with Et_2O at ¬35 °C. IR (cm^{-1}): 3070w, 2962m, 2882s, 2820s, 2704w, 1477m, 1445m, 1353s, 1321w, 1293m, 1258m, 1239w, 1173w, 1133s, 1108vs, 1097s, 1017w, 951s, 933m, 833w, 750m, 733w. UV-visible (THF) λ_{max} nm (ε, $M^{-1}cm^{-1}$): 745 (1700). Anal. Calcd for $C_{45}H_{75}KN_2O_6La$: C, 58.87; H, 8.23; N, 3.05. Found: C, 58.81; H, 8.17; N, 3.36. The results give a formula of $C_{45}H_{74.5}N_{2.2}$.

[K(crypt)][$(C_5Me_4H)_3$Ce], 2-Ce. In a procedure analogous to the preparation of **2-La**, **1-Ce** (55 mg, 0.11 mmol) and crypt (45 mg, 0.12 mmol) were dissolved in THF (2 mL) and reacted with KC_8 (22 mg, 0.16 mmol) to form a dark blue crystalline solid identified as [K(crypt)][$(C_5Me_4H)_3$Ce], **2-Ce**, (112 mg, 61%)**.** Single dark blue crystals of **2-Ce** suitable for X-ray diffraction were obtained by layer diffusion of the concentrated THF solution with Et_2O at ¬35 °C. IR (cm^{-1}): 3074w, 2961m 2883s, 2820s, 2704w, 1477m, 1456m, 1444m, 1354m, 1295m, 1258m, 1134s, 1108vs, 1080s, 1018m, 951s, 933m, 833w, 749m, 734w. UV-visible (THF) λ_{max} nm (ε, $M^{-1}cm^{-1}$): 874 (4100). Anal. Calcd for $C_{45}H_{75}KN_2O_6Ce$: C, 58.79; H, 8.22; N, 3.05. Found: C, 58.04; H, 8.34; N, 3.66. The results give a formula of $C_{45}H_{77}N_{2.4}$.

[K(crypt)][$(C_5Me_4H)_3$Sm], 2-Sm. In a procedure analogous to the preparation of **2-La**, **1-Sm** (29 mg, 0.056 mmol) and crypt (21 mg, 0.056 mmol) were dissolved in THF (2 mL) and reacted with KC_8 (10 mg, 0.074 mmol) to form a dark brown crystalline solid identified as [K(crypt)][$(C_5Me_4H)_3$Sm], **2-Sm**, (23 mg, 43%)**.** Single dark brown crystals of **2-Sm** suitable for X-ray diffraction were obtained by layer diffusion of the concentrated THF solution with Et_2O at ¬35 °C. IR (cm^{-1}): 3037w, 2911s, 2882vs, 2851s, 2817m, 2755w, 2717w, 1958w, 1477m, 1450m, 1444m, 1353s, 1264m, 1259m, 1237m, 1119s, 1106vs, 1028w, 949s, 932m, 877m, 818s, 754m, 657m. UV-visible (THF) λ_{max} nm (ε, $M^{-1}cm^{-1}$): 466 (200). Anal. Calcd for $C_{45}H_{75}KN_2O_6Sm$: C,

58.15; H, 8.13; N, 3.01. Found: C, 56.34; H, 8.01; N, 3.34. The results give a formula of $C_{45}H_{76}N_{2.3}$.

[K(crypt)][(C$_5$Me$_4$H)$_3$Gd], 2-Gd. In a procedure analogous to the preparation of **2-La**, **1-Gd** (7 mg, 0.01 mmol) and crypt (5 mg, 0.01 mmol) were dissolved in THF (2 mL) and reacted with KC_8 (3 mg, 0.02 mmol) to form a dark blue crystalline solid identified as [K(crypt)][(C$_5$Me$_4$H)$_3$Gd], **2-Gd**, (11 mg, 93%)**.** Single dark blue crystals of **2-Gd** suitable for X-ray diffraction were obtained by layer diffusion of the concentrated THF solution with Et_2O at ¬35 °C. IR (cm^{-1}): 3087w, 2961m, 2880s, 2820s, 2702w, 1477m, 1445m, 1353s, 1293m, 1258m, 1118s, 1108vs, 1100s, 952s, 933m, 833w, 750m, 734m. UV-visible (THF) λ_{max} nm (ε, M^{-1}cm^{-1}): 745 (2500). Anal. Calcd for $C_{45}H_{75}KN_2O_6Gd$: C, 57.72; H, 8.07; N, 2.99. Found: C, 56.40; H, 7.87; N, 2.92. The results give a formula of $C_{45}H_{74.8}N_2$.

[K(crypt)][(C$_5$Me$_4$H)$_3$Tb], 2-Tb. In a procedure analogous to the preparation of **2-La**, **1- Tb** (32 mg, 0.061 mmol) and crypt (28 mg, 0.08 mmol) were dissolved in THF (2 mL) and reacted with KC_8 (15 mg, 0.11 mmol) to form a dark blue crystalline solid identified as [K(crypt)][(C$_5$Me$_4$H)$_3$Tb], **2-Tb**, (47 mg, 83%)**.** Single dark blue crystals of **2-Tb** suitable for X-ray diffraction were obtained by layer diffusion of the concentrated THF solution with Et_2O at ¬35 °C. IR (cm^{-1}): 3089w, 2961sm, 2882s, 2818s, 2701m, 1478m, 1444m, 1351m, 1295m, 1257m, 1134s, 1108vs, 1080s, 1078m, 952s, 933m, 832w, 822w, 749m, 734m, 603w, 567w, 525w. UV-visible (THF) λ_{max} nm (ε, M^{-1}cm^{-1}): 784 (650). Anal. Calcd for $C_{45}H_{75}KN_2O_6Tb$: C, 57.61; H, 8.06; N, 2.99. Found: C, 51.76; H, 6.83; N, 3.01. The results give a formula of $C_{45}H_{70.8}N_{2.2}$.

[K(crypt)][(C$_5$Me$_4$H)$_3$Dy], 2-Dy. Similar to the preparation of **2-La**, **1-Dy** (25 mg, 0.05 mmol) and crypt (20 mg, 0.05 mmol) were dissolved in THF (2 mL) and reacted with KC_8 (11 mg, 0.08 mmol) to form dark brown crystalline solid identified as [K(crypt)][(C$_5$Me$_4$H)$_3$ Dy], **2-Dy**,

(32 mg, 68%)**.** Single dark brown crystals of **2-Dy** suitable for X-ray diffraction were obtained by layer diffusion of the concentrated THF solution with Et_2O at ¬35 °C. IR (cm^{-1}): 3093w, 2955m, 2882vs, 2725w, 1475m, 1442m, 1353s, 1296m, 1258m, 1173w, 1118m, 1105vs, 1078s, 951s, 930m, 828w, 752m. UV-visible (THF) λ_{max} nm (ε, $M^{-1}cm^{-1}$): 766 (200). Anal. Calcd for $C_{45}H_{75}KN_2O_6Dy$: C, 57.40; H, 8.03; N, 2.97. Found: C, 56.34; H, 7.48; N, 3.08. The results give a formula of $C_{45}H_{71.2}N_{2.1}$.

X-ray Data Collection, Structure Solution and Refinement for 1-Gd, Cp^{tet}_3Gd. An orange crystal of approximate dimensions 0.184 x 0.254 x 0.338 mm was mounted in a cryoloop and transferred to a Bruker SMART APEX II diffractometer. The APEX2[59] program package was used to determine the unit-cell parameters and for data collection (15 sec/frame scan time for a sphere of diffraction data). The raw frame data was processed using SAINT[60] and SADABS[61] to yield the reflection data file. Subsequent calculations were carried out using the SHELXTL[62] program. The systematic absences were consistent with the hexagonal space groups R3 and $R\bar{3}$. The centrosymmetric space group $R\bar{3}$ was assigned and later determined to be correct. The structure was solved using the coordinated of the dysprosium analog and refined on F^2 by full-matrix least-squares techniques. The analytical scattering factors[63] for neutral atoms were used throughout the analysis. Hydrogen atoms were located from a difference-Fourier map and refined (x,y,z and U_{iso}). The molecule was located on a three-fold rotation axis. Least-squares analysis yielded wR2 = 0.0500 and Goof = 1.145 for 138 variables refined against 1926 data (0.74 Å), R1 = 0.0183 for those 1881 data with $I > 2.0\sigma(I)$. The complex was refined as a two-component twin.

X-ray Data Collection, Structure Solution and Refinement for 1-Dy, Cp^{tet}_3Dy. A colorless crystal of approximate dimensions 0.163 x 0.188 x 0.300 mm was mounted in a cryoloop and transferred to a Bruker SMART APEX II diffractometer. The APEX2[59] program package was

used to determine the unit-cell parameters and for data collection (10 sec/frame scan time for a sphere of diffraction data). The raw frame data was processed using SAINT[60] and SADABS[61] to yield the reflection data file. Subsequent calculations were carried out using the SHELXTL[62] program. The systematic absences were consistent with the hexagonal space groups R3 and $R\bar{3}$. The centrosymmetric space group $R\bar{3}$ was assigned and later determined to be correct. The structure was solved by dual space methods and refined on F^2 by full-matrix least-squares techniques. The analytical scattering factors[63] for neutral atoms were used throughout the analysis. Hydrogen atoms were located from a difference-Fourier map and refined (x,y,z and U_{iso}). The molecule was located on a three-fold rotation axis. Least-squares analysis yielded wR2 = 0.0252 and Goof = 1.098 for 138 variables refined against 1961 data (0.73 Å), R1 = 0.0119 for those 1855 data with I > 2.0σ(I). The complex was refined as a two-component twin.

X-ray Data Collection, Structure Solution and Refinement for 2-La, [K(crypt)][Cp$^{tet}_3$La]. A black crystal of approximate dimensions 0.166 x 0.199 x 0.293 mm was mounted in a cryoloop and transferred to a Bruker SMART APEX II diffractometer. The APEX2[59] program package was used to determine the unit-cell parameters and for data collection (20 sec/frame scan time for a sphere of diffraction data). The raw frame data was processed using SAINT[60] and SADABS[61] to yield the reflection data file. Subsequent calculations were carried out using the SHELXTL[62] program. The diffraction symmetry was *mmm* and the systematic absences were consistent with the orthorhombic space group $P2_12_12_1$ that was later determined to be correct. The structure was solved by dual space methods and refined on F^2 by full-matrix least-squares techniques. The analytical scattering factors[63] for neutral atoms were used throughout the analysis. Hydrogen atoms were included using a riding model. Least squares analysis yielded wR2 = 0.0667 and Goof = 1.012 for 508 variables refined against 2062 data (0.73 Å), R1 = 0.0382 for

those 9911 data with I > 2.0σ(I). The absolute structure was assigned by refinement of the Flack parameter.[64, 65]

X-ray Data Collection, Structure Solution and Refinement for 2-Ce, [K(crypt)][Cp$^{tet}_3$Ce]. A black crystal of approximate dimensions 0.266 x 0.288 x 0.325 mm was mounted in a cryoloop and transferred to a Bruker SMART APEX II diffractometer. The APEX2[59] program package was used to determine the unit-cell parameters and for data collection (20 sec/frame scan time for a sphere of diffraction data). The raw frame data was processed using SAINT[60] and SADABS[61] to yield the reflection data file. Subsequent calculations were carried out using the SHELXTL[62] program. The diffraction symmetry was *mmm* and the systematic absences were consistent with the orthorhombic space group $P2_12_12_1$ that was later determined to be correct. The structure was solved by dual space methods and refined on F^2 by full-matrix least-squares techniques. The analytical scattering factors[63] for neutral atoms were used throughout the analysis. Hydrogen atoms were included using a riding model. Least squares analysis yielded wR2 = 0.0560 and Goof = 1.022 for 508 variables refined against 11618 data (0.74 Å), R1 = 0.0247 for those 10768 data with I > 2.0σ(I). The absolute structure was assigned by refinement of the Flack parameter. [64, 65]

X-ray Data Collection, Structure Solution and Refinement for 2-Sm, [K(crypt)][Cp$^{tet}_3$Sm]. A purple crystal of approximate dimensions 0.292 x 0.346 x 0.379 mm was mounted in a cryoloop and transferred to a Bruker SMART APEX II diffractometer. The APEX2[59] program package was used to determine the unit-cell parameters and for data collection (30 sec/frame scan time for a sphere of diffraction data). The raw frame data was processed using SAINT[60] and SADABS[61] to yield the reflection data file. Subsequent calculations were carried out using the SHELXTL[62] program. The diffraction symmetry was 2/*m,* and the systematic

absences were consistent with the monoclinic space groups *Cc*, and *C*2/*c*. It was later determined that space group *C*2/*c* was correct. The structure was solved by dual space methods and refined on F^2 by full-matrix least-squares techniques. The analytical scattering factors[63] for neutral atoms were used throughout the analysis. Hydrogen atoms were included using a riding model. Least-squares analysis yielded wR2 = 0.1301 and Goof = 1.194 for 508 variables refined against 11645 data (0.80 Å), R1 = 0.0564 for those 10067 data with $I > 2.0\sigma(I)$. There were several high residuals present in the final difference-Fourier map. It was not possible to determine the nature of the residuals although it was probable that diethyl ether and/or tetrahydrofuran solvents were present. The SQUEEZE[64] routine in the PLATON[65] program package was used to account for the electrons in the solvent accessible voids.

X-ray Data Collection, Structure Solution and Refinement for 2-Gd, [K(crypt)][Cp^{tet}_3Gd]. A black crystal of approximate dimensions 0.210 x 0.256 x 0.417 mm was mounted in a cryoloop and transferred to a Bruker SMART APEX II diffractometer. The APEX2[59] program package was used to determine the unit-cell parameters and for data collection (20 sec/frame scan time for a sphere of diffraction data). The raw frame data was processed using SAINT[60] and SADABS[61] to yield the reflection data file. Subsequent calculations were carried out using the SHELXTL[62] program. The diffraction symmetry was 2/*m,* and the systematic absences were consistent with the monoclinic space group $P2_1/c$ that was later determined to be correct. The structure was solved by dual space methods and refined on F^2 by full-matrix least-squares techniques. The analytical scattering factors[63] for neutral atoms were used throughout the analysis. Hydrogen atoms were included using a riding model. There were approximately 1.7 molecules of diethyl ether and 0.30 molecules of tetrahydrofuran solvents present. The partial mixed solvents (0.70 diethyl ether and 0.30 tetrahydrofuran) were included with partial site-

occupancy-factors and geometric constraints. All solvents were refined with equivalent anisotropic thermal parameters. Least-squares analysis yielded wR2 = 0.1301 and Goof = 1.083 for 557 variables refined against 12571 data (0.78 Å), R1 = 0.0508 for those 10459 data with I > 2.0σ(I).

X-ray Data Collection, Structure Solution and Refinement for 2-Tb, [K(crypt)][Cp$^{tet}_3$Tb]. A blue crystal of approximate dimensions 0.124 x 0.136 x 0.350 mm was mounted in a cryoloop and transferred to a Bruker SMART APEX II diffractometer. The APEX2[59] program package was used to determine the unit-cell parameters and for data collection (60 sec/frame scan time for a sphere of diffraction data). The raw frame data was processed using SAINT[60] and SADABS[61] to yield the reflection data file. Subsequent calculations were carried out using the SHELXTL[62] program. The diffraction symmetry was 2/*m,* and the systematic absences were consistent with the monoclinic space group $P2_1/c$ that was later determined to be correct. The structure was solved by dual space methods and refined on F^2 by full-matrix least-squares techniques. The analytical scattering factors[63] for neutral atoms were used throughout the analysis. Hydrogen atoms were included using a riding model. There were approximately 1.85 molecules of diethyl ether and 0.15 molecules of tetrahydrofuran solvents present. The partial mixed solvents (0.85 diethyl ether and 0.15 tetrahydrofuran) were included with partial site-occupancy-factors, geometric constraints, and equivalent anisotropic thermal parameters. Least-squares analysis yielded wR2 = 0.1065 and Goof = 1.052 for 590 variables refined against 12550 data (0.78 Å), R1 = 0.0416 for those 10435 data with I > 2.0σ(I).

X-ray Data Collection, Structure Solution and Refinement for 2-Dy, [K(crypt)][Cp$^{tet}_3$Dy]. A purple crystal of approximate dimensions 0.252 x 0.336 x 0.367 mm was mounted in a cryoloop and transferred to a Bruker SMART APEX II diffractometer. The APEX2[59]

program package was used to determine the unit-cell parameters and for data collection (30 sec/frame scan time for a sphere of diffraction data). The raw frame data was processed using SAINT[60] and SADABS[61] to yield the reflection data file. Subsequent calculations were carried out using the SHELXTL[62] program. The systematic absences were consistent with the hexagonal space groups $R3c$ and $R\bar{3}c$. The centrosymmetric space group $R\bar{3}c$ was assigned and later determined to be correct. The structure was solved by dual space methods and refined on F^2 by full-matrix least-squares techniques. The analytical scattering factors[63] for neutral atoms were used throughout the analysis. Hydrogen atoms were included using a riding model. The molecule and counter ion were located on three-fold rotation axes. The solvent molecules present (3.75 tetrahydrofuran, 0.75 diethyl ether) were disordered. One tetrahydrofuran was disordered over two positions and included using two components with partial site-occupancy-factors (50:50). A mixture of tetrahydrofuran and diethyl ether occupied a position with the composition of 0.25 each. O(3) and O(5) were located on two-fold rotation sites. The number of solvent molecules was consistent with the three-fold rotation symmetry (1.25 tetrahydrofuran x 3 = 3.75 and 0.25 diethyl ether x 3 = 0.75). Least-squares analysis yielded wR2 = 0.1336 and Goof = 1.065 for 206 variables refined against 4636 data (0.78 Å), R1 = 0.0445 for those 3422 data with $I > 2.0\sigma(I)$.

Computational Details

Density functional theory (DFT) structural optimizations of **2-Ln** and **3-Ln** (Ln= La, Ce, Pr, Nd, Sm, Gd, Tb, Dy) were performed using the hybrid meta-generalized gradient approximation (meta-GGA) functional, TPSSh.[66] DFT quadrature grids were of size 4 or larger in conjunction with tight energy convergence threshold of 10^{-8} Hartrees and one-electron density convergence threshold of 10^{-8}.[67] The geometry convergence threshold was 10^{-5} a.u. Solvent effects were included using the COSMO continuum solvent model, [68] with the following parameters to

model the THF solvent environment: dielectric constant = 7.520, refractive index = 1.405.[69] Due to the longer metal-ligand distances in the **2-Ln** complexes, it was necessary to increase the lanthanide metal atom radii used to construct the cavity to 2.584 Å (from the default 2.223 Å for all lanthanides), to obtain a continuous cavity. The default solvent radius (1.30 Å) was used. C_1 molecular symmetry was used for all calculations. For atoms on the ligands, double-ζ quality split valence basis sets with polarization functions on non-hydrogen atoms [def2-SV(P)] were used.[70] For the lanthanide atoms, large f-in-core quasi-relativistic Stuttgart-Cologne effective core potentials (ECPs) with corresponding triple-ζ quality basis sets [SCecp-mwb] were used.[71-73] For the time dependent density functional theory (TDDFT) calculations on **2-Ln** and **3-Ln** (Ln= La, Ce, Pr, Nd, Gd, Tb), the lanthanide basis sets were augmented with an additional diffuse p-function by downward extrapolation [SCecp-mwb-d].[74, 75] A gauge invariant implementation of the TPSSh functional was used.[76] For the ligand atoms, augmented polarized split valence basis (def2-SVPD) were employed.[77] All calculations were performed with the TURBOMOLE 7.2 package.[78, 79] Analysis was aided by VMD[80, 81] and Avogadro[82, 83] visualization tools.

References

(1) Evans, W. J. *Organometallics* **2016,** *35*, 3088-3100.

(2) Woen, D. H.; Evans, W. J., *Handbook on the Physics and Chemistry of Rare Earths*; Bünzli, J.-C. G.; Pecharsky, V. K., Eds.; Elsevier: Amsterdam, 2016; p 337-394.

(3) Meyer, G. *Chem. Rev.* **1988,** *88*, 93-107.

(4) Meyer, G., *The Rare Earth Elements: Fundamentals and Applications*; Atwood, D., Ed. John Wiley & Sons: Chichester, UK, 2012; p 161-173.

(5) Bochkarev, M. N. *Coord. Chem. Rev.* **2004,** *248*, 835-851.

(6) Nief, F., *Handbook on the Physics and Chemistry of Rare Earths*; Jr., K. A. G.; Bünzli, J.-C. G.; Pecharsky, V. K., Eds.; Elsevier: Amsterdam, 2010; p 241-300.

(7) Hitchcock, P. B.; Lappert, M. F.; Maron, L.; Protchenko, A. V. *Angew. Chem. Int. Ed.* **2008,** *47*, 1488-1491.

(8) Palumbo, C. T.; Darago, L. E.; Windorff, C. J.; Ziller, J. W.; Evans, W. J. *Organometallics* **2018,** *37*, 900-905.

(9) MacDonald, M. R.; Bates, J. E.; Ziller, J. W.; Furche, F.; Evans, W. J. *J. Am. Chem. Soc.* **2013,** *135*, 9857-9868.

(10) Fieser, M. E.; MacDonald, M. R.; Krull, B. T.; Bates, J. E.; Ziller, J. W.; Furche, F.; Evans, W. J. *J. Am. Chem. Soc.* **2015,** *137*, 369-382.

(11) MacDonald, M. R.; Ziller, J. W.; Evans, W. J. *J. Am. Chem. Soc.* **2011,** *133*, 15914-15917.

(12) MacDonald, M. R.; Bates, J. E.; Fieser, M. E.; Ziller, J. W.; Furche, F.; Evans, W. J. *J. Am. Chem. Soc.* **2012,** *134*, 8420-8423.

(13) Langeslay, R. R.; Fieser, M. E.; Ziller, J. W.; Furche, F.; Evans, W. J. *Chem. Sci.* **2015,** *6*, 517-521.

(14) MacDonald, M. R.; Fieser, M. E.; Bates, J. E.; Ziller, J. W.; Furche, F.; Evans, W. J. *J. Am. Chem. Soc.* **2013,** *135*, 13310-13313.

(15) Windorff, C. J.; MacDonald, M. R.; Meihaus, K. R.; Ziller, J. W.; Long, J. R.; Evans, W. J. *Chem. Eur. J.* **2016,** *22*, 772-782.

(16) Windorff, C. J.; Chen, G. P.; Cross, J. N.; Evans, W. J.; Furche, F.; Gaunt, A. J.; Janicke, M. T.; Kozimor, S. A.; Scott, B. L. *J. Am. Chem. Soc.* **2017,** *139*, 3970-3973.

(17) Su, J.; Windorff, C. J.; Batista, E. R.; Evans, W. J.; Gaunt, A. J.; Janicke, M. T.; Kozimor, S. A.; Scott, B. L.; Woen, D. H.; Yang, P. *J. Am. Chem. Soc.* **2018,** *140*, 7425-7428.

(18) Gun'ko, Y. K.; Hitchcock, P. B.; Lappert, M. F. *J. Organomet. Chem.* **1995,** *499*, 213-219.

(19) Cassani, M. C.; Duncalf, D. J.; Lappert, M. F. *J. Am. Chem. Soc.* **1998,** *120*, 12958-12959.

(20) Jaroschik, F.; Nief, F.; Le Goff, X. F.; Ricard, L. *Organometallics* **2007,** *26*, 1123-1125.

(21) Jaroschik, F.; Momin, A.; Nief, F.; Le Goff, X.-F.; Deacon, G. B.; Junk, P. C. *Angew. Chem. Int. Ed.* **2009,** *121*, 1137-1141.

(22) La Pierre, H. S.; Scheurer, A.; Heinemann, F. W.; Hieringer, W.; Meyer, K. *Angew. Chem. Int. Ed.* **2014,** *53*, 7158-7162.

(23) Fieser, M. E.; Ferrier, M. G.; Su, J.; Batista, E.; Cary, S. K.; Engle, J. W.; Evans, W. J.; Lezama Pacheco, J. S.; Kozimor, S. A.; Olson, A. C.; Ryan, A. J.; Stein, B. W.; Wagner, G. L.; Woen, D. H.; Vitova, T.; Yang, P. *Chem. Sci.* **2017,** *8*, 6076-6091.

(24) Meihaus, K. R.; Fieser, M. E.; Corbey, J. F.; Evans, W. J.; Long, J. R. *J. Am. Chem. Soc.* **2015,** *137*, 9855-9860.

(25) Corbey, J. F.; Woen, D. H.; Palumbo, C. T.; Fieser, M. E.; Ziller, J. W.; Furche, F.; Evans, W. J. *Organometallics* **2015,** *34*, 3909-3921.

(26) Huh, D. N.; Kotyk, C. M.; Gembicky, M.; Rheingold, A. L.; Ziller, J. W.; Evans, W. J. *Chem. Commun.* **2017,** *53*, 8664-8666.

(27) Lauher, J. W.; Hoffmann, R. *J. Am. Chem. Soc.* **1976,** *98*, 1729-1742.

(28) Bursten, B. E.; Rhodes, L. F.; Strittmatter, R. J. *J. Am. Chem. Soc.* **1989,** *111*, 2756-2758.

(29) Bursten, B. E.; Rhodes, L. F.; Strittmatter, R. J. *J. Am. Chem. Soc.* **1989,** *111*, 2758-2766.

(30) Strittmatter, R. J.; Bursten, B. E. *J. Am. Chem. Soc.* **1991,** *113*, 552-559.

(31) Lukens, W. W.; Andersen, R. A. *Organometallics* **1995,** *14*, 3435-3439.

(32) Denning, R. G.; Harmer, J.; Green, J. C.; Irwin, M. *J. Am. Chem. Soc.* **2011,** *133*, 20644-20660.

(33) Fang, M.; Lee, D. S.; Ziller, J. W.; Doedens, R. J.; Bates, J. E.; Furche, F.; Evans, W. J. *J. Am. Chem. Soc.* **2011,** *133*, 3784-3787.

(34) Coles, M. P.; Hitchcock, P. B.; Lappert, M. F.; Protchenko, A. V. *Organometallics* **2012,** *31*, 2682-2690.

(35) Peterson, J. K.; MacDonald, M. R.; Ziller, J. W.; Evans, W. J. *Organometallics* **2013,** *32*, 2625-2631.

(36) Zachmanoglou, C. E.; Docrat, A.; Bridgewater, B. M.; Parkin, G.; Brandow, C. G.; Bercaw, J. E.; Jardine, C. N.; Lyall, M.; Green, J. C.; Keister, J. B. *J. Am. Chem. Soc.* **2002,** *124*, 9525-9546.

(37) Woen, D. H.; Chen, G. P.; Ziller, J. W.; Boyle, T. J.; Furche, F.; Evans, W. J. *Angew. Chem. Int. Ed.* **2017,** *56*, 2050-2053.

(38) Ryan, A. J.; Darago, L. E.; Balasubramani, S. G.; Chen, G. P.; Ziller, J. W.; Furche, F.; Long, J. R.; Evans, W. J. *Chem. Eur. J.* **2018,** *24*, 7702-7709.

(39) Ryan, A. J.; Ziller, J. W.; Evans, W. J. *Chem. Sci.* **2020,** *11*, 2006-2014.

(40) Woen, D. H.; Huh, D. N.; Ziller, J. W.; Evans, W. J. *Organometallics* **2018,** *37*, 3055-3063.

(41) Lappert, M. F.; Singh, A.; Atwood, J. L.; Hunter, W. E. *Chem. Commun.* **1981**, 1190-1191.

(42) Schumann, H.; Glanz, M.; Hemling, H.; Ekkehard Hahn, F. *Z. Anorg. Allg. Chem.* **1995,** *621*, 341-345.

(43) Xie, Z.; Chui, K.; Liu, Z.; Xue, F.; Zhang, Z.; Mak, T. C. W.; Sun, J. *J. Organomet. Chem.* **1997,** *549*, 239-244.

(44) Evans, W. J.; Rego, D. B.; Ziller, J. W. *Inorg. Chem.* **2006,** *45*, 10790-10798.

(45) Stults, S. D.; Andersen, R. A.; Zalkin, A. *Organometallics* **1990,** *9*, 115-122.

(46) Minasian, S. G.; Krinsky, J. L.; Rinehart, J. D.; Copping, R.; Tyliszczak, T.; Janousch, M.; Shuh, D. K.; Arnold, J. *J. Am. Chem. Soc.* **2009,** *131*, 13767-13783.

(47) Windorff, C. J.; Dumas, M. T.; Ziller, J. W.; Gaunt, A. J.; Kozimor, S. A.; Evans, W. J. *Inorg. Chem.* **2017,** *56*, 11981-11989.

(48) Evans, D. F. *J. Chem. Soc.* **1959**, 2003-2005.

(49) Becconsall, J. K. *Mol. Phys.* **1968,** *15*, 129-139.

(50) Schubert, E. M. *J. Chem. Educ.* **1992,** *69*, 62.

(51) Dorenbos, P. *J. Phys.: Condens. Matter* **2003,** *15*, 575-594.

(52) Bergbreiter, D. E.; Killough, J. M. *J. Am. Chem. Soc.* **1978,** *100*, 2126-2134.

(53) Soller, B. S.; Sun, Q.; Salzinger, S.; Jandl, C.; Pöthig, A.; Rieger, B. *Macromolecules* **2016,** *49*, 1582-1589.

(54) Shestakov, B. G.; Mahrova, T. V.; Larionova, J.; Long, J.; Cherkasov, A. V.; Fukin, G. K.; Lyssenko, K. A.; Scherer, W.; Hauf, C.; Magdesieva, T. V.; Levitskiy, O. A.; Trifonov, A. A. *Organometallics* **2015,** *34*, 1177-1185.

(55) Evans, W. J.; Lee, D. S.; Johnston, M. A.; Ziller, J. W. *Organometallics* **2005,** *24*, 6393-6397.

(56) Goodwin, C. A. P.; Joslin, K. C.; Lockyer, S. J.; Formanuik, A.; Morris, G. A.; Ortu, F.; Vitorica-Yrezabal, I. J.; Mills, D. P. *Organometallics* **2015,** *34*, 2314-2325.

(57) Chilton, N. F.; Goodwin, C. A.; Mills, D. P.; Winpenny, R. E. *Chem. Commun.* **2015,** *51*, 101-103.

(58) Goodwin, C. A.; Chilton, N. F.; Vettese, G. F.; Moreno Pineda, E.; Crowe, I. F.; Ziller, J. W.; Winpenny, R. E.; Evans, W. J.; Mills, D. P. *Inorg. Chem.* **2016,** *55*, 10057-10067.

(59) *Apex2 Version 2014.11-0*, Bruker AXS: Madison, WI, 2014.

(60) *SAINT Version 8.36a*, Bruker AXS, Inc.: Madison, WI, 2013.

(61) Sheldrick, G. M. *SADABS, Version 2014/5*, Bruker AXS, Inc.: Madison, WI 2014.

(62) Sheldrick, G. M. *SHELXTL, Version 2014/7*, Bruker AXS, Inc.: Madison, WI, 2014.

(63) *International Tables for Crystallography*; Dordrecht: Kluwer Academic Publishers 1992; Vol. C.

(64) Spek, A. *Acta Crystallogr. D:* **2009,** *65*, 148-155.

(65) Spek, A. *Acta Crystallogr. C:* **2015,** *71*, 9-18.

(66) Staroverov, V. N.; Scuseria, G. E.; Tao, J. M.; Perdew, J. P. *J. Chem. Phys.* **2003,** *119*, 12129-12137.

(67) Eichkorn, K.; Treutler, O.; Öhm, H.; Häser, M.; Ahlrichs, R. *Chem. Phys. Lett.* **1995,** *240*, 283-290.

(68) Klamt, A.; Schuurmann, G. *Perkin Trans. 2* **1993**, 799-805.

(69) *CRC Handbook of Chemistry and Physics*; 81 ed.; CRC Press: Boca Raton, FL, 2008; p 136.

(70) Weigend, F.; Ahlrichs, R. *Phys. Chem. Chem. Phys.* **2005,** *7*, 3297-3305.

(71) Hülsen, M.; Weigand, A.; Dolg, M. *Theor. Chem. Acc.* **2009,** *122*, 23-29.

(72) Dolg, M.; Stoll, H.; Preuss, H. *Theor. Chem. Acc.* **1993,** *85*, 441-450.

(73) Dolg, M.; Stoll, H.; Savin, A.; Preuss, H. *Theor. Chem. Acc.* **1989,** *75*, 173-194.

(74) Bauernschmitt, R.; Ahlrichs, R. *Chem. Phys. Lett.* **1996,** *256*, 454-464.

(75) Brown, A.; Kemp, C. M.; Mason, S. F. *J. Chem. Soc.* **1971**, 751.

(76) Bates, J. E.; Furche, F. *J. Chem. Phys.* **2012,** *137*, 164105.

(77) Weigend, F. *Phys. Chem. Chem. Phys.* **2006,** *8*, 1057-1065.

(78) *TURBOMOLE* 7.2; a development of University of Karlsruhe and Forschungszentrum Karlsruhe GmbH, 1989-2007, TURBOMOLE GmbH, since 2007: available from http://www.turbomole.com, 2017.

(79) Acevedo, O.; Jorgensen, W. L. *WIREs Comput. Mol. Sci.* **2014,** *4*, 422-435.

(80) *VMD* 1.9: available from http://www.ks.uiuc.edu/Research/vmd/.

(81) Humphrey, W.; Dalke, A.; Schulten, K. *J. Mol. Graphics Modell.* **1996,** *14*, 33-38.

(82) *Avogadro: An Open-Source Molecular Builder and Visualization Tool*, 1.1.0.

(83) Hanwell, M. D.; Curtis, D. E.; Lonie, D. C.; Vandermeersch, T.; Zurek, E.; Hutchison, G. R. *J. Cheminform.* **2012,** *4*, 17.

CHAPTER 3

Synthesis of Heteroleptic Bis(cyclopentadienyl) Amide Yttrium(II) Complexes, [K(2.2.2-cryptand)][$Cp^X_2Y(NR_2)$], and Their C–H Bond Activated Y(III) Derivatives ($Cp^X = C_5Me_5, C_5Me_4H$)[a]

Introduction

As described in the Introduction, the first examples of crystallographically-characterizable molecular complexes of the +2 oxidation state for the rare-earth ions beyond Eu, Yb, Sm, Tm, Dy, and Nd, were initially accomplished via reduction of the homoleptic tris(cyclopentadienyl) complexes Cp''_3Ln^{III} and Cp'_3Ln^{III} ($Cp'' = C_5H_3(SiMe_3)_2$; $Cp' = C_5H_4SiMe_3$), which formed (Cp''_3Ln^{II}) and (Cp'_3Ln^{II}), respectively, eq. 3.1.[1-5]

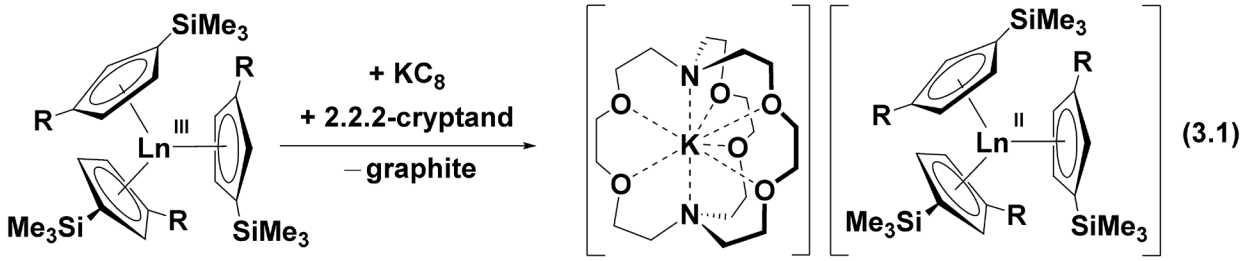

(3.1)

R = H; Ln = Y, La, Ce, Pr, Nd, Sm, Gd, Tb, Dy, Ho, Er, Tm, Lu
R = $SiMe_3$; Ln = La, Ce, Pr, Nd

Homoleptic complexes of the general formula $(LnA_3)^{1-}$ (A = anion) for the rare earth metals beyond Eu Yb, Sm, Tm, Dy, and Nd have subsequently been characterized by X-ray crystallography for A = Cp′, Cp″, C_5Me_4H (Cp^{tet}), C_5H_4Me (Cp^{Me}), $C_5H_4CMe_3$ (Cp^t), NR_2 (R = $SiMe_3$), and 2,6-Ad_2-4-*t*-Bu-C_6H_2O ($OAr^{Ad,Ad,t\text{-}Bu}$).[1-11] One notable exception to the ligand list above is A = C_5Me_5 because the homoleptic $(C_5Me_5)_3Ln$ complexes are highly reactive, sterically

[a]Portions of this chapter have been submitted for publication: Jenkins, T.F.; Bekoe, S.; Ziller, J.W.; Furche, F.; Evans, W.J. *Organometallics.*

crowded species that react with THF which is the common solvent used in LnA_3 reductions.[12, 13] This is unfortunate since C_5Me_5 is an excellent ligand for the isolation, stabilization, and generation of crystalline rare-earth metal complexes.[14] This study was initiated to see if an Y(II) complex containing C_5Me_5 could be isolated from a heteroleptic precursor, namely $(C_5Me_5)_2Y(NR_2)$.

Complexes of the new Ln(II) ions with formulas other than the initially discovered homoleptic complexes, $(LnA_3)^{1-}$, have subsequently been crystallographically characterized, but few contain Y(II).[15-21] Although many Y(II) complexes have been identified by EPR spectroscopy using coupling to the 100% abundant ^{89}Y ($I = ½$) nucleus as a diagnostic tool, isolation has been much more challenging compared to their lanthanide analogs.[7, 9, 10, 22, 23] While the first example of the Y(II) ion was in the anionic complex $(Cp'_3Y^{II})^{1-}$,[2] the only other crystallographically-characterizable Y(II) species are $[K(crypt)][Y(OAr^{Ad,Ad,t-Bu})_3]$,[10] $[K(18\text{-crown-6})_2][Y(NR_2)_3]$,[11] and the mixed ligand complex $[K(crypt)][Cp''_2YCp]$[23] (crypt = 2.2.2-cryptand; Cp = C_5H_5). Reductions of Cp_3Y,[23] Cp''_3Y,[23] Cp^{tet}_3Y,[7] Cp^{t}_3Y,[9] Cp^{Me}_3Y,[23] $Y(NR_2)_3$,[22] and $Y(OAr^{t-Bu,t-Bu,Me})_3$[10] as well as the 3:1 Cp''_2YCp^{Me}:$Cp''YCp^{Me}_2$ mixture[23] gave EPR signals characteristic of Y(II), but none of these reduction reactions provided structural data.

Reported here is the synthesis and X-ray crystal structure of the first Y(II) complex containing C_5Me_5 as a ligand along with a C–H bond activated derivative. C–H bond activation has been observed in several Ln(II) systems including (a) the $[((^{Ad,Me}ArO)_3mes)Ln^{II}]^{1-}$ complexes which form $[((^{Ad,Me}ArO)_3mes)Ln^{III}H]^{1-}$ compounds, which co-crystallize with the Ln(II) compounds,[18, 19] (b) $[(C_5H_2{}^tBu_3)_2Nd^{II}(\mu\text{-I})K(18\text{-crown-6})]$, which forms $[(C_5H_2{}^tBu_3)(\eta^5\text{-}C_3H_2{}^tBu_2CMe_2CH_2\text{-}\kappa C)Nd^{III}(\mu\text{-I})K(18\text{-crown-6})]$,[15] (c) attempts to isolate indenyl Ln(II) complexes, which resulted in the metalated $[K(crypt)][(C_9H_7)_2Dy(\mu\text{-}\eta^5\text{:}\eta^1\text{-}C_9H_6)]_2$ complex,[23] and (d) the isolation of $(Cp''_2YH)_2$ from the reduction of Cp''_3Y.[24] C–H bond activation has also been

observed in uranium chemistry in reduction of U(III) species to U(II) products.[25-30] Specifically, C–H activation was observed with the $[(^{Ad,Me}ArO)_3mes]^{3-}$ ligand system described above,[31] as well as the U analog of the complexes examined in this study.[32]

The generality of the $(C_5Me_5)_2Y(NR_2)$ reduction reaction was also investigated with the tetramethylcyclopentadienyl analog, $(C_5Me_4H)_2Y(NR_2)$.[33] Both types of ligand in this precursor are known to form homoleptic Ln(II) complexes: crystallographically-characterizable $[(C_5Me_4H)_3Ln]^{1-}$ complexes are known for Ln = La, Ce, Pr, Nd, Sm, Gd, Tb, and Dy and $[Ln(NR_2)_3]^{1-}$ complexes for Ln = Nd, Gd, Tb, Dy, Ho, Er, and Y. Given the utility of C_5Me_4H and NR_2 ligands for making homoleptic Ln(II) complexes, it was of interest to determine if heteroleptic Ln(II) complexes could be synthesized and crystallographically-characterized.

Results

Reduction of $(C_5Me_5)_2Y(NR_2)$ and $(C_5Me_4H)_2Y(NR_2)$ (R = $SiMe_3$). Treatment of colorless $(C_5Me_5)_2Y(NR_2)$, **1**, in THF in the presence of 2.2.2-cryptand (crypt) with KC_8 generated a dark blue/purple solution, **2**, which had EPR and UV-visible spectra consistent with Y(II). Similarly, a solution of $(C_5Me_4H)_2Y(NR_2)$, **3**, in THF in the presence of crypt reacted with KC_8 and generated a dark blue/purple solution, **4**, with EPR and UV-visible spectra similar to the spectra reported for **2**. The 298 K EPR spectra of **2** and **4** in Figures 3.1 and 3.2 both contain isotropic signals with two-line hyperfine patterns as expected for ^{89}Y ($I = ½$). Simulations of the data gave $g_{iso} = 1.975$ for both complexes with hyperfine constants of $A_{iso} = 74.5$ G for **2** and 71.2 G for **4**. These data can be compared with EPR parameters of other Y(II) species in Table 3.1. The UV-visible spectra of **2** and **4** are discussed below.

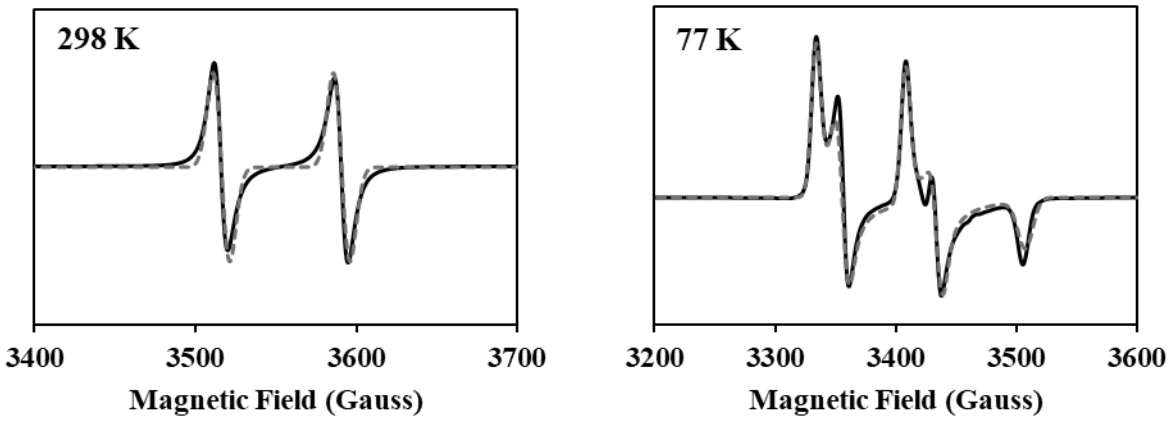

Figure 3.1. X-band EPR experimental (solid line) and simulated (dotted line) spectra of **2** obtained by reduction of $(C_5Me_5)_2Y(NR_2)$ collected at 298 K (left; mode: perpendicular; g_{iso} = 1.975; A_{iso} = 74.5 G; ν = 9.824 GHz; *P* = 0.2152 mW; modulation amplitude = 4.0 G) and 77K (right; mode: perpendicular; g_x = 1.999, g_y = 1.985, g_z = 1.942; A_x = 74.3 G, A_y = 78.2 G, A_z = 77.2 G; ν = 9.431 GHz; *P* = 0.006812 mW; modulation amplitude = 4.0 G).

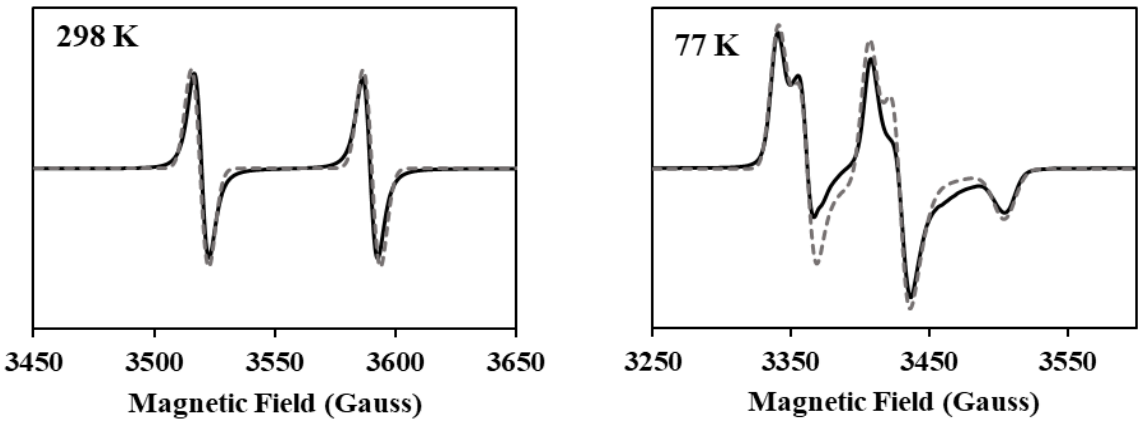

Figure 3.2. X-band EPR experimental (solid line) and simulated (dotted line) spectra of **4** obtained by reduction of $(C_5Me_4H)_2Y(NR_2)$ collected at 298 K (left; mode: perpendicular; g_{iso} = 1.975; A_{iso} = 71.2 G; ν = 9.827 GHz; *P* = 0.2154 mW; modulation amplitude = 4.0 G) and 77 K (right; mode:

perpendicular; $g_x = 1.998$, $g_y = 1.985$, $g_z = 1.941$; $A_x = 66.0$ G, $A_y = 66.9$ G, $A_z = 65.4$ G; $\nu = 9.436$ GHz; $P = 0.2155$ mW; modulation amplitude = 4.0 G).

Table 3.1. Comparison of EPR Parameters of reduction products of YA_3 complexes (A = anionic ligand), 298 K.

Compound Reduced	g_{iso}	A_{iso} **(G)**	A_{iso} **(MHz)**
$[C_5H_3(SiMe_3)_2]_2Y(C_5H_5)$ [23]	1.990	34.6	96.4
$[C_5H_3(SiMe_3)_2]_3Y$ [23]	1.991	36.1	100.6
$(C_5H_4SiMe_3)_3Y$ [2]	1.991	36.6	102.0
$(C_5H_5)_3Y(THF)$ [23]	1.991	42.8	119.3
$(C_5H_4Me)_3Y(THF)$ [23]	1.990	46.9	130.6
$(C_5Me_4H)_3Y$ [7]	1.986	64.8	180.1
3, $(C_5Me_4H)_2Y[N(SiMe_3)_2]$	1.975	71.2	196.8
1, $(C_5Me_5)_2Y[N(SiMe_3)_2]$	1.975	74.5	206.0
$Y[N(SiMe_3)_2]_3$ [22]	1.976	110	304.2
$Y(OAr^{Ad,Ad,t\text{-}Bu})_3$ [10]	1.980	153.3	424.8

At 77 K, the spectrum of **2**, Fig 3.1, features a rhombic signal that was best simulated with $g_x = 1.999$, $g_y = 1.985$, and $g_z = 1.942$ and hyperfine coupling constants $A_x = 74.3$ G, $A_y = 78.2$ G, and $A_z = 77.2$ G. Similarly, the 77 K spectrum of **4**, Fig 3.2, was best simulated with $g_x = 1.998$,

g_y = 1.985, and g_z = 1.941 and hyperfine coupling constants of A_x = 66.0 G, A_y = 66.9 G, and A_z = 65.4 G. The anisotropy in the 77 K EPR spectra of **2** and **4** is consistent with a change in symmetry between homoleptic complexes, which have axial spectra, and these heteroleptic complexes of Y(II). Upon brief thawing of the dark colored solutions to room temperature and re-cooling, the EPR spectra of the solutions did not change noticeably.

UV-Visible Spectroscopy. The UV-visible spectra of the dark solutions of **2** and **4** are shown in Figure 3.3 in comparison to the spectra of the crystallographically-characterized homoleptic complexes, $[K(crypt)][(C_5H_4SiMe_3)_3Y]$, and $[K(18\text{-crown-6})_2][Y(NR_2)_3]$.[2, 11] Extinction coefficients were estimated based on the concentration of the Y(III) precursors **1** and **3** assuming complete reduction. Hence, the absorptivity values are underestimates if complete reduction does not occur. The spectra of both **2** and **4** have the large extinction coefficients characteristic of Y(II).

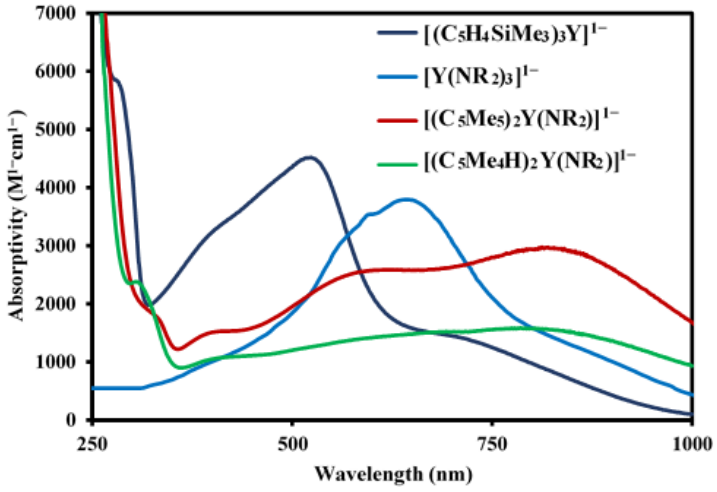

Figure 3.3. UV-vis spectra of **2** and **4** plotted for comparison with the spectra of crystallographically-characterized $[(C_5H_4SiMe_3)_3Y]^{1-}$ and $[Y(NR_2)_3]^{1-}$.

Thermal Stability. Unfortunately, the solutions of **2** and **4** are not stable at room temperature and decompose to colorless products within a few hours. Freshly reduced solutions of $(C_5Me_5)_2Y(NR_2)$ and $(C_5Me_4H)_2Y(NR_2)$ were evaluated following protocols similar to those used for [K(crypt)][Cp′$_3$Ln] and [K(crypt)][Cp″$_3$Ln].[4, 5] The absorption spectra for **2** and **4** as a function of time are shown in Figure 3.4. The observation of isosbestic points in both spectra indicates that decomposition proceeds cleanly for **2** and **4**. The concentrations of Y(II) in **2** and **4** were tracked at λ_{max} = 515 nm for each solution. The decompositions were best modeled with first-order kinetics as shown in the plots of $\log_e$[Y(II)] versus time in Figure 3.5. Although $[(C_5H_4SiMe_3)_3Ln]^{1-}$ and $[(C_5H_3(SiMe_3)_2)_3Ln]^{1-}$ were found to decompose through second-order kinetics,[5] [K(crypt)][$(C_5H_4SiMe_3)_3$Lu], the most reactive $(Cp'_3Ln)^{1-}$ complex, proceeded through a first-order pathway, with a decomposition rate of $5.99(7)\times10^{-4}$ s^{1-} for comparison.[4] The solution of **2** was determined to have a decomposition rate of $2.92(1)\times10^{-5}$ s^{1-} compared to $2.09(3)\times10^{-4}$ s^{1-} for **4.** These rates result in calculated $t_{1/2}$ values of 1.16×10^3 s for [K(crypt)][$(C_5H_4SiMe_3)_3$Lu], 2.38×10^4 s for [K(crypt)][$(C_5Me_5)_2Y(NR_2)$], and 3.32×10^3 s for [K(crypt)][$(C_5Me_4H)_2Y(NR_2)$]. This contrasts with $[Y(NR_2)_3]^{1-}$ which decomposes within 10 seconds and was not measurable at room temperature.[11]

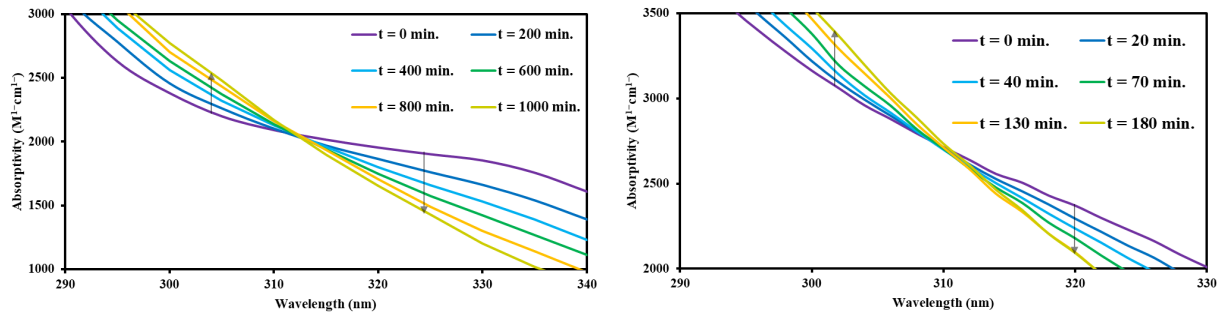

Figure 3.4. (left) Overlay of UV-visible spectra of **2** during decomposition. The absorbance remains constant at λ = 315 nm. (right) Overlay of UV-visible spectra of **4** during decomposition. The absorbance remains constant at λ = 310 nm.

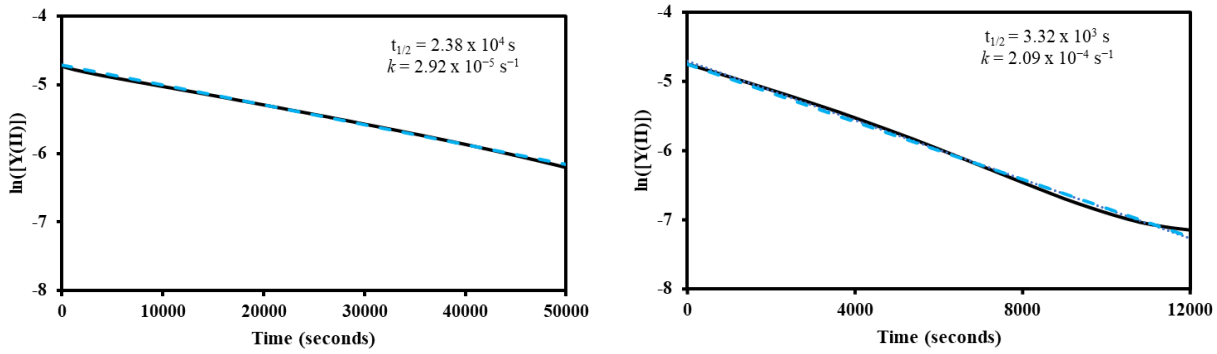

Figure 3.5. (left) Absorption of **2** collected at 9.0 mM concentration in THF at room temperature. Absorptions were measured at λ_{max} = 515 nm every 15 min. (right) Absorption of **4** collected at 9.0 mM concentration in THF at room temperature. Absorptions were measured at λ_{max} = 515 nm every 15 min.

Structural Analysis: The $(C_5Me_5)_2Y(NR_2)$ Reduction Product. Pentane diffusion into the blue THF solution of **2** at −35 °C produced single crystals that were identified by X-ray crystallography to be a mixture of an Y(II) complex, [K(crypt)][$(C_5Me_5)_2Y(NR_2)$], **5** and an Y(III) derivative, [K(crypt)][$(C_5Me_5)_2Y\{N(SiMe_3)(SiMe_2CH_2)$-$\kappa C,\kappa N\}$], **6**, formally derived from C–H bond activation of one of the methyl groups of the trimethylsilyl substituents on the amide ligand in **5**.

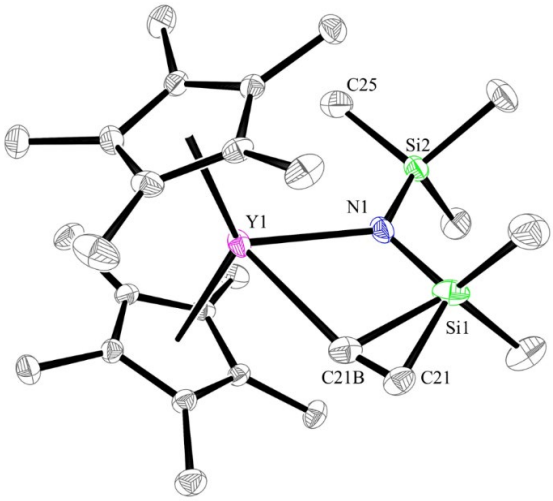

Figure 3.6. Displacement ellipsoid plot of 75:25 disordered structure of [K(crypt)][$(C_5Me_5)_2YN(SiMe_3)_2$], **5**, and [K(crypt)][$(C_5Me_5)_2Y\{N(SiMe_3)(SiMe_2CH_2)$-$\kappa$C,$\kappa$N$\}$], **6**, respectively, with ellipsoids drawn at the 50% probability level. Hydrogen atoms and the $[K(crypt)]^{1+}$ counter-cation were omitted for clarity.

Two different batches of single crystals containing this Y(II)/Y(III) mixture of **5** and **6** were isolated. Structural data for each single crystal were modelled differently. In one crystal, the data were modeled with a 75:25 mixture of complexes **5:6**,while a 70:30 model best fit the data for the other crystal. Both mixtures crystallized in the triclinic $P\bar{1}$ space group, with disordering of one Me group from an $SiMe_3$ unit on the $N(SiMe_3)_2$ ligand. As shown in Figure 3.6, the structures are similar except for C21 and C21B. The 3.523(2) Å Y…C21 distance is associated with the Y(II) complex, **5,** while the 2.638(7) Å Y–C21B distance is associated with the Y(III) complex, **6**. For comparison, the Y^{III}–C bond distance in the previously reported heteroleptic complex, $(C_5Me_5)_2Y[CH(SiMe_3)_2]$, is 2.468(7) Å and the closest Y…C($SiMe_3$) distances are 2.878(7) and 4.446(7) Å.[34] Also consistent with these assignments are the N1–Si1–C21 and N1–Si1–C21B angles of 115.51(8)° and 88.7(2)°, respectively, which are in the range observed in normal Ln–

NR_2 bonds and the range of cyclometalated complexes derived from NR_2 ligands.[35-39] The Y–(C_5Me_5 ring centroid) and Y–N distances are the same for **5** and **6**. Structural data on **5** and **6** from the crystal with a 75:25 ratio ~~is~~ are compared to $(C_5Me_5)_2Y(NR_2)$ and $(C_5Me_5)_2Y[CH(SiMe_3)_2]$ in Table 3.2.

Table 3.2. Selected bond lengths and angles of a 75:25 mixture of [K(crypt)][$(C_5Me_5)_2Y\{N(SiMe_3)_2\}$], **5**, and [K(crypt)][$(C_5Me_5)_2Y\{N(SiMe_3)(SiMe_2CH_2)$-$\kappa C,\kappa N\}$], **6**, and structurally related $(C_5Me_5)_2Y[N(SiMe_3)_2]$ and, $(C_5Me_5)_2Y[CH(SiMe_3)_2]$.[34]

	Y–(C_5Me_5 ring centroid) Distances (Å)	Y–N, Y–C Distances (Å)	Y–C($SiMe_3$) Distances (Å)	Y–N–Si, Y–C–Si angles (°)
$[(C_5Me_5)_2Y\{N(SiMe_3)_2\}]^{1-}$, 5	2.441	2.336 (1)	3.523(2)	114.31(7), 124.05(8)
$[(C_5Me_5)_2Y\{N(SiMe_3)(SiMe_2CH_2)$-$\kappa C,\kappa N\}]^{1-}$, 6	2.441	2.336 (1)	2.638(7), 3.762(2)	114.31(7), 124.05(8)
$(C_5Me_5)_2Y[N(SiMe_3)_2]$[a], [34]	2.378, 2.404	2.253(5)	3.181(8), 3.421(8)	114.0(3), 120.2(3)
	2.391, 2.400	2.274(5)	2.970(6), 3.800(7)	107.1(3), 129.7(3)
$(C_5Me_5)_2Y[CH(SiMe_3)_2]$ [34]	2.381, 2.382	2.468(7)	2.878(7), 4.446(7)	97.1(3), 138.6(4)

[a] This complex crystallized with two asymmetric molecules in the unit cell.

Comparison of bond distances is one of the commonly used analyses to compare rare earth Ln(II) and Ln(III) complexes.[40] Structural analyses on [K(crypt)][$(C_5Me_5)_2Y(NR_2)$], **5**, with the Y(III) precursor, $(C_5Me_5)_2Y(NR_2)$, is complicated by the fact that the latter complex has two molecules in the unit cell with somewhat different features.[34] Both molecules have similar Y–N distances of 2.253(5) and 2.274(5) Å, and a narrow range of Y–(C_5Me_5 ring centroid) distances of 2.378-2.404 Å. However, one molecule has a Y….C(Me) distance of 2.970(6) Å and a Y–Si–C angle of 107.1(3)° which is associated with an agostic interaction of a methyl group with the metal center, while the other molecule has less acute angles and Y…C(Me) distances that are >0.200 Å longer. Upon reduction of **1** to **5**, the Y–N distance increases by 0.072 Å and the average Y–(C_5Me_5 ring centroid) distance increases by 0.048 Å. This is consistent with reduction of the metal center, but the distances are on the long end of the range of bond distance changes previously found for $4d^0$ Y(III) to $4d^1$ Y(II) complexes, 0.020-0.032 Å.[40, 41] The Y–N–Si angles in **5** are similar to those in the molecule of **1** which does not have an agostic interaction. The 3.523(2) Å Y^{II}…C21(Me) distance in **5** is long for an agostic interaction. This is consistent with the expectation that an Y(II) ion would be less likely to participate in an agostic interaction than an Y(III) ion.

Structural Analysis: The $(C_5Me_4H)_2Y(NR_2)$ Reduction Product. Attempts to crystallize the dark solution of **4** obtained by reduction of $(C_5Me_4H)_2Y(NR_2)$ through both layering and vapor diffusion methods only yielded crystals containing ~10% of the Y(II) product, [K(crypt)][$(C_5Me_4H)_2Y(NR_2)$], **7**, and ~90% of the Y(III) cyclometalated product, [K(crypt)][$(C_5Me_4H)_2Y\{N(SiMe_3)(SiMe_2CH_2)$-$\kappa C,\kappa N\}$], **8**, which co-crystallized with

[K(crypt)][C_5Me_4H], Figure 3.7. Unfortunately, the data on this structure were not of sufficient quality to discuss bond lengths.

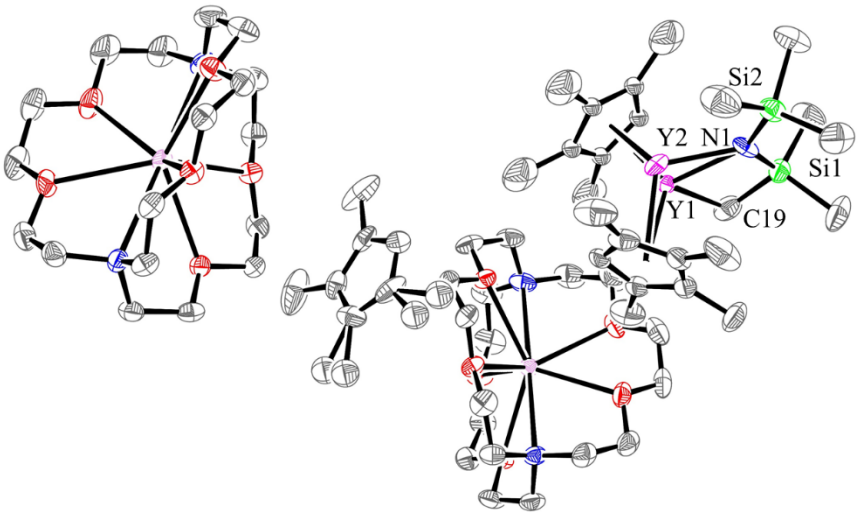

Figure 3.7. Displacement ellipsoid plot of 10:90 disordered structure of [K(crypt)][$(C_5Me_4H)_2Y(NR_2)$]/[$(C_5Me_4H)_2Y\{N(SiMe_3)(SiMe_2CH_2)$-$\kappa C$, $\kappa N\}$], that crystallizes with [K(crypt)][C_5Me_4H], with ellipsoids drawn at the 50 % probability level. Hydrogen atoms omitted for clarity.

Theoretical Analysis. Electronic structure calculations on $[(C_5Me_5)_2Y(NR_2)]^{1-}$ and $[(C_5Me_4H)Y(NR_2)_2]^{1-}$ were carried out by Samuel Bekoe from the research group of Professor Filipp Furche at the density functional level of theory using the TPSSh[42] functional with Grimme's D3 dispersion correction.[43, 44] All structures were initially optimized starting from the crystal structures without symmetry constraints. The solvent optimized structure of $[(C_5Me_5)_2Y(NR_2)]^{1-}$ resulted in a C_2-symmetric structure that exhibited a small second-order Jahn-Teller distortion into a C_1 symmetric minimum. The energy change associated with this distortion is less than 1 kcal/mol

and hence the electron configuration can be understood qualitatively using C_1 symmetry. The optimized structure closely approximates the X-ray data with the optimized Y–N distance ~0.04 Å longer than the experimentally observed distance. The average closest Y…C($SiMe_3$) distance in the optimized structure is 3.720 Å, approximately 1 Å outside the expected distance to form a bond. Molecular orbital plots and population analysis revealed a highest occupied molecular orbital with $4d_z^2$-like character, Figure 3.8 (left). The HOMO has electron density on two methyl carbon atoms of the $(NR_2)^{1-}$ ligand.

Structure optimization of $[(C_5Me_4H)_2Y(NR_2)]^{1-}$ resulted in a C_s symmetric minimum with molecular orbital plots and population analysis revealing a highest occupied molecular orbital with $4d_z^2$-like character, Figure 3.8 (right). The Y–N distance from the optimized structure is 2.374 Å, which is similar to the Y–N distance, 2.336(1) Å, in $[(C_5Me_5)_2Y\{N(SiMe_3)_2\}]^{1-}$, **5.** The average distance of Y to the closest C in the amide methyl groups is 3.526 Å, approximately 1 Å larger than would be expected to form a bond. Again, there are small amounts of HOMO electron density on two of the $(NR_2)^{1-}$ methyl groups.

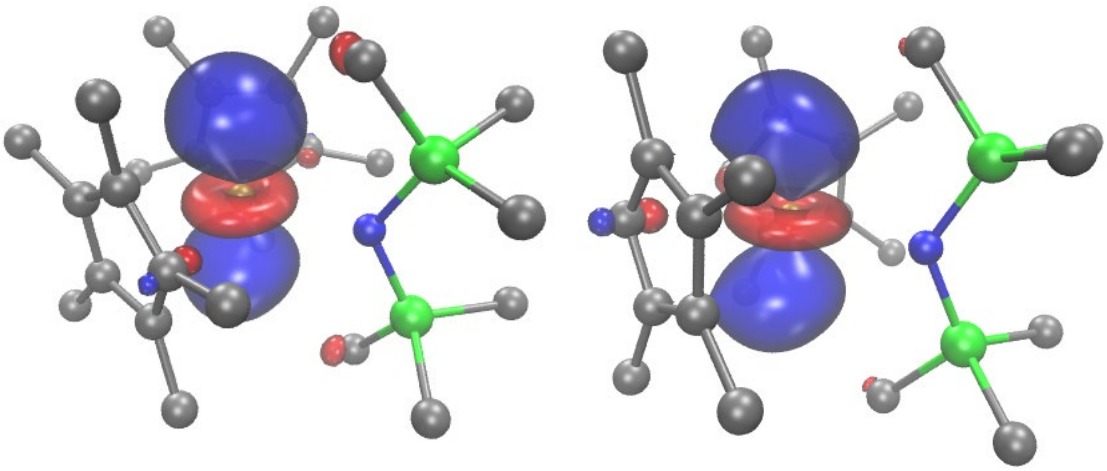

Figure 3.8. (left) Calculated d_z^2-like HOMO of $[(C_5Me_5)_2Y(NR_2)]^{1-}$, plotted with a contour value of 0.05 with hydrogen atoms excluded for clarity. (right) Calculated d_z^2-like HOMO of $[(C_5Me_4H)_2Y(NR_2)]^{1-}$, plotted with a contour value of 0.05 with hydrogens excluded for clarity.

TDDFT analyses were performed on the solvent optimized structure of $[(C_5Me_5)_2Y(NR_2)]^{1-}$ and $[(C_5Me_4H)_2Y(NR_2)]^{1-}$. TDDFT calculations on $[(C_5Me_5)_2Y(NR_2)]^{1-}$ are compared with the observed spectrum for **2** is shown in Figure 3.9. There are characteristic $4d_z^2 \rightarrow 5p_z$ transitions in the 550-750 nm region and 4d-4d transitions at 350-500 nm. A 4d-ligand transition is predicted at 330 nm. The multiple features in the predicted spectrum for $[(C_5Me_5)_2Y(NR_2)]^{1-}$ match the spectrum of the solution of **2** and are consistent with the reduction of **1**. TDDFT calculations on $[(C_5Me_4H)_2Y(NR_2)]^{1-}$ are compared with the observed spectrum for **4** in Figure 3.10. The predicted spectrum differs from that of $[(C_5Me_5)_2Y(NR_2)]^{1-}$ in Figure 3.9 just as the experimental spectrum of **4** differs from that of **2**. The predicted band centered around 850 nm arises from 4d-5p transitions and the 400 nm band is assigned as a 4d-ligand transition, which is at a lower energy than in the C_5Me_5 complex.

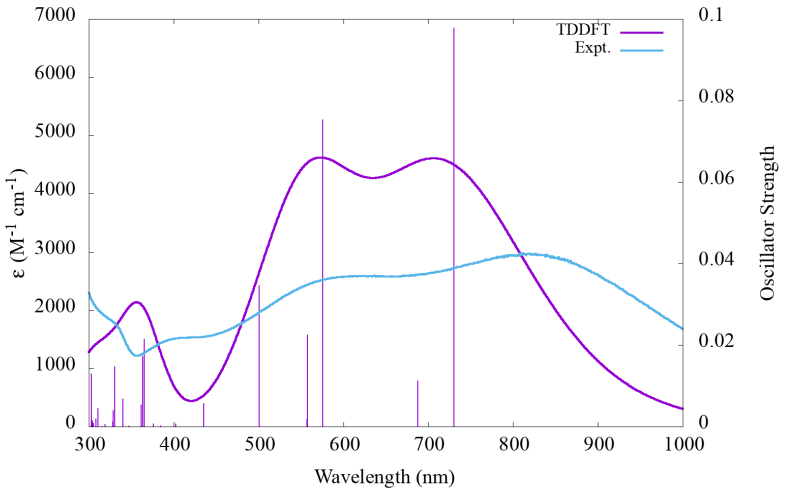

Figure 3.9. Theoretical UV-visible spectrum of $[(C_5Me_5)_2Y(NR_2)]^{1-}$ in purple with computed TDDFT oscillator strengths shown as vertical lines. The computed intensities were scaled by a factor 0.3 to ease comparison with the experimental spectrum of **2** in blue.

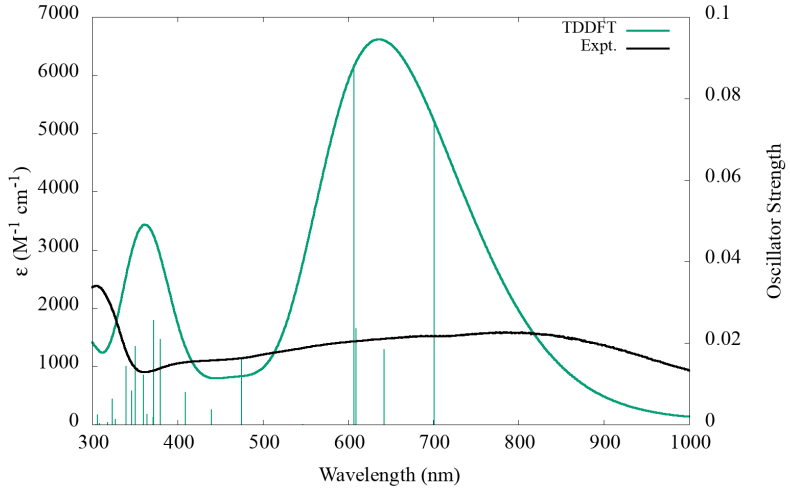

Figure 3.10. Theoretical UV-visible spectrum of $[(C_5Me_4H)_2Y(NR_2)]^{1-}$ in C_1-symmetry, shown in green with computed TDDFT oscillator strengths shown as vertical lines. The computed intensities were scaled by a factor 0.7 to ease comparison with the experimental spectrum of **4** in black.

Discussion

Reductions of $(C_5Me_5)_2Y(NR_2)$, **1**, and $(C_5Me_4H)_2Y(NR_2)$, **3**, form dark blue solutions, **2**, and **4**, respectively, that have UV-visible and EPR spectra consistent with the presence of Y(II). Their respective 74.5 G and 71.2 G hyperfine coupling constants, A_{iso}, fit well with previous correlations that Y(II) complexes of more electron donating ligands have higher A_{iso} values , Table

1. The *A* value for the C_5Me_4H containing solution, 71.2 G, is in between those of its homoleptic analogs, 64.8 G for the reduction product of $(C_5Me_4H)_3Y$[7] and 110 G for $[Y(NR_2)_3]^{1-}$.[22] The fact that the value for **4** is closer to the value of the $(C_5Me_4H)_3Y$ reduction product is consistent with the fact that there are two C_5Me_4H ligands and only one NR_2 ligand. This contrasts with the previously reported *A* value, 34.6 G, for the product of reducing the heteroleptic Cp''_2YCp complex,[23] which is less than the *A* values for both of the respective homoleptic complexes, 36.1 G for the $Cp"_3Y$ reduction product and 42.8 G for the Cp_3Y reduction product. Hence, the *A* values are not necessarily additive depending on the identity of the ligands.

Both heteroleptic reduction products, **2** and **4**, decompose readily at room temperature and attempts to crystallize the Y(II) products at low temperature formed crystals that contained $[N(SiMe_3)(SiMe_2CH_2)]^{2-}$ ligands formed by apparent C–H bond activation of a trimethylsilyl group. Cyclometalation of the $[N(SiMe_3)_2]^{1-}$ ligand is a common reaction,[35-39] and as described in the introduction, C–H bond activation has been observed in other reductions attempting to form Ln(II) and U(II) complexes.[15, 18, 19, 23-30, 32, 45] The fact that the precursor $(C_5Me_5)_2Y(NR_2)$, **1**, had an agostic interaction of a methyl C–H with the yttrium metal center in one complex of the two present in the unit cell suggests that this reaction could occur with little structural change.

The product crystallized from the reduction of $(C_5Me_5)_2Y(NR_2)$, **1**, contained a mixture of the Y(II) complex, **[**K(crypt)][$(C_5Me_5)_2Y(NR_2)$], **5**, and the cyclometalate. [$(C_5Me_5)_2Y${$N(SiMe_3)(SiMe_2CH_2)$-*κC,κN*}], **6**. In the reduction of the tetramethyl analog $(C_5Me_4H)_2Y(NR_2)$, **3**, only a 10% mixture of the Y(II) complex, [K(crypt)][$(C_5Me_4H)_2Y(NR_2)$], **7**, and 90% of the cyclometalated complex, [K(crypt)][$(C_5Me_4H)_2Y${$N(SiMe_3)(SiMe_2CH_2)$-*κC*:*κN*}], **8**, was isolated. This difference is consistent with the first-order decomposition kinetics observed with half-lives of 6.6 h and 55 min for the C_5Me_5, **2**, and C_5Me_4H, **4**, reduced solutions,

respectively. Interestingly, both heteroleptic systems, **5** and **7**, are more thermally stable than the homoleptic yttrium analogs, $[(C_5Me_4H)_3Y]^{1-}$ [7]and $[Y(NR_2)_3]^{1-}$.[11] The solutions produced from reducing $(C_5Me_4H)_3Y$ and $Y(NR_2)_3$ decompose too fast to give good kinetic data at room temperature.

The DFT calculations on both $[(C_5Me_5)_2Y(NR_2)]^{1-}$, and $[(C_5Me_4H)_2Y(NR_2)]^{1-}$show HOMOs with electron density on the C–H bond which is consistent with the reactivity observed. The possibility of a facile C–H bond activation decomposition pathway is consistent with the fact that isosbestic points are observed in each case, indicating clean decomposition of both **2** and **4**. The difference in stability of **2** and **4** is not great enough to make major conclusions about C_5Me_5 vs C_5Me_4H ligands in this system. Since the more electron donating C_5Me_5 is slightly more stable according to the decomposition data, the difference in donor strength of the ligand is apparently not a main factor.

Conclusion

Reduction of the bis(pentamethylcyclopentadienyl) yttrium amide complex, $[(C_5Me_5)_2Y(NR_2)]$, **1**, has generated the first C_5Me_5 complex of Y(II), $[K(crypt)][(C_5Me_5)_2Y(NR_2)]$, **5**. This complex is highly reactive and decomposes to the C–H bond activation product, $[K(crypt)][(C_5Me_5)_2Y\{N(SiMe_3)(SiMe_2CH_2)$-$\kappa C,\kappa N\}]$, **6,** overnight. This reactivity is consistent with DFT studies which show delocalization of the HOMO of the Y(II) complex onto a C–H bond from one trimethylsilyl group of the amide ligand which is activated to form **6**. A similar reduction occurs with, $(C_5Me_4H)_2Y(NR_2)$, **3**, but the Y(II) reaction product, $[K(crypt)][(C_5Me_4H)_2Y(NR_2)]$, **7**, is less stable than **5** and

[K(crypt)][$(C_5Me_4H)_2Y\{N(SiMe_3)(SiMe_2CH_2)$-$\kappa C,\kappa N\}$], **8**, an Y(III) cyclometallation product, was predominantly isolated.

Experimental Details

All manipulations and syntheses described below were conducted with the rigorous exclusion of air and water using standard Schlenk line and glovebox techniques under an argon or dinitrogen atmosphere. Solvents were sparged with UHP argon and dried by passage through columns containing Q-5 and molecular sieves prior to use. Deuterated NMR solvents were dried over NaK alloy, degassed by three freeze-pump-thaw cycles, and vacuum transferred before use. KC_8, $(C_5Me_5)_2YN(SiMe_3)_2$, and $(C_5Me_4H)_2Y(NR_2)$ were prepared as previously described. [33, 34, 46] 2.2.2-cryptand (crypt) (Aldrich) was dried under 10^{-5} Torr for 12 h before use. UV-Visible spectroscopy was performed using an Agilent Cary 60 Scan UV-visible spectrophotometer in a 1 mm quartz cuvette. Infrared spectra were collected as compressed solids on an Agilent Cary 630 ATR-FTIR. Elemental analyses were conducted on a Perkin-Elmer 2400 Series II CHNS elemental analyzer.

Synthesis of [K(crypt)][$(C_5Me_5)_2YN(SiMe_3)_2$]/[$(C_5Me_5)_2Y\{N(SiMe_3)(SiMe_2CH_2)$-$\kappa C,\kappa N\}$], 5/6. $(C_5Me_5)_2YNR_2$ (90 mg, 0.17 mmol) and 2.2.2-cryptand (76 mg, 0.20 mmol) were charged into a vial and stirred in 5 mL of THF for 20 min. A vial was charged with KC_8 (40 mg, 0.30 mmol) and both vials were place in the freezer for 2 h. The yellow THF solution was added to the KC_8 and stirred for 5 min. This solution was filtered and layered using chilled pentane. After placing in the freezer at −35°C for 24 h, dark black/ purple crystals containing **2**/**3** were isolated (104 mg, 61 %). UV-vis (THF) λ_{max} nm (ε, $M^{1-}cm^{1-}$): 815 (3000), 583 (2500), 405 (1500). IR (cm^{1-}): 2877s, 2810s, 1476vw, 1455vw, 1442w, 1353s, 1293w, 1258w, 1237w, 1173vw, 1130s,

1101vs, 1079vs, 948vs, 930vs, 875s, 831s, 819vs, 772w, 750w. Anal. Calcd for $C_{44}H_{84}KN_3O_6Si_2Y$: C, 56.5; H, 9.05; N, 4.49. Found: C, 56.9; H, 9.5; N, 4.38. The results give a formula of $C_{45}H_{90}N_3$.

Synthesis of [K(crypt)]$_2$[(C$_5$Me$_4$H)$_2$YNR$_2$]/[(C$_5$Me$_4$H)$_2$Y{N(SiMe$_3$)(SiMe$_2$CH$_2$)-*κC,κN*}][C$_5$Me$_4$H], 7/8. $(C_5Me_4H)_2YN(SiMe_3)_2$ (55 mg, 0.11 mmol) was charged into a vial with 2.2.2-cryptand (43 mg, 0.11 mmol) and 5 mL of THF. The pale-yellow solution was stirred for 20 min and another vial was charged with KC_8 (30 mg, 0.22 mmol). The vials were placed in the −35°C freezer for 2 h, followed by addition of the THF solution to the KC_8 vial. The solution was stirred for 5 min, filtered, layered using chilled pentane and placed in the freezer at −35 °C which after 12 h produced dark purple crystals of **7/8** (64 mg, 61 %). UV-vis (THF) λ_{max} nm (ε, $M^{1-}cm^{1-}$): 791 (1600), 670 (1500), 403 (1100). IR (cm^{1-}): 2877s, 2807s, 1628vw, 1476w, 1455vw, 1442w, 1353s, 1293w, 1258w, 1237vw, 1173vw, 1130s, 1101vs, 1079vs, 946vs, 930vs, 831s, 819w, 750s, 704w. Anal. Calcd. for $C_{42}H_{80}KN_3O_6Si_2Y$: C, 55.6; H, 8.89; N, 4.63. Found: C, 56.0; H, 8.81; N, 2.93. The results suggest low N composition, but the C/H ratios are similar. Calcd: 0.525; Found: 0.534.

X-ray Data Collection, Structure Solution and Refinement for [K(crypt)][(C$_5$Me$_5$)$_2$YN*]/{(C$_5$Me$_5$)$_2$Y[N(SiMe$_3$)(SiMe$_2$CH$_2$)-*κC,κN*]}, 5/6 (75%/ 25%). A purple crystal of approximate dimensions 0.067 x 0.366 x 0.402 mm was mounted in a cryoloop and transferred to a Bruker SMART APEX II diffractometer. The APEX2[47] program package was used to determine the unit-cell parameters and for data collection (30 sec/frame scan time for a sphere of diffraction data). The raw frame data was processed using SAINT[48] and SADABS[49] to yield the reflection data file. Subsequent calculations were carried out using the SHELXTL[50] program. There were no systematic absences nor any diffraction symmetry other than the Friedel

condition. The centrosymmetric triclinic space group $P\bar{1}$ was assigned and later determined to be correct. The structure was solved by direct methods and refined on F^2 by full-matrix least-squares techniques. The analytical scattering factors[51] for neutral atoms were used throughout the analysis. Hydrogen atoms were included using a riding model. Atom C(21) was disordered. C(21) was refined as 75% CH_3 and C(21B) was refined as 25% CH_2 to account for a mixture of and Y^{2+} and Y^{3+}. Least-squares analysis yielded wR2 = 0.0862 and Goof = 1.041 for 539 variables refined against 15627 data (0.68 Å), R1 = 0.0380 for those 13739 data with I > 2.0σ(I).

X-ray Data Collection, Structure Solution and Refinement for [K(crypt)][$(C_5Me_5)_2$YN*]/{$(C_5Me_5)_2$Y[N($SiMe_3$)($SiMe_2CH_2$)-*κC,κN*]}, 5/6 (70%/ 30%). A purple crystal of approximate dimensions 0.042 x 0.224 x 0.318 mm was mounted in a cryoloop and transferred to a Bruker SMART APEX II diffractometer. The APEX2[47] program package was used to determine the unit-cell parameters and for data collection (30 sec/frame scan time for a sphere of diffraction data). The raw frame data was processed SAINT[48] and SADABS[49] to yield the reflection data file. Subsequent calculations were carried out using the SHELXTL [50] program. There were no systematic absences nor any diffraction symmetry other than the Friedel condition. The centrosymmetric triclinic space group $P\bar{1}$ was assigned and later determined to be correct. The structure was solved by direct methods and refined on F^2 by full-matrix least-squares techniques. The analytical scattering factors[51] for neutral atoms were used throughout the analysis. Hydrogen atoms were included using a riding model. Atom C(21) was disordered. C(21) was refined as 70% CH_3 and C(21B) was refined as 30% CH_2 to account for a mixture of and Y^{2+} and Y^{3+}. Least-squares analysis yielded wR2 = 0.0933 and Goof = 1.038 for 539 variables refined against 12564 data (0.75 Å), R1 = 0.0387 for those 10354 data with I > 2.0σ(I).

X-ray Data Collection, Structure Solution and Refinement for [K(crypt)]$_2$[$(C_5Me_4H)_2Y(NR_2)$]/{$(C_5Me_4H)_2Y[N(SiMe_3)(SiMe_2CH_2)$-*κC,κN*]}[$C_5Me_4H$], 7/8 (10%/ 90%). An orange crystal of approximate dimensions 0.063 x 0.149 x 0.366 mm was mounted in a cryoloop and transferred to a Bruker SMART APEX II diffractometer system. The APEX2[47] program package was used to determine the unit-cell parameters and for data collection (180 sec/frame scan time). The raw frame data was processed SAINT[48] and SADABS[49] to yield the reflection data file. Subsequent calculations were carried out using the SHELXTL[50] program package. There were no systematic absences nor any diffraction symmetry other than the Friedel condition. The centrosymmetric triclinic space group $P\bar{1}$ was assigned and later determined to be correct. The structure was solved by direct methods and refined on F^2 by full-matrix least-squares techniques. The analytical scattering factors[51] for neutral atoms were used throughout the analysis. Hydrogen atoms were included using a riding model. Several atoms were disordered and included using multiple components with partial site-occupancy-factors. The yttrium atom exhibited an approximate 90:10 disorder Y(1):Y(2). The SIMU restraint was applied to the disordered yttrium atom. Carbon atoms C(10) to C(18B) were refined using equivalent anisotropic displacement parameters (EADP) and geometrical restraints (SAME). Least-squares analysis yielded wR2 = 0.2108 and Goof = 1.019 for 835 variables refined against 16133 data (0.80 Å), R1 = 0.0772 for those 9686 data with $I > 2.0\sigma(I)$.

Computational Details. Electronic structure calculations on $[(C_5Me_5)_2Y(NR_2)]^{1-}$ and $[(C_5Me_4H)Y(NR_2)_2]^{1-}$ were carried out at the density functional level of theory using the TPSSh[42] functional with Grimme's D3[43, 44] dispersion correction in C_1 symmetry. Scalar relativistic effective core potentials (ECPs) [52] with the def2-TZVP[53] basis set were used for Y and polarized split-valence basis sets with diffuse functions def2-SVP[54] were used for the lighter atoms. DFT

quadrature grids of size 4 were used throughout [55]. The continuum solvation model COSMO[56] with a dielectric constant of 7.5218[57] and a refractive index of 1.3 for THF was included to account for solvent effects. All structures were initially optimized starting from the X-ray structures without symmetry constraints and with geometry convergence thresholds of 10^{-4} a.u and energy convergence of 10^{-8} a.u. Optimized structures were confirmed to be minima on the potential energy surface by vibrational analysis using finite differences of gradients. Re-optimization of the C_1 symmetrized structures with symmetry constraints were carried out and compared to the total energy to the one obtained in C_1. Vertical excitation energies and oscillator strengths of the solvent optimized structures were carried within the time-dependent density functional theory (TDDFT) framework using def2-SVPD[58] basis sets for the ligands and def2-TZVP basis set for Y. UV-visible spectra were simulated using Gaussian line profiles with a root mean-square width of 0.2 eV. Molecular orbitals and electronic transitions and states were analyzed with VMD[59] and Mulliken population analysis (MPA). All calculations were carried out with the TURBOMOLE program suite, V-7.4.1. [60] Excitation energies, oscillator strengths, and dominant orbital contributions of the electronic excitations of **5** and **7** are summarized in Tables 3.3 and 3.4, respectively.

Table 3.3. Electronic excitation summary for $[(C_5Me_5)_2Y(NR_2)]^{1-}$ computed using the TPSSh functional with the def2-SVP basis set for ligand atoms. Only transitions above 10% contribution to the overall excitation are listed.

Wavelength (nm)	Oscillator Strength (length)	Dominant Contributions			Assignment
		Occupied	Virtual	% weight	
730.5	0.098	126a	128a	99.2	$4d_z^2 \rightarrow 5p_z$
687.7	0.011	126a	129a	97.7	$4d_z^2 \rightarrow 5p_x$
575.9	0.075	126a	130a	99.6	$4d_z^2 \rightarrow 5p_y$
557.9	0.022	126a	131a	73.1	$4d_z^2 \rightarrow 5p_x$
			132a	24.3	$4d_z^2 \rightarrow 4d_{yz}$
500.5	0.035	126a	133a	97.0	$4d_z^2 \rightarrow 4d_{xy}$
365.2	0.021	126a	138a	38.8	$4d_z^2 \rightarrow 4d_{yz}$
			139a	19.1	$4d_z^2 \rightarrow 5p_z+4d_{xy}$
			140a	15.7	
363.4	0.017	126a	138a	24.8	$4d_z^2 \rightarrow 4d_{yz}$
			139a	24.5	$4d_z^2 \rightarrow 5p_z+4d_{xy}$
			142a	22.3	$4d_z^2 \rightarrow 4d_{xy}$
			145a	10.4	$4d_z^2 \rightarrow 4d_{xy}$
330.3	0.015	126a	143a	86.1	$4d_z^2 \rightarrow$ ligand

Table 3.4. Electronic excitation summary for $[(C_5Me_4H)_2Y(NR_2)]^{1-}$ in C_1-symmetry computed using the TPSSh functional with the def2-SVPD basis set for ligand atoms. Only transitions above 10% contribution to the overall excitation are listed.

Wavelength (nm)	Oscillator Strength (length)	Dominant Contributions			Assignment
		Occupied	Virtual	% weight	
701.1	0.043	118a	120a	98.5	$4d_z^2 \rightarrow 5p_z$
642.4	0.043	118a	121a	97.7	$4d_z^2 \rightarrow 5p_x$
606.8	0.028	118a	122a	88.1	$4d_z^2 \rightarrow 5p_y$
			123a	10.1	$4d_z^2 \rightarrow 5s+5p_x$
475.2	0.024	118a	125a	95.3	$4d_z^2 \rightarrow 4d_{xy}$
409.2	0.030	118a	127a	94.9	$4d_z^2 \rightarrow$ ligand
371.7	0.028	118a	133a	53.9	$4d_z^2 \rightarrow 4d_{xy}$
			128a	20.0	$4d_z^2 \rightarrow$ ligand
			130a	11.1	$4d_z^2 \rightarrow 5p_z$

References

(1) Hitchcock, P. B.; Lappert, M. F.; Maron, L.; Protchenko, A. V. *Angew. Chem. Int. Ed.* **2008,** *47*, 1488-1491.

(2) MacDonald, M. R.; Ziller, J. W.; Evans, W. J. *J. Am. Chem. Soc.* **2011,** *133*, 15914-15917.

(3) MacDonald, M. R.; Bates, J. E.; Fieser, M. E.; Ziller, J. W.; Furche, F.; Evans, W. J. *J. Am. Chem. Soc.* **2012,** *134*, 8420-8423.

(4) MacDonald, M. R.; Bates, J. E.; Ziller, J. W.; Furche, F.; Evans, W. J. *J. Am. Chem. Soc.* **2013,** *135*, 9857-9868.

(5) Palumbo, C. T.; Darago, L. E.; Windorff, C. J.; Ziller, J. W.; Evans, W. J. *Organometallics* **2018,** *37*, 900-905.

(6) Woen, D. H.; Huh, D. N.; Ziller, J. W.; Evans, W. J. *Organometallics* **2018,** *37*, 3055-3063.

(7) Jenkins, T. F.; Woen, D. H.; Mohanam, L. N.; Ziller, J. W.; Furche, F.; Evans, W. J. *Organometallics* **2018,** *37*, 3863-3873.

(8) Ryan, A. J.; Darago, L. E.; Balasubramani, S. G.; Chen, G. P.; Ziller, J. W.; Furche, F.; Long, J. R.; Evans, W. J. *Chem. Eur. J.* **2018,** *24*, 7702-7709.

(9) Angadol, M. A.; Woen, D. H.; Windorff, C. J.; Ziller, J. W.; Evans, W. J. *Organometallics* **2019,** *38*, 1151-1158.

(10) Moehring, S. A.; Miehlich, M.; Hoerger, C. J.; Meyer, K.; Ziller, J. W.; Evans, W. J. *Inorg. Chem.* **2020,** *59*, 3207-3214.

(11) Ryan, A. J.; Ziller, J. W.; Evans, W. J. *Chem. Sci.* **2020,** *11*, 2006-2014.

(12) Evans, W. J.; Davis, B. L. *Chem. Rev.* **2002,** *102*, 2119-2136.

(13) Evans, W. J.; Davis, B. L.; Champagne, T. M.; Ziller, J. W. *Proceedings of the National Academy of Sciences* **2006,** *103*, 12678-12683.

(14) Evans, W. J. *Inorg. Chem.* **2007,** *46*, 3435-3449.

(15) Jaroschik, F.; Nief, F.; Le Goff, X.-F.; Ricard, L. *Organometallics* **2007,** *26*, 1123-1125.

(16) Jaroschik, F.; Momin, A.; Nief, F.; Le Goff, X.-F.; Deacon, G. B.; Junk, P. C. *Angew. Chem. Int. Ed.* **2009,** *121*, 1137-1141.

(17) Kelly, R. P.; Maron, L.; Scopelliti, R.; Mazzanti, M. *Angew. Chem. Int. Ed.* **2017,** *56*, 15663-15666.

(18) Fieser, M. E.; Palumbo, C. T.; La Pierre, H. S.; Halter, D. P.; Voora, V. K.; Ziller, J. W.; Furche, F.; Meyer, K.; Evans, W. J. *Chem. Sci.* **2017,** *8*, 7424-7433.

(19) Palumbo, C. T.; Halter, D. P.; Voora, V. K.; Chen, G. P.; Chan, A. K.; Fieser, M. E.; Ziller, J. W.; Hieringer, W.; Furche, F.; Meyer, K.; Evans, W. J. *Inorg. Chem.* **2018,** *57*, 2823-2833.

(20) Palumbo, C. T.; Darago, L. E.; Dumas, M. T.; Ziller, J. W.; Long, J. R.; Evans, W. J. *Organometallics* **2018,** *37*, 3322-3331.

(21) Gould, C. A.; McClain, K. R.; Yu, J. M.; Groshens, T. J.; Furche, F.; Harvey, B. G.; Long, J. R. *J. Am. Chem. Soc.* **2019,** *141*, 12967-12973.

(22) Fang, M.; Lee, D. S.; Ziller, J. W.; Doedens, R. J.; Bates, J. E.; Furche, F.; Evans, W. J. *J. Am. Chem. Soc.* **2011,** *133*, 3784-3787.

(23) Corbey, J. F.; Woen, D. H.; Palumbo, C. T.; Fieser, M. E.; Ziller, J. W.; Furche, F.; Evans, W. J. *Organometallics* **2015,** *34*, 3909-3921.

(24) Coles, M. P.; Hitchcock, P. B.; Lappert, M. F.; Protchenko, A. V. *Organometallics* **2012,** *31*, 2682-2690.

(25) Simpson, S. J.; Turner, H. W.; Andersen, R. A. *Inorg. Chem.* **1981,** *20*, 2991-2995.

(26) Dormond, A.; El Bouadili, A. A.; Moïse, C. *Chem. Commun.* **1985**, 914-916.

(27) Fortier, S.; Wu, G.; Hayton, T. W. *J. Am. Chem. Soc.* **2010,** *132*, 6888-6889.

(28) Fortier, S.; Kaltsoyannis, N.; Wu, G.; Hayton, T. W. *J. Am. Chem. Soc.* **2011,** *133*, 14224-14227.

(29) Hervé, A.; Bouzidi, Y.; Berthet, J.-C.; Belkhiri, L.; Thuéry, P.; Boucekkine, A.; Ephritikhine, M. *Inorg. Chem.* **2015,** *54*, 2474-2490.

(30) Rookes, T. M.; Wildman, E. P.; Balázs, G.; Gardner, B. M.; Wooles, A. J.; Gregson, M.; Tuna, F.; Scheer, M.; Liddle, S. T. *Angew. Chem. Int. Ed.* **2018,** *57*, 1332-1336.

(31) La Pierre, H. S.; Scheurer, A.; Heinemann, F. W.; Hieringer, W.; Meyer, K. *Angew. Chem. Int. Ed.* **2014,** *53*, 7158-7162.

(32) Wedal, J. C.; Bekoe, S.; Ziller, J. W.; Furche, F.; Evans, W. J. *Organometallics* **2020,** *39*, 3425-3432.

(33) Lorenz, S. E.; Schmiege, B. M.; Lee, D. S.; Ziller, J. W.; Evans, W. J. *Inorg. Chem.* **2010,** *49*, 6655-6663.

(34) Den Haan, K. H.; De Boer, J. L.; Teuben, J. H.; Spek, A. L.; Kojic-Prodic, B.; Hays, G. R.; Huis, R. *Organometallics* **1986,** *5*, 1726-1733.

(35) Deacon, G. B.; Forsyth, C. M.; Junk, P. C.; Wang, J. *Inorg. Chem.* **2007,** *46*, 10022-10030.

(36) Niemeyer, M. *Inorg. Chem.* **2006,** *45*, 9085-9095.

(37) Wang, J.; Gardiner, M. G. *Chem. Commun.* **2005**, 1589-1591.

(38) Deacon, G. B.; Forsyth, C. M. *Chem. Commun.* **2002**, 2522-2523.

(39) Karl, M.; Harms, K.; Seybert, G.; Massa, W.; Fau, S.; Frenking, G.; Dehnicke, K. *Z. Anorg. Allg. Chem.* **1999,** *625*, 2055-2063.

(40) Evans, W. J. *Organometallics* **2016,** *35*, 3088-3100.

(41) Fieser, M. E.; MacDonald, M. R.; Krull, B. T.; Bates, J. E.; Ziller, J. W.; Furche, F.; Evans, W. J. *J. Am. Chem. Soc.* **2015,** *137*, 369-382.

(42) Staroverov, V. N.; Scuseria, G. E.; Tao, J. M.; Perdew, J. P. *J. Chem. Phys.* **2003,** *119*, 12129-12137.

(43) Grimme, S.; Antony, J.; Ehrlich, S.; Krieg, H. *J. Chem. Phys.* **2010,** *132*, 154104.

(44) Grimme, S. *J. Comput. Chem.* **2006,** *27*, 1787-1799.

(45) Palumbo, C. T.; Halter, D. P.; Voora, V. K.; Chen, G. P.; Ziller, J. W.; Gembicky, M.; Rheingold, A. L.; Furche, F.; Meyer, K.; Evans, W. J. *Inorg. Chem.* **2018,** *57*, 12876-12884.

(46) Bergbreiter, D. E.; Killough, J. M. *J. Am. Chem. Soc.* **1978,** *100*, 2126-2134.

(47) *Apex2 Version 2014.11-0*, Bruker AXS: Madison, WI, 2014.
(48) *SAINT Version 8.36a*, Bruker AXS, Inc.: Madison, WI, 2013.

(49) Sheldrick, G. M. *SADABS, Version 2014/5*, Bruker AXS, Inc.: Madison, WI 2014.

(50) Sheldrick, G. M. *SHELXTL, Version 2014/7*, Bruker AXS, Inc.: Madison, WI, 2014.

(51) *International Tables for Crystallography*; Dordrecht: Kluwer Academic Publishers 1992; Vol. C.

(52) Andrae, D.; Häußermann, U.; Dolg, M.; Stoll, H.; Preuß, H. *Theor. Chem. Acc.* **1990,** *77*, 123-141.

(53) Weigend, F.; Ahlrichs, R. *Phys. Chem. Chem. Phys.* **2005,** *7*, 3297-3305.

(54) Schäfer, A.; Horn, H.; Ahlrichs, R. *J. Chem. Phys.* **1992,** *97*, 2571-2577.

(55) Treutler, O.; Ahlrichs, R. *J. Chem. Phys.* **1995,** *102*, 346-354.

(56) Klamt, A.; Schuurmann, G. *Perkin Trans. 2* **1993**, 799-805.

(57) *CRC Handbook of Chemistry and Physics*; 81 ed.; CRC Press: Boca Raton, FL, 2008; p 136.

(58) Rappoport, D.; Furche, F. *J. Chem. Phys.* **2010,** *133*, 134105.

(59) *VMD* 1.9: available from http://www.ks.uiuc.edu/Research/vmd/.

(60) *TURBOMOLE V7.4.1 2019, a development of University of Karlsruhe and Forschungszentrum Karlsruhe GmbH, 1989-2007, TURBOMOLE GmbH, since 2007; available from http://www.turbomole.com.*

CHAPTER 4

Synthesis of a 2-Isocyanophenolate Ligand, $(2\text{-}CNC_6H_4O)^{1-}$, by Ring-Opening of Benzoxazole with Rare-Earth Metal Complexes*

Introduction

Benzoxazole, C_7H_5NO, Figure 4.1 left, and its derivatives are important building blocks for the synthesis of pharmaceutical agents,[1] natural products,[2] functional materials,[3] and agrochemical compounds.[4] Due to these numerous applications, the functionalization of benzoxazole has been explored extensively.[1, 4-11] Benzoxazole is also an interesting ligand for metals since it is a neutral heteroatomic version of the indenyl ligand, $(C_9H_7)^{1-}$, and it can function as an N-heterocyclic carbene (NHC) with a variety of transition metals including chromium,[12] iron,[13] tungsten,[14] rhenium,[15] and platinum,[16] Figure 4.1 right.

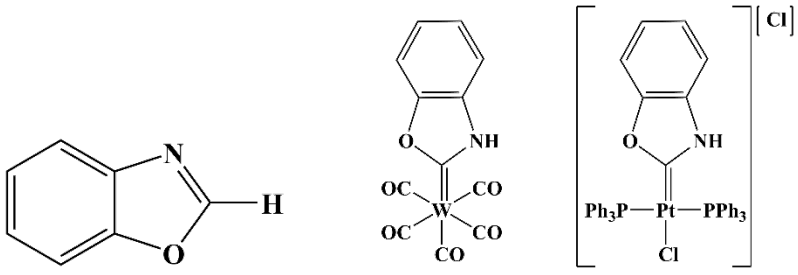

Figure 4.1. (left) Structure of benzoxazole. (right) Tungsten and platinum complexes of benzoxazole (NHC) ligands.[14, 16]

*Portions of this chapter have been published: Dumas, M.T.; Jenkins, T.F.; Wedal, J.C.; Ziller, J.W.; Furche, F.; Evans, W.J. *Organometallics*. **2021**, *40*(6), 735-741. DOI: 10.1021/acs.organomet.1c00002

Reactions of the lithium salt of deprotonated benzoxazole, $Li(C_7H_4NO)$, with $(C_5H_5)_2TiCl_2$ and $M(CO)_6$ (M = Cr, W), led to heterobimetallic ring-opened products containing the 2-isocyanophenolate ligand, $[(C_5H_5)_2Ti[\mu\text{-}2\text{-}CNC_6H_4O\text{-}\kappa C{:}\kappa O]_XM(CO)_4]$ (x = 1, 2), in 10-50% yields, eq 4.1. However, reaction of only $(C_5H_5)_2TiCl_2$ with the lithium salt did not lead to any isolable products.[17]

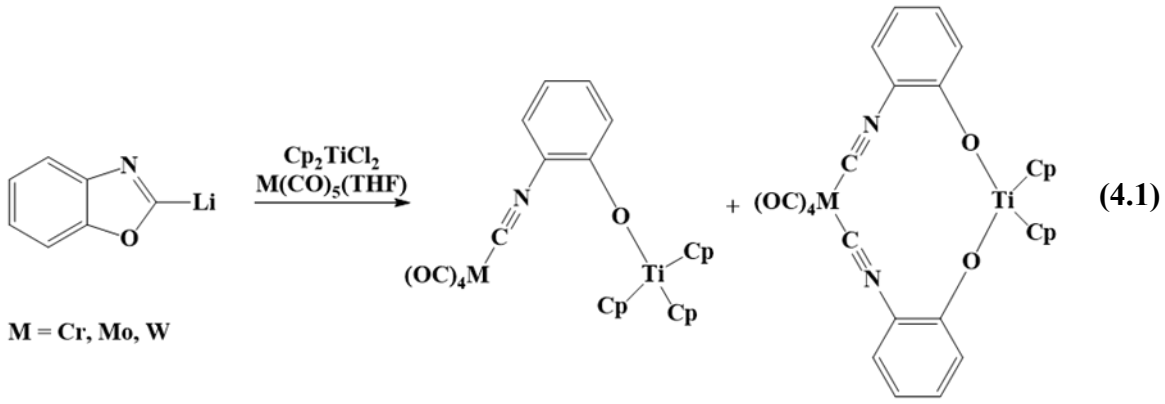

Although rare-earth metal complexes containing benzoxazole have not been reported in the literature, the capacity of ytterbium trifuoromethanesulfonate, $Yb(OTf)_3$, (OTf = CF_3SO_3) to catalyze the ring-opening of benzoxazole in a C–N bond forming reaction with 1,3-diphenylprop-2-ynol and similar substrates has been described, eq 4.2.[18]

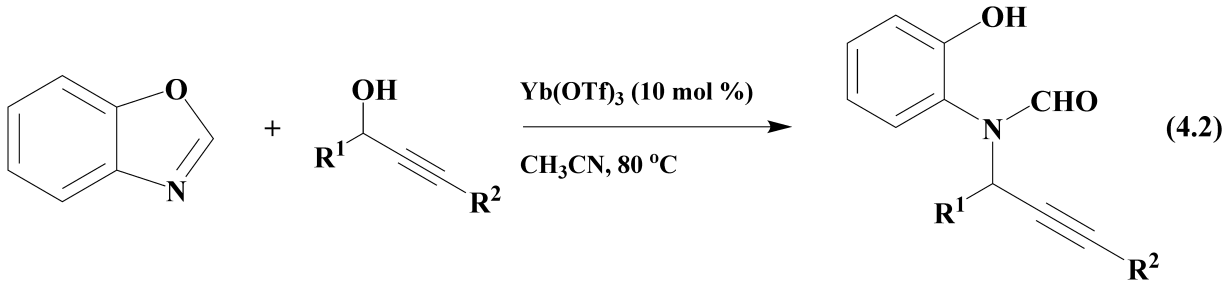

Dr. Megan Dumas explored the chemistry of benzoxazole with the rare-earth metals by examining reactions with the bis(pentamethylcyclopentadienyl) allyl complexes $(C_5Me_5)_2Ln(\eta^3\text{-}C_3H_5)$ (Ln = Y, Tb, Dy). Dr. Dumas obtained crystals of bimetallic ring-opened 2-

isocyanophenolate products, $[(C_5Me_5)_2Ln(\mu\text{-}2\text{-}CNC_6H_4O\text{-}\kappa C{:}\kappa O)]_2$ for Ln = Y, Dy, and Tb, but did not have time to bring the project to a publishable form before she graduated. This Chapter describes the completion of this project with full analysis and interpretation of the data. Efforts to isolate the product of reducing the Y complex are also presented.

Results & Discussion

Synthesis. When a colorless solution of benzoxazole in hexane was added to yellow solutions of $(C_5Me_5)_2Ln(\eta^3\text{-}C_3H_5)$ (Ln = Y, Dy, Tb) in hexane, the mixtures immediately became deep blood red. The allyl ligand can act as a base and deprotonate the benzoxazole, generating an oxazolyl anion in the presence of a bis(pentamethylcyclopentadienyl) cation, $[(C_5Me_5)_2Ln]^{1+}$, which can readily form crystallographically-characterizable organometallic complexes. X-ray crystallography was used to identify the structures of the products of the three reactions as the ring-opened 2-isocyanophenolate dimers, $[(C_5Me_5)_2Ln(\mu\text{-}2\text{-}CNC_6H_4O\text{-}\kappa C{:}\kappa O)]_2$, **1-Ln**, Figure 4.2, eq 4.3.

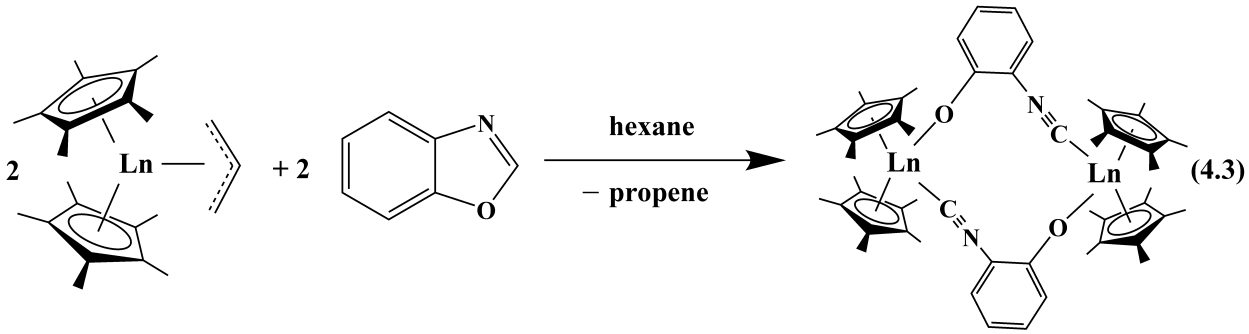

The ^{1}H NMR spectrum of **1-Y** matches its crystallographically-determined structure with a single C_5Me_5 resonance consistent with a single type of product as well as four separate aromatic CH signals. The ^{13}C NMR spectrum of the yttrium complex contained a doublet due to coupling with the ^{89}Y nucleus which has a nuclear spin of I = ½ with a resonance of 167.15 ppm (J_{YC} = 24

Hz). This is consistent with the presence of an isocyano-yttrium linkage as found crystallographically for C21. The complexes $(C_5Me_5)_2Y[CH(SiMe_3)_2](CNCMe_3)$ and $(C_5Me_5)_2Y[\eta^2\text{-}C(CH_2(3,5\text{-}Me_2C_6H_3))=N(2,6\text{-}Me_2C_6H_3)](CNCMe_3)$, feature isocyanide ^{13}C resonances at 149.27 ppm (J_{YC} = 10.9 Hz) and 155.29 ppm (J_{YC} = 7.5 Hz), respectively.[19] The complex $(C_5Me_5)_2Y(NC_6H_{10}O)(CNCMe_3)$ has a reported resonance of 150.7 ppm, although no J_{YC} coupling constant is reported.[20] Apparently, the benzoxazole was deprotonated by the allyl complexes and the ring-opened product was captured on both ends by $[(C_5Me_5)_2Ln]^{1+}$ cations.

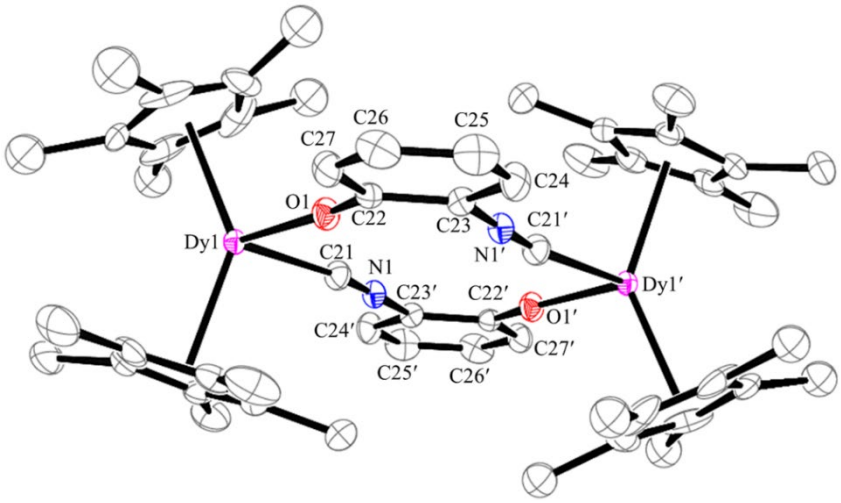

Figure 4.2. ORTEP depiction of $[(C_5Me_5)_2Dy(\mu\text{-}CNC_6H_4O\text{-}\kappa C{:}\kappa O)]_2$, **1-Dy**, with thermal ellipsoids drawn at the 50% probability level. Hydrogen atoms and co-crystallized solvent molecules have been omitted for clarity. **1-Y,** and **1-Tb** are isomorphous with **1-Dy**.

Structure. The bimetallic complex has two bent metallocene units oriented such that the four cyclopentadienyl ring centroids define a plane not a tetrahedron. The twelve-membered ring comprised of Ln1, O1, C22, C23, N1′, C21′, Ln1′, O1′, C22′, C23′, N1, and C21 in the **1-Ln** complexes is planar to within 0.024 Å. This plane makes an 89.5° angle with the plane of the four

C_5Me_5 ring centroids in **1-Dy** and **1-Tb** and an 89.4° angle in **1-Y** as shown in the side on view of **1-Tb**, Figure 4.3.

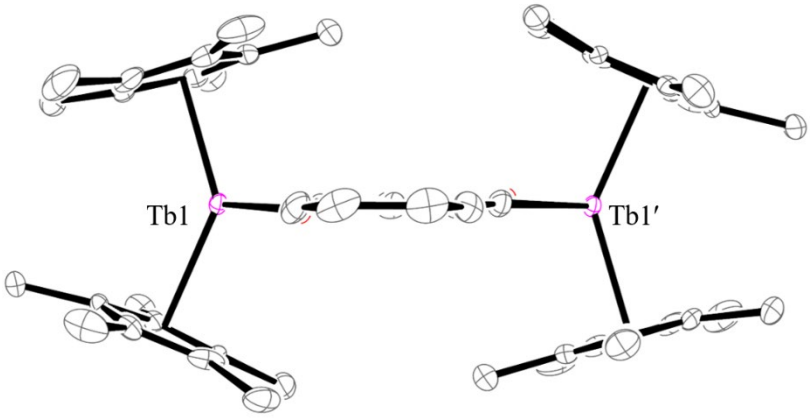

Figure 4.3. ORTEP representation of $[(C_5Me_5)_2Tb(\mu\text{-}2\text{-}CNC_6H_4O\text{-}\kappa C{:}\kappa O)]_2$, **1-Tb**, shown along the plane of the Ln-containing twelve membered ring, with thermal ellipsoids drawn at the 50% probability level. Hydrogen atoms and co-crystallized solvent molecules have been omitted for clarity.

The three **1-Ln** complexes are isomorphous and their bond distances differ according to the difference in their 8-coordinate ionic radii which are 1.019, 1.040, and 1.027 Å for Y, Tb, and Dy, respectively.[21] The local coordination environment around each metal can be compared to that of $(C_5Me_5)_2YMe(THF)$ and $[(C_5Me_5)_2Y(\mu\text{-}O_2CEt)]_2$.[22, 23] Table 4.1 shows that these compounds have Y–(C_5Me_5 ring centroid) distances similar to those of **1-Y**. The Y–O distance in **1-Y** is shorter than the Y–O(THF) distance in $(C_5Me_5)_2YMe(THF)$ which is consistent with a formally anionic versus neutral oxygen donor atom ligand. The Y–C distance in **1-Y** is longer than the Y–C(Me) distance in $(C_5Me_5)_2YMe(THF)$ which is consistent with a formally neutral versus anionic carbon donor atom ligand.

Table 4.1. Selected structural parameters for **1-Y** and structurally similar complexes.

	Y–(C_5Me_5 ring centroid) (Å)	Y–O (Å) Distance	Y–C (Å) Distance
$[(C_5Me_5)_2Y(\mu\text{-}2\text{-}CNC_6H_4O\text{-}\kappa C{:}\kappa O)]_2$, **1-Y**	2.367, 2.417	2.130(1)	2.530(2)
$(C_5Me_5)_2Y(Me)(THF)$[23]	2.320, 2.444	2.379(8)	2.44(2)
$[(C_5Me_5)_2Y(\mu\text{-}O_2CEt)]_2$[22]	2.372, 2.430	2.227(3), 2.252(3)	--

The Ln–C(NR) distances in **1-Y** can also be compared with the literature isocyanide complexes $(C_5Me_5)_2Y(NC_6H_{10}O)(CNCMe_3)$[20, 24] The yttrium–isocyanide bond distance in **1-Y**, 2.530(2)Å, is in between the 2.578(4) Å distance in $(C_5Me_5)_2Y(NC_6H_{10}O)(CNCMe_3)$ and the 2.4927(19) and 2.496(2) Å distances in $((C_5Me_5)_2Y[\mu\text{-}N(SiMe_3)NC])_2$.

UV-Vis Spectroscopy. The UV-vis spectra of **1-Ln** in hexane show overlapping broad absorbance peaks between 350 and 550 nm responsible for the dark red color, Figure 4.4. Intensely-colored complexes are not common for trivalent rare earth metals and the large extinction coefficients observed are consistent with Laporte allowed charge transfer transitions involving the C_5Me_5 and 2-isocyanophenolate ligands.

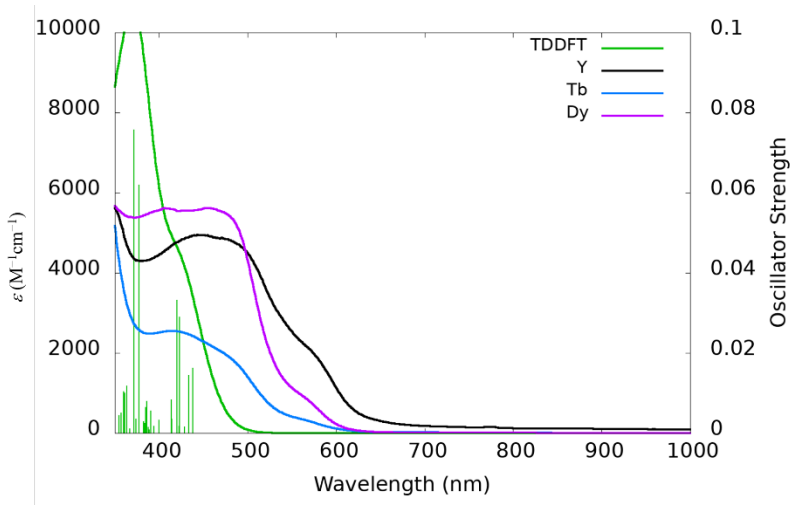

Figure 4.4. UV-Vis spectra of $[(C_5Me_5)_2Dy(\mu\text{-}2\text{-}CN(C_6H_4)O\text{-}\kappa C\text{:}\kappa O)]_2$, **1-Dy** (purple) **1-Y** (black), **1-Tb** (blue), and the simulated spectrum of **1-Y** with TDDFT oscillator strengths shown as vertical lines (green).

Electronic Structure Calculations. To gain further insight into the electronic structure of the ring-opened product, geometry optimization calculations on **1-Y** were performed by Justin C. Wedal from the Evans Group in collaboration with the Filipp Furche Group. In the optimized ground state structure, the highest occupied molecular orbital (HOMO) resides in the π system of the C_5Me_5 rings while the first lowest unoccupied molecular orbital (LUMO) is a π^* orbital on the $(CNC_6H_4O)^{1-}$ ligand, Figure 4.5. Time-dependent density functional theory (TDDFT) calculations were performed to analyze the experimental UV-Vis spectrum, Figure 4.4. All the computed absorptions are $\pi \rightarrow \pi^*$ transitions, from the occupied C_5Me_5 π system to the unoccupied (CNC_6H_4O) π^* system and do not involve any significant metal character.

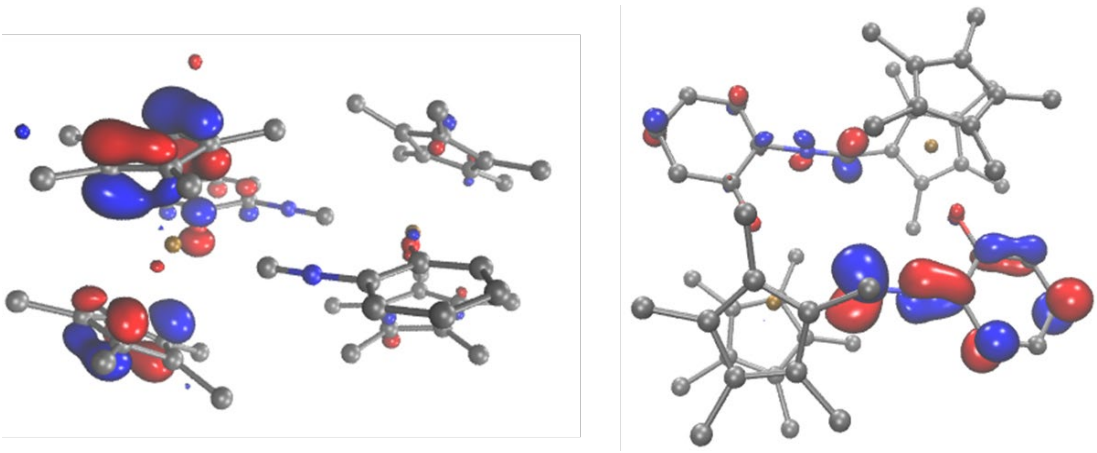

Figure 4.5. HOMO (left) and LUMO (right) of **1-Y**, plotted with contour value 0.05.

DFT calculations were also carried out on the product of reducing **1-Y** to investigate if the mono-reduced species, labelled **2-Y**, would contain Y(II) or a radical in the bimetallic ring. The α-spin HOMO of **2-Y** is purely ligand-based and is a π^* orbital on the CNC_6H_4O ligand, Figure 4.6, reminiscent of the LUMO of **1-Y**, Figure 4.5. The α-spin LUMO of **2-Y** is also a π^* orbital on the CNC_6H_4O ligand. The lowest α-spin unoccupied orbital for **2-Y** with significant metal character was LUMO +3 and exhibits π bonding character between the empty 4d orbitals on Y and the isocyanide moiety of the CNC_6H_4O ligand, Figure 4.6.

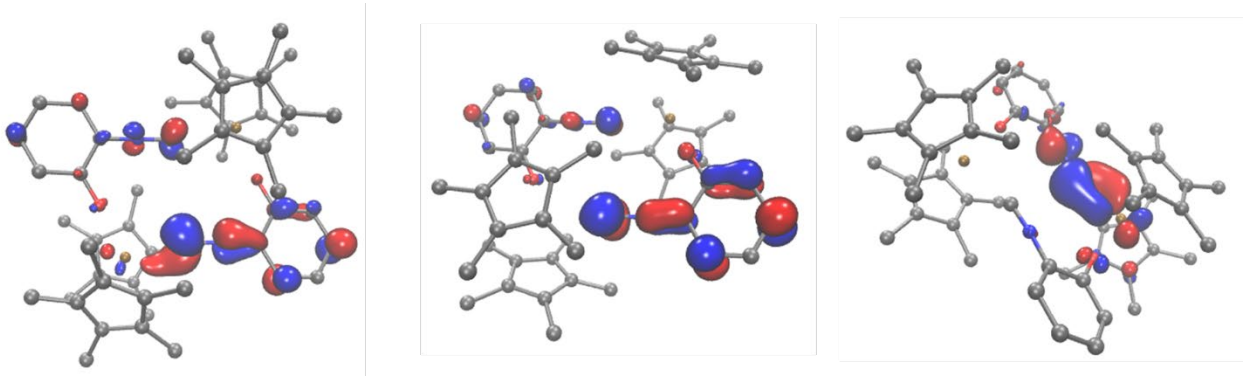

Figure 4.6. HOMO (left), LUMO (middle), and LUMO +3 (right) of **2-Y**, plotted with contour value 0.05. Hydrogen atoms have been omitted for clarity.

TDDFT calculations on **2-Y** show a new absorption band compared to **1-Y**, Figure 4.7. This new band is comprised of transitions from the occupied HOMO of **2-Y** into unoccupied π/π^* orbitals and do not have any significant metal character. The electronic structure calculations support the experimental observations described below that reduction of **1-Y** is ligand-based and not yttrium-based.

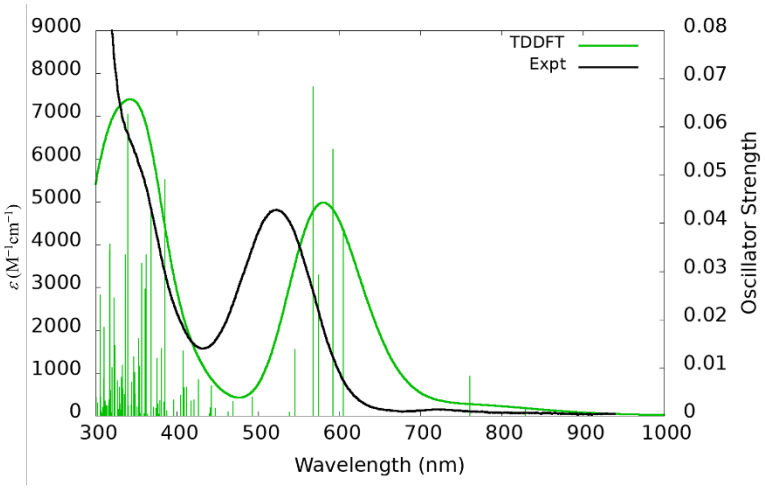

Figure 4.8. Experimental UV-vis spectrum of **2-Y** (black-red) and the simulated spectrum of **2-Y** with TDDFT oscillator strengths shown as vertical lines (green).

Reduction of 1-Y. The reduction of **1-Y** did not generate an isolable crystalline complex. Reduction of a dark red solution of **1-Y** and 2.2.2-cryptand with KC_8 did not result in an obvious color change that is typical when dark blue-black Y(II) complexes are formed.[25-29] However, the UV-vis spectrum of the product, **2-Y**, differed from that of **1-Y** and matched that calculated by TDDFT, Figure 4.7, for a complex with the twelve-membered ring reduced by one electron. EPR spectra were obtained that also substantiated the results of the DFT calculations. Specifically, the EPR spectrum of **2-Y** at 298 K exhibited a complicated pattern, which was best simulated with g

= 2.0027 and a hyperfine splitting of A = 5.16 G, Figure 4.8. The EPR spectrum of **2-Y** at 77 K was more difficult to model. A simulation with g = 2.0027, and A = 10.6 G is shown in Figure 4.8.

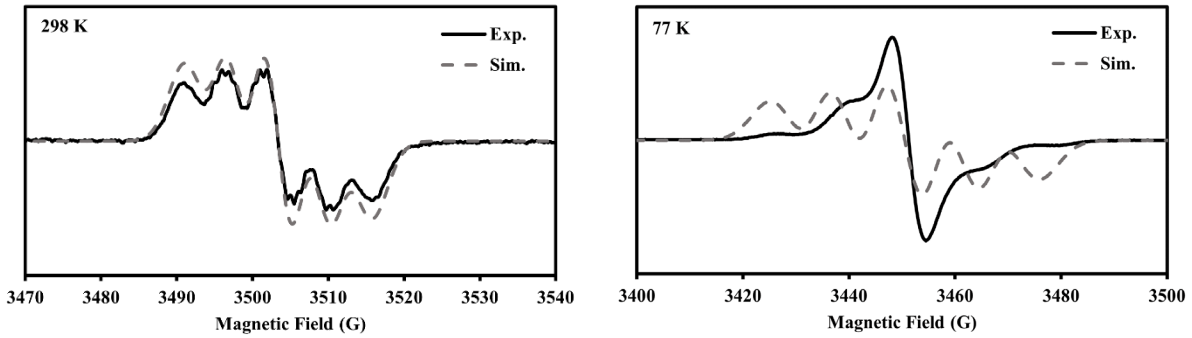

Figure 4.8. Experimental and simulated EPR spectra of **2-Y** at 298 K (left; mode = perpendicular; g_{iso} = 2.00256, A_{iso} = 5.2 G; ν = 9.819 GHz; *P* = 2.021; modulation amplitude = 10.02 mT) and at 77 K (right; mode = perpendicular; g_{iso} = 2.0027, A_{iso} = 10.6 G; ν = 9.674 GHz; *P* = 2.021; modulation amplitude = 10.02 mT).

The EPR spectra are consistent with an organic radical in the 12-membered ring with coupling to two ^{14}N (*I* = 1) nuclei. The spectra match the prediction of the DFT calculations and clearly eliminate the formation of an Y(II) complex, which would be expected to have a two-line pattern based on the nuclear spin of ^{89}Y(*I* = ½).[28, 30] Further characterization of **2-Y** was complicated by its high solubility and X-ray quality single crystals of the product were not isolated. Attempts to make a crystalline analog with 18-crown-6 were similarly unsuccessful.

Conclusion

The allyl complexes $(C_5Me_5)_2Ln(\eta^3\text{-}C_3H_5)$ of Y, Tb, and Dy can deprotonate benzoxazole and form ring-opened 2-isocyanophenolate complexes, $[(C_5Me_5)_2Ln(\mu\text{-}2\text{-}CNC_6H_4O\text{-}\kappa C{:}\kappa O)]_2$, **1-Ln**, as identified by X-ray crystallography. The allyl complexes constitute an effective means to deprotonate a substrate and provide metallocene cations to complex the resulting anion. The **1-Ln** products have central 12-membered metallo-heterocyclic rings that can be reduced to radical species with extensive coupling to the ring components. The experimental results are completely consistent with the electronic structure calculations on the yttrium system.

Experimental Details

All manipulations and syntheses described below were conducted with the rigorous exclusion of air and water using standard Schlenk line and glovebox techniques under an argon or dinitrogen atmosphere. Solvents were sparged with UHP argon and dried by passage through columns containing Q-5 and molecular sieves prior to use. Deuterated NMR solvents were dried over NaK alloy, degassed by three freeze-pump-thaw cycles, and vacuum transferred before use. ^{1}H NMR spectra and ^{13}C{^{1}H} NMR spectra were recorded on Bruker AVANCE600 or GN500 MHz spectrometer operating at 151 MHz or 125 MHz, respectively for ^{13}C at room temperature unless otherwise stated and referenced internally to residual protio-solvent resonances. Elemental analyses were conducted on a Perkin-Elmer 2400 Series II CHNS elemental analyzer. UV-visible spectra were collected at room temperature using a Varian Cary 50 Scan UV-visible spectrophotometer. EPR spectra were collected using X-band frequency (9.3–9.8 GHz) on a Bruker EMX spectrometer equipped with an ER041XG microwave bridge, and the magnetic field

was calibrated with DPPH (g = 2.0036). EPR simulations were performed as least-squares fits of the experimental spectra using the EasySpin software package.[31] Infrared (IR) transmittance measurements were taken as compressed solids on a Thermo Scientific Nicolet iS5 spectrophotometer with an iD5 ATR attachment. 2.2.2-cryptand (Sigma-Aldrich) and 18-crown-6 (Sigma-Aldrich) were placed under vacuum (10^{-3} Torr) before use. Anhydrous $LnCl_3$ (Ln = Y, Tb, Dy),[32] $(C_5Me_5)_2Ln(\eta^3–C_3H_5)$ (Y,[33] Tb,[34] Dy[34]), KC_8,[35] and KC_5Me_5[33] were prepared according to the literature.

Synthesis of $[(C_5Me_5)_2Y(\mu\text{-}2\text{-}CNC_6H_4O\text{-}\kappa C{:}\kappa O)]_2$, 1-Y. In an argon glovebox free of coordinating solvents, a colorless solution of benzoxazole (31 mg, 0.260 mmol) in hexane (5 mL) was added to a bright yellow solution of $(C_5Me_5)_2Y(\eta^3\text{-}C_3H_5)$ (100 mg, 0.250 mmol) in hexane (5 mL). After addition, the reaction mixture immediately became a deep blood red. The deep blood red solution was stirred overnight. The solution was filtered, and insoluble purple solids were discarded. The solvent was removed from the deep red solution under reduced pressure, and the dark red solids were extracted into hexane again (10 mL). The solution was filtered, and the solvent was removed from the deep red solution under reduced pressure, yielding **1-Y** as a blood red solid (107 mg, 0.112 mmol, 90%). Dark red crystals of **1-Y** suitable for X-ray diffraction were grown from a concentrated solution of hexane at –35 °C. ^{1}H NMR (500 MHz, C_6D_6): δ 7.15 (d, 1 H, J_{HH} = 6 Hz, O(C_6H_4)NC), 7.06 (m, 1 H, J_{HH} = 6 Hz, O(C_6H_4)NC), 6.71 (d, 1 H, J_{HH} = 6 Hz, O(C_6H_4)NC), 6.40 (t, 1 H, J_{HH} = 6 Hz, O(C_6H_4)NC), 2.07 (s, 30 H, C_5Me_5). ^{13}C NMR (125 MHz, C_6D_6): δ 167.15 (d, J_{YC} = 24 Hz, O(C_6H_4)N*C*), 137.53 O(C_6H_4)NC), 131.94 O(C_6H_4)NC), 128.96 O(C_6H_4)NC), 125.33 O(C_6H_4)NC), 122.45 O(C_6H_4)NC), 116.85 O(C_6H_4)NC), 115.06 (C_5Me_5), 11.21 (C_5Me_5). IR (cm^{-1}): 3696w, 3667w, 3650w, 3056w, 2961w, 2904m, 2855m, 2723w, 2367w, 2362w, 2358w, 2355w, 2349w, 2324w, 1630w, 1589m, 1571w, 1536w, 1514w, 1496w,

1477w, 1467m, 1452m, 1377w 1345w, 1317m, 1279m, 1279m, 1250w, 1237w, 11944w, 1171w, 1141m, 1106w, 1106w, 1062w, 1020w, 982w, 972w, 937w, 920w, 885w, 887w, 872w, 862w, 803w, 778w, 744s, 609s, 592s, 590s, 578s, 575s, 568w, 562m, 561m, 558s. UV-Vis (hexane) λ = 575 nm, ε = 1980 $M^{-1}cm^{-1}$; λ = 489 nm, ε = 4710 $M^{-1}cm^{-1}$; λ_{max} = 443 nm, ε = 4950 $M^{-1}cm^{-1}$. Anal. Calcd for $C_{54}H_{68}N_2O_2Y_2$: C, 67.90%; H, 7.18%; N, 2.93%. Found: C, 68.16%; H, 7.17%; N, 2.73%.

Synthesis of [$(C_5Me_5)_2Dy(\mu$-2-CNC_6H_4O-$\kappa C:\kappa O)]_2$, 1-Dy. In an analogous procedure to **1-Y**, colorless benzoxazole (38 mg, 0.32 mmol) and deep yellow $(C_5Me_5)_2Dy(\eta^3$-$C_3H_5)$ (150 mg, 0.317 mmol) were combined in hexane (15 mL) to isolate **1-Dy** as a deep blood red solid (143 mg, 0.129 mmol, 81%). Dark red crystals of **1-Dy** suitable for X-ray diffraction were grown from a concentrated solution of hexane at –30 °C. IR (cm^{-1}): 3739w, 3632w, 3378w, 2981w, 2957m, 2921s, 2852m, 2725w, 2361w, 2343w, 2324w, 1631w, 1589w, 1574w, 1559w, 1534w, 1497m, 1497m, 1497m, 1475m, 1446m, 1377w, 1344w, 1344w, 1344w, 1313w, 1289w, 1277m, 1264m, 1253w, 1214w, 1171s, 1151s, 1141s, 1099w, 1031w, 1021w, 985w, 884w, 872w, 811w, 739s, 721w, 676m, 668s, 655w, 649w, 644w, 638w, 633w, 626w, 621s, 614w, 608w, 603m, 595w, 595w, 591w, 588w, 582w, 578s, 573s, 566s, 561s, 556m, 551s. UV-Vis (hexane) λ = 570 nm, ε = 800 $M^{-1}cm^{-1}$; λ = 455 nm, ε = 5620 $M^{-1}cm^{-1}$; λ_{max} = 405 nm, ε = 5620 $M^{-1}cm^{-1}$. Anal. Calcd for $C_{54}H_{68}N_2O_2Dy_2$: C, 58.85%; H, 6.22%; N, 2.54%. Found: C, 60.71%; H, 6.80%; N, 2.31%. Fmla: $C_{61}H_{82}N_2$, matches within 0.2% with inclusion of hexane (C_6H_{14}).

Synthesis of [$(C_5Me_5)_2Tb(\mu$-2-CNC_6H_4O-$\kappa C:\kappa O)]_2$, 1-Tb. In an analogous procedure to **1-Y**, colorless benzoxazole (38 mg, 0.319 mmol) and deep yellow $(C_5Me_5)_2Tb(\eta^3$-$C_3H_5)$ (150 mg, 0.319 mmol) were combined in hexane (15 mL) to isolate **1-Tb** as a deep blood red solid (159 mg, 0.145 mmol, 91%). Dark red crystals of **1-Tb** suitable for X-ray diffraction were grown from a

concentrated solution of hexane at –30 °C. IR (cm^{-1}): 3733w, 3388w, 3061w, 298w, 2964w, 2908m, 2855m, 2729w, 2598w, 2361w, 2344w, 2322w, 1630w, 1582m, 1535w, 1496w, 1667s, 1452s, 1377w, 1341w, 1315s, 1452s, 1377w, 1341w, 1315s, 1278s, 1262m, 1172w, 1141s, 1100w, 1061w, 1034w, 1022w, 988w, 920w, 883w, 870w, 861m, 803w, 790w, 775w, 742s, 694w, 668w, 665w, 644w, 633w, ,627w, 625w, 618w, 614w, 610w, 603m, 595s, 590s, 586m, 579m, 572m, 569m, 567w, 562m, 555w. UV-Vis (hexane) λ = 564 nm, ε = 330 $M^{-1}cm^{-1}$; λ = 489 nm, ε = 1700 $M^{-1}cm^{-1}$; λ_{max} = 415 nm, ε = 2550 $M^{-1}cm^{-1}$). Anal. Calcd for $C_{54}H_{68}N_2O_2Tb_2$: C, 59.23%; H, 6.26%; N, 2.56%. Found: C, 58.84%; H, 6.42%; N, 2.37%.

Reduction of 1-Y to 2-Y. 1-Y (121 mg, 0.126 mmol) and 2.2.2-cryptand (48 mg, 0.126 mmol) were dissolved in THF (3 mL) to form a deep blood red solution. The red solution, a KC_8 column, an EPR tube, a collection vial and several pipets were chilled to –30 °C. The –30 °C solution was passed through the –30 °C KC_8, which resulted in no color change. A small aliquot of the solution was removed, diluted by a factor of three, and frozen in an EPR tube. An EPR spectrum was collected at 77 K and 298 K.

X-ray Data Collection, Structure Solution and Refinement for 1-Y. A red crystal of approximate dimensions 0.221 x 0.226 x 0.318 mm was mounted on a glass fiber and transferred to a Bruker SMART APEX II diffractometer. The APEX2 [36] program package was used to determine the unit-cell parameters and for data collection (20 sec/frame scan time for a sphere of diffraction data). The raw frame data was processed using SAINT [37] and SADABS [38] to yield the reflection data file. Subsequent calculations were carried out using the SHELXTL [39] program. There were no systematic absences nor any diffraction symmetry other than the Friedel condition. The centrosymmetric triclinic space group $P\bar{1}$ was assigned and later determined to be correct. The structure was solved by dual space methods and refined on F^2 by full-matrix least-squares

techniques. The analytical scattering factors [40] for neutral atoms were used throughout the analysis. Hydrogen atoms were included using a riding model. The molecule was a dimmer located about an inversion center. Several atoms were disordered and included using multiple components with partial site-occupancy-factors. There was one molecule of *n*-hexane solvent present. The solvent was located on an inversion center. Least-squares analysis yielded wR2 = 0.0660 and Goof = 1.052 for 394 variables refined against 6472 data (0.74 Å), R1 = 0.0271 for those 5882 data with I > 2.0σ(I).

X-ray Data Collection, Structure Solution and Refinement for 1-Tb. A violet crystal of approximate dimensions 0.159 x 0.177 x 0.261 mm was mounted in a cryoloop and transferred to a Bruker SMART APEX II diffractometer. The APEX2 [36] program package was used to determine the unit-cell parameters and for data collection (45 sec/frame scan time for a sphere of diffraction data). The raw frame data was processed using SAINT [37] and SADABS [38] to yield the reflection data file. Subsequent calculations were carried out using the SHELXTL [39] program. There were no systematic absences nor any diffraction symmetry other than the Friedel condition. The centrosymmetric triclinic space group $P\bar{1}$ was assigned and later determined to be correct. The structure was solved by dual space methods and refined on F^2 by full-matrix least-squares techniques. The analytical scattering factors [40] for neutral atoms were used throughout the analysis. Hydrogen atoms were included using a riding model. The molecule was a dimmer and located about an inversion center. Disordered atoms were included using multiple components with partial site-occupancy-factors. There was one molecule of *n*-hexane present. The solvent was located on an inversion center. Least-squares analysis yielded wR2 = 0.0382 and Goof = 1.075 for 404 variables refined against 7620 data (0.73 Å), R1 = 0.0165 for those 6400 data with I > 2.0σ(I).

X-ray Data Collection, Structure Solution and Refinement for 1-Dy. A violet crystal of approximate dimensions 0.100 x 0.170 x 0.348 mm was mounted on a glass fiber and transferred to a Bruker SMART APEX II diffractometer. The APEX2 [36] program package was used to determine the unit-cell parameters and for data collection (30 sec/frame scan time for a sphere of diffraction data). The raw frame data was processed using SAINT [37] and SADABS [38] to yield the reflection data file. Subsequent calculations were carried out using the SHELXTL [39] program. There were no systematic absences nor any diffraction symmetry other than the Friedel condition. The centrosymmetric triclinic space group $P\bar{1}$ was assigned and later determined to be correct. The structure was solved by dual space methods and refined on F^2 by full-matrix least-squares techniques. The analytical scattering factors [40] for neutral atoms were used throughout the analysis. Hydrogen atoms were included using a riding model. The molecule was a dimmer located about an inversion center. Several atoms were disordered and included using multiple components with partial site-occupancy-factors. There was one molecule of n-hexane solvent present. The solvent was located on an inversion center. Least-squares analysis yielded wR2 = 0.0592 and Goof = 1.077 for 304 variables refined against 6491 data (0.74 Å), R1 = 0.0241 for those 6052 data with $I > 2.0\sigma(I)$.

Computational Details. DFT calculations were performed by Justin C. Wedal of the Evans Group in collaboration with the research group of Filipp Furche and completed using the TPSSh hybrid meta-generalized gradient density functional approximation.[41] For TDDFT of **1-Ln**, A Gaussian line broadening of 0.15 eV was applied and the computed excitation energies were empirically red shifted by 0.1 eV. To ease comparison, the computed intensities were scaled by a factor of 0.5. Effective core potentials (ECPs)[42] with polarized triple-ζ (def2-TZVP[43]) basis sets were used for Y and split-valence basis sets with polarization for non-hydrogen atoms (def2-

SV(P)[44]) were used elsewhere. For TDDFT of **2-Y**, the vertical electron affinity of **1-Y** was computed using spin-unrestricted Kohn-Sham DFT theory. To account for solvation of this radical anion species, the polarizable continuum model COSMO[45] for THF (ε = 7.52) was used.[46] A Gaussian line broadening of 0.15 eV was applied and the computed intensities were scaled by a factor of 0.5 to ease comparison. All calculations were performed with TURBOMOLE V7.4.1.[47,48]

References

(1) Dunwell, D. W.; Evans, D. *J. Med. Chem.* **1977,** *20*, 797-801.

(2) Chaney, M. O.; Demarco, P. V.; Jones, N. D.; Occolowitz, J. L. *J. Am. Chem. Soc.* **1974,** *96*, 1932-1933.

(3) Taki, M.; Wolford, J. L.; O'Halloran, T. V. *J. Am. Chem. Soc.* **2004,** *126*, 712-713.

(4) Sawada, Y.; Yanai, T.; Nakagawa, H.; Tsukamoto, Y.; Yokoi, S.; Yanagi, M.; Toya, T.; Sugizaki, H.; Kato, Y.; Shirakura, H.; Watanabe, T.; Yajima, Y.; Kodama, S.; Masui, A. *Pest Management Science* **2003,** *59*, 25-35.

(5) Corro, M.; Besora, M.; Maya, C.; Álvarez, E.; Urbano, J.; Fructos, M. R.; Maseras, F.; Pérez, P. J. *ACS Catalysis* **2014,** *4*, 4215-4222.

(6) Teo, Y. C.; Riduan, S. N.; Zhang, Y. *Green Chemistry* **2013,** *15*, 2365-2368.

(7) Nguyen, T. B.; Ermolenko, L.; Al-Mourabit, A. *J. Am. Chem. Soc.* **2013,** *135*, 118-121.

(8) Yao, L.; Zhou, Q.; Han, W.; Wei, S. *Eur. J. Org. Chem.* **2012,** *2012*, 6856-6860.

(9) Ai, W.; Zhou, W.; Du, Z.; Du, Y.; Zhang, H.; Jia, X.; Xie, L.; Yi, M.; Yu, T.; Huang, W. *J. Mater. Chem.* **2012,** *22*, 23439-23446.

(10) Viirre, R. D.; Evindar, G.; Batey, R. A. *J. Org. Chem.* **2008,** *73*, 3452-3459.

(11) Do, H.-Q.; Daugulis, O. *J. Am. Chem. Soc.* **2007,** *129*, 12404-12405.

(12) Hahn, F. E.; Tamm, M.; Lügger, T. *Angew. Chem. Int. Ed.* **1994,** *33*, 1356-1359.

(13) Hahn, F. E.; Tamm, M. *Chem. Commun.* **1993**, 842-844.

(14) Hahn, F. E.; Tamm, M. *J. Organomet. Chem.* **1993,** *456*, C11-C14.

(15) Ng, C.-O.; Yiu, S.-M.; Ko, C.-C. *Inorg. Chem.* **2014,** *53*, 3022-3031.

(16) Hahn, F. E.; Klusmann, D.; Pape, T. *Eur. J. Inorg. Chem.* **2008,** *2008*, 4420-4424.

(17) An, J.; van Niekerk, L.; Esterhuysen, C.; Raubenheimer, H. G. *Dalton Trans.* **2002**, 2386-2389.

(18) Liu, W.; Sun, Y.; Zhao, H.; Li, B.; Chen, S. *ChemCatChem* **2016,** *8*, 2894-2897.

(19) Den Haan, K. H.; Luinstra, G. A.; Meetsma, A.; Teuben, J. H. *Organometallics* **1987,** *6*, 1509-1515.

(20) Evans, W. J.; Fujimoto, C. H.; Ziller, J. W. *Organometallics* **2001,** *20*, 4529-4536.

(21) Shannon, R. D. *Acta Crystallogr. Sect. A: Found. Crystallogr.* **1976,** *32*, 751-767.

(22) MacDonald, M. R.; Langeslay, R. R.; Ziller, J. W.; Evans, W. J. *J. Am. Chem. Soc.* **2015,** *137*, 14716-14725.

(23) Den Haan, K. H.; De Boer, J. L.; Teuben, J. H.; Smeets, W. J. J.; Spek, A. L. *J. Organomet. Chem.* **1987,** *327*, 31-38.

(24) Evans, W. J.; Montalvo, E.; Champagne, T. M.; Ziller, J. W.; DiPasquale, A. G.; Rheingold, A. L. *Organometallics* **2009,** *28*, 2897-2903.

(25) Ryan, A. J.; Ziller, J. W.; Evans, W. J. *Chem. Sci.* **2020,** *11*, 2006-2014.

(26) Moehring, S. A.; Miehlich, M.; Hoerger, C. J.; Meyer, K.; Ziller, J. W.; Evans, W. J. *Inorg. Chem.* **2020,** *59*, 3207-3214.

(27) Jenkins, T. F.; Woen, D. H.; Mohanam, L. N.; Ziller, J. W.; Furche, F.; Evans, W. J. *Organometallics* **2018,** *37*, 3863-3873.

(28) MacDonald, M. R.; Ziller, J. W.; Evans, W. J. *J. Am. Chem. Soc.* **2011,** *133*, 15914-15917.

(29) Fang, M.; Lee, D. S.; Ziller, J. W.; Doedens, R. J.; Bates, J. E.; Furche, F.; Evans, W. J. *J. Am. Chem. Soc.* **2011,** *133*, 3784-3787.

(30) Fieser, M. E.; MacDonald, M. R.; Krull, B. T.; Bates, J. E.; Ziller, J. W.; Furche, F.; Evans, W. J. *J. Am. Chem. Soc.* **2015,** *137*, 369-382.

(31) Stoll, S.; Schweiger, A. *Journal of Magnetic Resonance* **2006,** *178*, 42-55.

(32) Taylor, M. D. *Chem. Rev.* **1962,** *62*, 503-511.

(33) Evans, W. J.; Kozimor, S. A.; Brady, J. C.; Davis, B. L.; Nyce, G. W.; Seibel, C. A.; Ziller, J. W.; Doedens, R. J. *Organometallics* **2005,** *24*, 2269-2278.

(34) Demir, S.; Zadrozny, J. M.; Nippe, M.; Long, J. R. *J. Am. Chem. Soc.* **2012,** *134*, 18546-18549.

(35) Bergbreiter, D. E.; Killough, J. M. *J. Am. Chem. Soc.* **1978,** *100*, 2126-2134.

(36) *Apex2 Version 2014.11-0*, Bruker AXS: Madison, WI, 2014.

(37) *SAINT Version 8.36a*, Bruker AXS, Inc.: Madison, WI, 2013.

(38) Sheldrick, G. M. *SADABS, Version 2014/5*, Bruker AXS, Inc.: Madison, WI 2014.

(39) Sheldrick, G. M. *SHELXTL, Version 2014/7*, Bruker AXS, Inc.: Madison, WI, 2014.

(40) *International Tables for Crystallography*; Dordrecht: Kluwer Academic Publishers 1992; Vol. C.

(41) Staroverov, V. N.; Scuseria, G. E.; Tao, J. M.; Perdew, J. P. *J. Chem. Phys.* **2003,** *119*, 12129-12137.

(42) Andrae, D.; Häußermann, U.; Dolg, M.; Stoll, H.; Preuß, H. *Theor. Chem. Acc.* **1990,** *77*, 123-141.

(43) Weigend, F.; Ahlrichs, R. *Phys. Chem. Chem. Phys.* **2005,** *7*, 3297-3305.

(44) Schäfer, A.; Horn, H.; Ahlrichs, R. *J. Chem. Phys.* **1992,** *97*, 2571-2577.

(45) Schäfer, A.; Klamt, A.; Sattel, D.; Lohrenz, J. C. W.; Eckert, F. *Phys. Chem. Chem. Phys.* **2000,** *2*, 2187-2193.

(46) 81 ed.; CRC Press: Boca Raton, FL, 2008; p 136.

(47) Balasubramani, S. G.; Chen, G. P.; Coriani, S.; Diedenhofen, M.; Frank, M. S.; Franzke, Y. J.; Furche, F.; Grotjahn, R.; Harding, M. E.; Hättig, C.; Hellweg, A.; Helmich-Paris, B.; Holzer, C.; Huniar, U.; Kaupp, M.; Marefat Khah, A.; Karbalaei Khani, S.; Müller, T.; Mack, F.; Nguyen, B. D.; Parker, S. M.; Perlt, E.; Rappoport, D.; Reiter, K.; Roy, S.; Rückert, M.; Schmitz, G.; Sierka, M.; Tapavicza, E.; Tew, D. P.; van Wüllen, C.; Voora, V. K.; Weigend, F.; Wodyński, A.; Yu, J. M. *J. Chem. Phys.* **2020,** *152*, 184107.

(48) *TURBOMOLE V7.4.1 2019, a development of University of Karlsruhe and Forschungszentrum Karlsruhe GmbH, 1989-2007, TURBOMOLE GmbH, since 2007; available from http://www.turbomole.com.*

EPILOGUE

Collectively, the synthesis and reactivity of +2 rare earth metal ion complexes described in this dissertation, as well as results reported in the literature, appears to be influenced by three factors, at least. These include: 1) electron donating strength of the ancillary ligands 2) steric saturation of the complex from the ligand environment, and 3) identity of the rare earth metal.

Previous electrochemical studies by Bercaw et al. and Lappert et al. suggested that alkyl substituents on cyclopentadienyl ligands render the ligand more electron donating while silyl substituents have a contrary effect.[1, 2] However, as described in the Introduction, the silyl-substituted $(C_5H_4SiMe_3)_3^{3-}$ ligand set allowed for the isolation of new Ln^{2+} ions for the entire series of rare earth metals as well as the alkyl substituted $(C_5Me_4H)_3^{3-}$ ligand set, described in Chapter 2. Based on these results, no correlation between ancillary ligand strength and +2 ion thermal stability is readily apparent.

Steric factors play an important role in rare earth metal chemistry.[3] Specifically, the steric saturation of ligand environment can influence the stability of +2 rare earth metal ions. For example, the $(C_5Me_4H)_3^{3-}$ ligand environment allowed for +2 ions to be isolable for the metals La, Ce, Pr, Nd, Sm, Gd, Tb, and Dy while the $(C_5Me_5)_3^{3-}$ ligand set is sterically crowded and consequently cannot stabilize Ln(II) ions. In addition, comparison of the mono- and di- silyl substituted cyclopentadienyl ligands, as discussed in Chapter 1, show that the smaller, mono-silyl substituted Cp ligand set can allow for the entire series of Ln(II) ions to be isolated, while the larger, di-silyl substituted Cp ligand set only allows the larger metals La, Ce, Pr, Nd to be isolated.

Moreover, in the heteroleptic Ln^{2+} complexes described in Chapter 3; the steric factors of the ancillary ligands are similar. In fact, by replacing one C_5Me_5 ligand for an amide, NR_2 (R =

$SiMe_3$), the first C_5Me_5 containing complex of a new Ln^{2+} ion was isolated. Similarly, for C_5Me_4H, the $(C_5Me_4H)_3^{3-}$ ligand environment is too sterically crowded to render Y^{2+} isolable, but by replacing a C_5Me_4H ligand with an NR_2 ligand, an Y^{2+} complex can be generated with slightly better thermal stability than the homoleptic analogue. Likewise, in Appendix B, the impact of exchanging the NR_2 ligand for an $OAr^{tBu,tBu,Me}$ ligand affected the thermal stability of the Y^{2+} complex. Clearly, steric factors of the ligands play an important role in heteroleptic Ln(II) complexes as well.

In terms of the identity of the rare earth metal ion, size is the predominant factor. As described above, only the larger rare earth metals were isolable using the larger ligand, $C_5H_3(SiMe_3)_2$, compared with the entire series of Ln^{2+} with the ligand, $C_5H_4SiMe_3$. As described in Appendix B, efforts to synthesize and reduce $(C_5Me_5)_2Ln(NR_2)$ complexes for Ce, Nd, and Lu reveal a similar pattern. The Ce and Nd complexes can be reduced and are more thermally stable than the Y analogue, while the Lu complex is less thermally stable than Y. This is consistent with the trend in ionic radii for these elements Ce and Nd are larger than Y which is larger than Lu.[4] This means that as the metal center gets smaller, the steric saturation of the complex increases, and lowers the thermal stability of the Ln(II) complex.

In conclusion, the stability of +2 complexes appears to involve a relationship between steric and electronic factors of the ligands as well as the identity of the rare earth metal ion. Consequently, through judicious choice of the ancillary ligands and rare earth metal, heteroleptic Ln^{2+} complexes should be isolable for the entire series of metals.

References

(1) Cassani, M. C.; Duncalf, D. J.; Lappert, M. F. *J. Am. Chem. Soc.* **1998,** *120*, 12958-12959.

(2) Zachmanoglou, C. E.; Docrat, A.; Bridgewater, B. M.; Parkin, G.; Brandow, C. G.; Bercaw, J. E.; Jardine, C. N.; Lyall, M.; Green, J. C.; Keister, J. B. *J. Am. Chem. Soc.* **2002,** *124*, 9525-9546.

(3) Evans, W. J. *Inorg. Chem.* **2007,** *46*, 3435-3449.

(4) Shannon, R. D. *Acta Crystallogr. Sect. A: Found. Crystallogr.* **1976,** *32*, 751-767.

APPENDIX A

Reactivity of [K(crypt)][$(C_4Me_5H)_3Ln$] (Ln = La, Ce) with *tert*-Butyl Isocyanide

Introduction

As described in Chapter 2, Ln^{2+} ions were successfully isolated and crystallographically-characterized for La, Ce, Pr, Nd, Sm, Gd, Tb, and Dy by reduction of the homoleptic compounds, $Cp^{tet}_3Ln^{III}$ ($Cp^{tet} = C_5Me_4H$), which formed $(Cp^{tet}_3Ln^{II})^{1-}$ products, eq. A.1. Sm and Dy adopted "traditional" $4f^{n+1}$ electron configurations, while the other metals were assigned "non-traditional " $4f^n5d^1$ configurations based on UV-visible spectroscopic and structural analyses corroborated by DFT calculations. These $4f^n5d^1$ ions were more stable for the larger metals, La and Ce, than for the smaller metal, Tb. This Appendix describes the reactivity of the [K(crypt)][$(C_5Me_4H)_3Ln$] for Ln = La, Ce with *tert*-butyl isocyanide, $Me_3C–N{\equiv}C$.

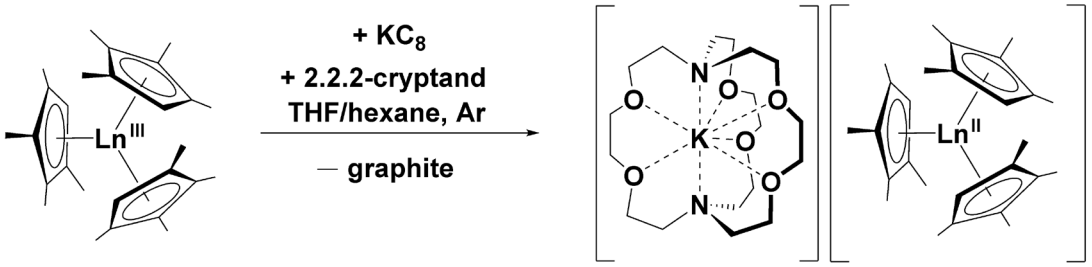

(A.1)

Ln = La, Ce, Pr, Nd, Sm, Gd, Tb, Dy

Reactions with *tert*-butyl isocyanide and rare earth metals have been previously reported with the $(C_5Me_5)_3^{3-}$ ligand system.[1, 2] The tris-pentamethyl analogues of the tris-tetramethylcyclopentadienyl complexes, $(C_5Me_5)_3Ln$, are sterically crowded and display unusual reactivity.[3] Reactions of $(C_5Me_5)_3Ln$ for Ln = La, Nd, and Sm, with *tert*-butyl isocyanide displayed different reactivity for Sm compared to La and Nd. The Sm complex, $(C_5Me_5)_3Sm$, formed a trimetallic product, $[(C_5Me_5)_2Sm(CNCMe_3)(\mu\text{-}CN)]_3$, while the La and Nd complexes formed

adducts, $[(C_5Me_5)_3Ln(CNCMe_3)_n]$ (Ln = La, n = 2; Ln = Nd, n = 1). However, these complexes involve Ln(III) ions. Consequently, the reactivity of $[K(crypt)][(C_5Me_4H)_3Ln^{II}]$ with *tert*-butyl isocyanide was investigated with the most stable non-traditional Ln^{2+} ions, La and Ce.

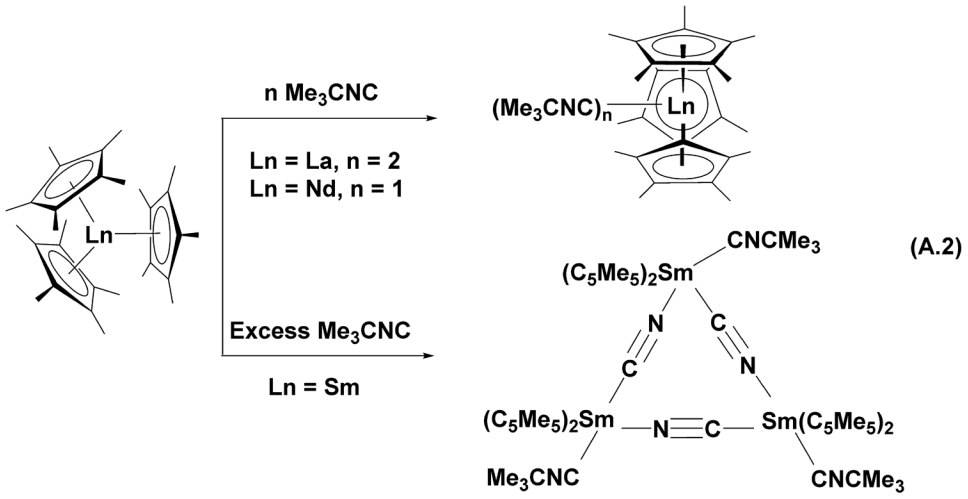

(A.2)

Results & Discussion

Treatment of a dark blue THF solution of $[K(crypt)][(C_5Me_4H)_3Ln]$ with a slight excess of *tert*-butyl isocyanide, added via syringe, at room temperature, resulted in dark yellow/ orange solutions, Ln = La, **1**; Ln = Ce, **2**, which generated an EPR active species. The 298 K EPR spectra of **1** and **2** in Figures A.1 and A.2, respectively, contain isotropic signals with hyperfine coupling. The 298 K spectrum of **1** contains a multi-line pattern, which may indicate coupling between ^{139}La (I = 7/2) and ^{14}N (I = 1), Fig A.1. The assignment of this pattern was challenging to identify, but the g_{iso} value was found to be 1.92. The 298 K spectrum of **2** contains a three-line hyperfine pattern consistent with an ^{14}N-centered organic radical, with an A_{iso} value of 13.0 G and a g_{iso} value of 2.003, Fig A.2. The 77 K EPR spectrum of **1** contains unresolved hyperfine coupling, complicating the assignment of this signal as axial or rhombic, Fig A.1. The 77 K EPR spectrum of **2** contains a rhombic signal with g_x = 2.022, g_y = 2.003, and g_z = 1.979 and no hyperfine coupling, Fig A.2.

This is consistent with a carbon centered radical since the only carbon isotope with a non-zero nuclear spin, ^{13}C, is not abundant enough to detect.

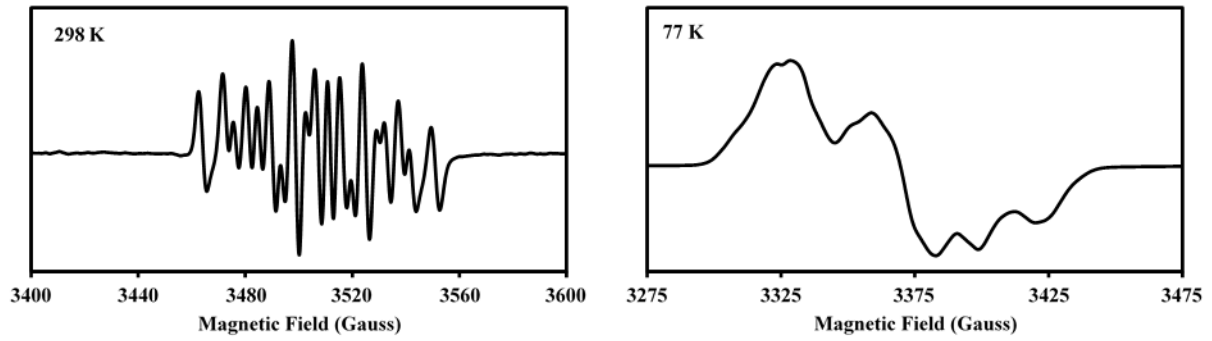

Figure A.1. X-band EPR experimental spectra of **1** obtained by collected at 298 K (left; mode: perpendicular; g_{iso} = 1.92; ν = 9.838 GHz; *P* = 2.154 mW; modulation amplitude = 4.0 G) and 77K (right; mode: perpendicular; ν = 9.433 GHz; *P* = 0.2154 mW; modulation amplitude = 4.0 G).

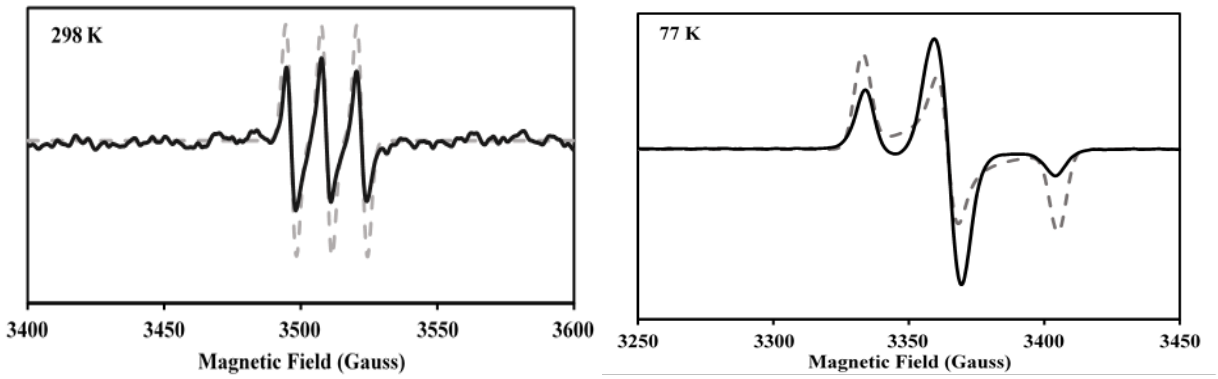

Figure A.2. X-band EPR experimental (solid line) and simulated (dotted line) spectra of **2** obtained by collected at 298 K (left; mode: perpendicular; g_{iso} =2.003; A_{iso} = 13.0 G; ν = 9.836 GHz; *P* = 2.155 mW; modulation amplitude = 4.0 G) and 77K (right; mode: perpendicular; g_x = 2.022, g_y =2.003, g_z =1.979; ν = 9.432 GHz; *P* = 2.156 mW; modulation amplitude = 4.0 G).

These reactions could be performed at room temperature or −35°C with no differences in reactivity. Two different crystals were isolated following repeated addition of tBu–NC to THF solutions of [K(crypt)][$(C_5Me_4H)_3Ln$] at room temperature. When the THF solution was layered under chilled Et_2O and placed in freezer at −35 °C, small colorless crystals were obtained overnight, which were determined to be [K(crypt)][CN]. Evidently a reductive N–C bond cleavage occurred, removing a tert-butyl group, and generating a cyanide anion. This can be attributed to the highly reducing La(II) ion present and has precedent in Sm(II) chemistry.[1, 3]

Another attempt to crystallize the reaction products yielded small colorless crystals determined to be [K(crypt)][^{t}Bu–NH–COO]. The carbamate anion presumably is a product of hydrolysis. The presence of water is confirmed based on the water molecules present in this crystal structure as well as the structure of [K(crypt)][CN] described above.

The ORTEP diagrams of the two crystal structures are shown in Figures A.3 and A.4, respectively. Both crystal structures feature $[K(crypt)]^+$ countercations (crypt = 2.2.2-cryptand) with no water is bound to the K^+ ions. The cyanide structure contains a C–N bond distance of 1.130(2) Å. Powder diffraction crystallographic methods determined the C–N bond distance to be 1.15 Å, while reported crystallographic data on H–CN, determined the C–N bond distance to be 1.16 Å.[4] In the cyanide structure, a hydrogen bonding interaction occurs between N(3) from the cyano unit with a proton from a neighboring water molecule. One hydrogen of the water molecule is oriented toward N3, at a distance of 2.16(2) Å, while the oxygen from the water, O7, is farther away, 2.978(2) Å. The N–H–O angle is close to 180°, with the unbound H atom pointing away from the $[K(crypt)]^{1+}$ countercation.

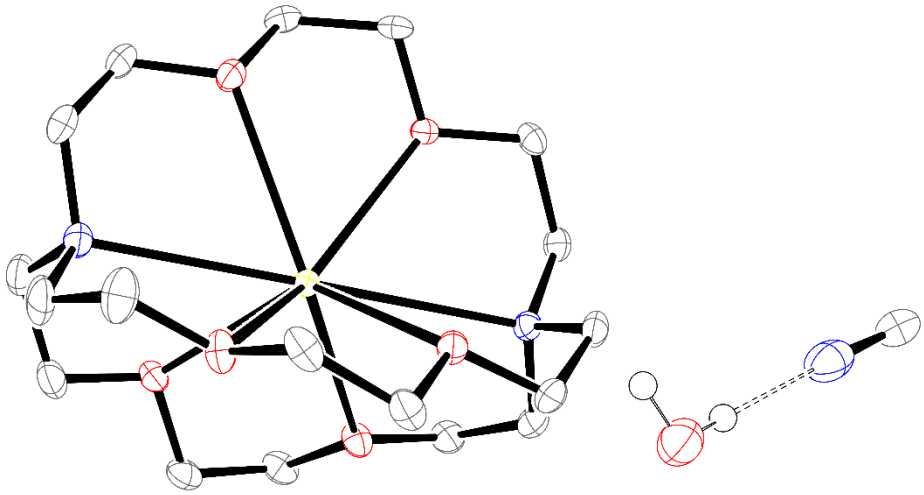

Figure A.3. Displacement ellipsoid plot of [K(crypt)][CN]·H_2O with $[K(crypt)]^{1+}$ countercations included with ellipsoids drawn at the 50% probability level. Hydrogen atoms are included only for water, all other atoms excluded for clarity. Hydrogen bonds shown as double dashed lines.

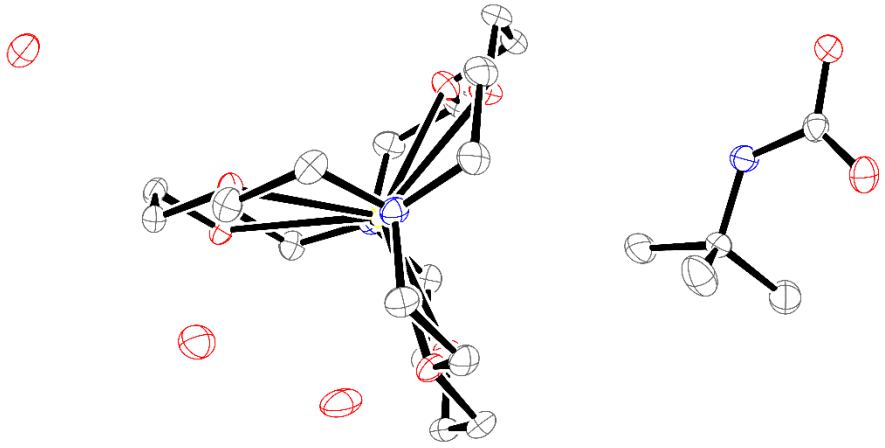

Figure A.4. Displacement ellipsoid plot of [K(crypt)][^{t}Bu–NH–COO] with $[K(crypt)]^{1+}$ countercations included with ellipsoids drawn at the 50% probability level. Hydrogen atoms are excluded for clarity.

Conclusion

Reactions of the complexes, $(Cp^{tet}_3Ln)^{1-}$ (Ln = La, Ce), with tBu–NC, generated solutions that were EPR active, but no crystallographic data were obtainable on Ln-containing compounds. The only crystals isolated were identified as products of C-C bond cleavage, [K(crypt)][CN], and hydrolysis, [K(crypt)][tBu–NH–COO].

Experimental Details

All manipulations and syntheses described below were conducted with the rigorous exclusion of air and water using standard Schlenk line and glovebox techniques under an argon or dinitrogen atmosphere. Solvents were sparged with UHP argon and dried by passage through columns containing Q-5 and molecular sieves prior to use. [K(crypt)][$(C_5Me_4H)_3$Ln] for Ln = La, Ce were prepared as previously described.[5] *tert*-Butyl isocyanide was dried over molecular sieves and degassed by three freeze-pump-thaw cycles under 10^{-5} Torr before use.

Reaction of tBu–NC with [K(crypt)][$(C_5Me_4H)_3$La]. Treatment of a dark blue 5mL THF solution of (50 mg) [K(crypt)][$(C_5Me_4H)_3$La] with a slight excess of tert-butyl isocyanide, added dropwise, at room temperature resulted in a dark yellow/ orange solution which was layered under Et_2O. The THF/Et_2O mixture was placed in freezer at −35 °C. Overnight, small colorless crystals were obtained which were determined to be [K(crypt)][CN]. Another attempt to crystallize the reaction products yielded small colorless crystals determined to be [K(crypt)][^{t}Bu–NH–COO].

Reaction of tBu–NC with [K(crypt)][$(C_5Me_4H)_3$Ce]. Treatment of a dark blue 5mL THF solution of (50 mg) [K(crypt)][$(C_5Me_4H)_3$Ce] with a slight excess of tert-butyl isocyanide, added dropwise, at room temperature resulted in a dark yellow/ orange solution which was layered under Et_2O. The THF/Et_2O mixture was placed in freezer at −35 °C.

References

(1) Evans, W. J.; Drummond, D. K. *Organometallics* **1988,** *7*, 797-802.

(2) Evans, W. J.; Mueller, T. J.; Ziller, J. W. *Chem. Eur. J.* **2010,** *16*, 964-975.

(3) Evans, W. J. *Inorg. Chem.* **2007,** *46*, 3435-3449.

(4) Dulmage, W. J.; Lipscomb, W. N. *Acta Crystallographica* **1951,** *4*, 330-334.

(5) Jenkins, T. F.; Woen, D. H.; Mohanam, L. N.; Ziller, J. W.; Furche, F.; Evans, W. J. *Organometallics* **2018,** *37*, 3863-3873.

APPENDIX B

Attempts to Synthesize Cp^X_2LnA Complexes for Reduction Studies

($Cp^X = C_5Me_4H, C_5Me_5$; Ln = Nd, Sm, Y, Lu; A = $N(SiMe_3)_2$, $OAr^{t\text{-}Bu,t\text{-}Bu,Me}$, BH_4)

Introduction

As described in Chapter 3, heteroleptic yttrium complexes of the type $Cp^X_2Y^{III}(NR_2)$ (Cp^X = C_5Me_5, C_5Me_4H; R = $SiMe_3$) can be reduced in THF in the presence of 2.2.2-cryptand (crypt) with KC_8 to form $[K(crypt)][Cp^X_2Y^{II}(NR_2)]$ products which decompose to $[K(crypt)][Cp^X_2Y^{III}\{N(SiMe_3)(SiMe_2CH_2)$-$\kappa$C,$\kappa$N$\}]$. This heteroleptic Y^{2+} complex is the first crystallographically-characterized complex of a non-traditional ion with C_5Me_5 as a ligand. This is significant because C_5Me_5 is well established rare earth chemistry as an suitable ligand for stabilizing and crystallizing Ln-containing compounds.[1] Comparisons between the heteroleptic C_5Me_5 complex and the C_5Me_4H complex revealed that the C_5Me_5 complex was slightly more thermally stable, although both complexes decomposed significantly before crystallographic evidence was obtained. This Appendix describes the synthesis of heteroleptic Ln(II) complexes to explore the generality of the $Cp^X_2Ln(NR_2)$ system to other rare earth metals (Ln = Ce, Nd, Sm, Lu) as well as explore the generality of the $Cp^*_2Y(A)$ system to other anionic ligands (A = BH_4, $OAr^{tBu,tBu,Me}$).

Since the isolation and crystallographic-characterization of the rare earth metal series in the +2 oxidation state in the homoleptic $(Cp'_3Ln)^{1-}$ series, the thermal stability of these new $4f^n5d^1$ ions has been of paramount importance.[2] Comparison of the thermal stability of the $(Cp'_3Ln)^{1-}$ series and the isolable $(Cp''_3Ln)^{1-}$ complexes which are only known for the largest rare earth metals, Ln = La, Ce, Pr, and Nd, suggests that the size and number of substituents on the

cyclopentadienyl ring plays an important role in allowing Ln(II) ions to be thermally stable enough to isolate.[3] Since Cp″ contains one more $SiMe_3$ group than Cp′, Cp″ occupies more space and thus, only the largest rare earth metals can be stabilized in the $Cp''_3{}^{3-}$ ligand environment. Consequently, since the heteroleptic complex, $Cp^X_2Y(NR_2)$, was not thermally stable enough to generate a purely Y(II) system for crystallographically-characterization, the identity of the metal was investigated in this ligand framework for Ce, Nd, Sm, and Lu. Similarly, while the homoleptic $(C_5Me_5)_3Ln$ complexes are sterically overcrowded species that display unusual reactivity for Ln(III) ions and are not stable species upon reduction[4], by exchanging one C_5Me_5 ligand for a NR_2 ligand, an Y(II) ion was successfully generated upon reduction of a Y(III) precursor, although the complex had limited thermal stability. Subsequently, the thermal stability of $[(C_5Me_5)_2Y(A)]^{1-}$ complexes was investigated for A = BH_4, $OAr^{tBu,tBu,Me}$.

Results & Discussion

$(C_5Me_5)_2Y(A)$ (A = BH_4, $OAr^{tBu,tBu,Me}$). The heteroleptic complex, $(C_5Me_5)_2Y(BH_4)$, was previously reported from the Evans group but the reductive capabilities of this complex were not established. Treatment of a THF solution at – 35 °C or – 78 °C of $(C_5Me_5)_2Y(BH_4)$ in the presence of 2.2.2-cryptand (crypt) and KC_8 generated a dark blue solution, **1**, that rapidly lost color within 5 minutes. The thermal instability of this complex precluded characterization via UV-visible and EPR spectroscopy. The heteroleptic complex, $(C_5Me_5)_2Y(OAr^{tBu,tBu,Me})$, was synthesized for reductive studies. Treatment of a THF solution at – 35 °C of $(C_5Me_5)_2Y(OAr^{tBu,tBu,Me})$ in the presence of crypt and KC_8 generated a dark blue solution, **2**, with UV-visible and EPR spectroscopic data indicative of Y(II), although crystallographic-characterization was unsuccessful. The 298 K EPR spectrum of **2** contains a two-line hyperfine pattern, consistent with ^{89}Y (I = ½), Figure B.1. The data were best simulated with g_{iso} = 1.981 and A_{iso} = 83.5 G. The 77

K EPR spectrum of **2** is similar to the 77 K EPR spectra obtained for $[(C_5Me_5)_2Y^{II}(NR_2)]^{1-}$, Figure B.1. Specifically, a rhombic signal is observed which was best modeled as $g_x = 2.000$, $g_y = 1.985$, and $g_z = 1.959$ and hyperfine values of $A_x = 73.7$ G, $A_y = 80.3$ G, and $A_z = 74.2$ G.

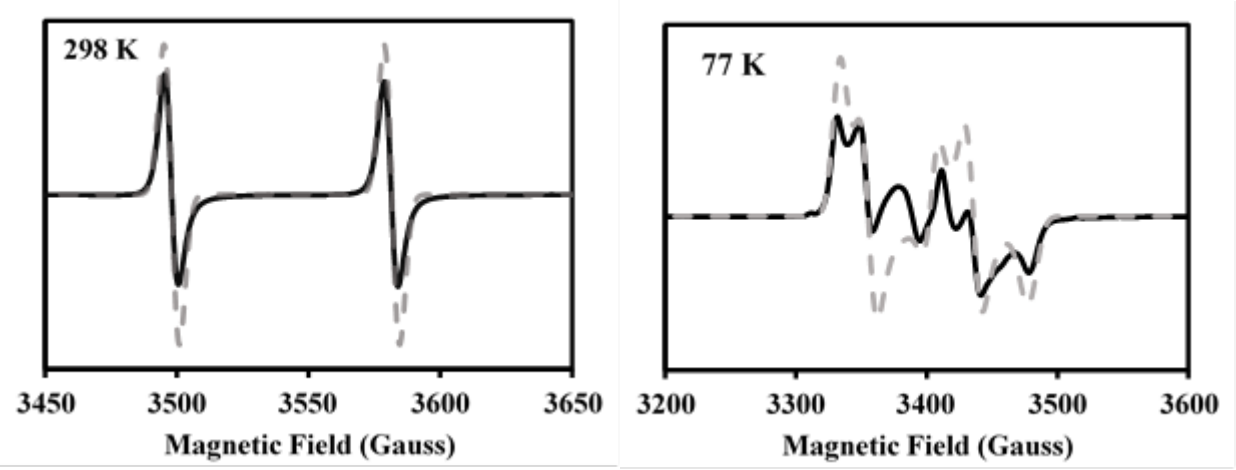

Figure B.1. X-band EPR experimental (solid line) and simulated (dotted line) spectra of **2** obtained by reduction of $(C_5Me_5)_2Y(OAr^{tBu,tBu,Me})$ collected at 298 K (left; mode: perpendicular; g_{iso} = 1.981; A_{iso} = 83.5 G; ν = 9.816 GHz; P = 0.002151 mW; modulation amplitude = 4.0 G) and 77K (right; mode: perpendicular; $g_x = 2.000$, $g_y = 1.985$, $g_z = 1.959$; $A_x = 73.7$ G, $A_y = 80.3$ G, $A_z = 74.2$ G; ν = 9.435 GHz; P = 0.002153 mW; modulation amplitude = 4.0 G).

UV-visible spectroscopy collected on **2** reveals that the absorption spectrum of **2** is similar to the reported spectra for $Cp^X_2Y(NR_2)$, Figure B.2. The absorptivities reported are calculated assuming complete reduction of the Y(III) complex, thus these values can be considered underestimates. Specifically, three absorptions were identified with ε values > 1000 $M^{1-}cm^{1-}$ like those for the NR_2 analogue. These values are consistent with the formation of Y(II).[2, 5-7]

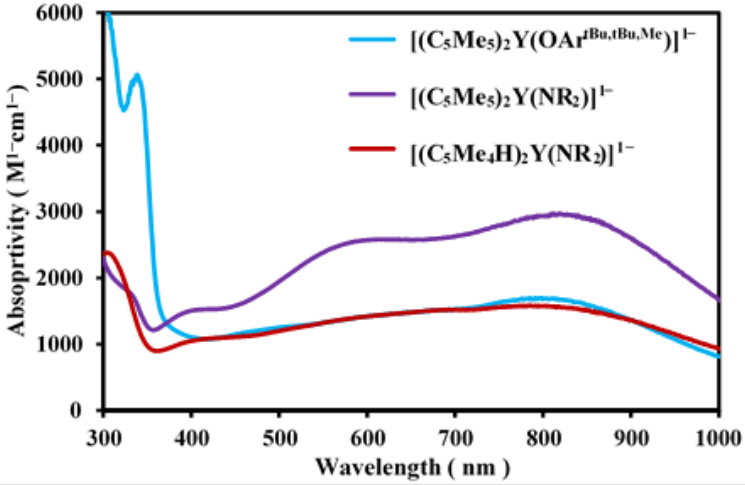

Figure B.2. UV-visible spectrum of **2,** solution formed upon reducing $(C_5Me_5)_2Y(OAr^{tBu,tBu,Me})$, plotted with $[(C_5Me_5)_2Y(NR_2)]^{1-}$ and $[(C_5Me_4H)_2Y(NR_2)]^{1-}$ for comparison.

$(C_5Me_5)_2Ln(NR_2)$ (Ln = Ce, Nd, Sm, Lu). The $(C_5Me_5)_2Ln(NR_2)$ complex has been previously reported for Ce as well as Sm. The C_5Me_4H analogue has not been reported for Sm but was synthesized during these studies although crystallographic evidence was not obtained. However, the analogous Lu complex, $(C_5Me_5)_2Lu(NR_2)$ was synthesized using the same procedure and was crystallographically characterized, Figure B.3.

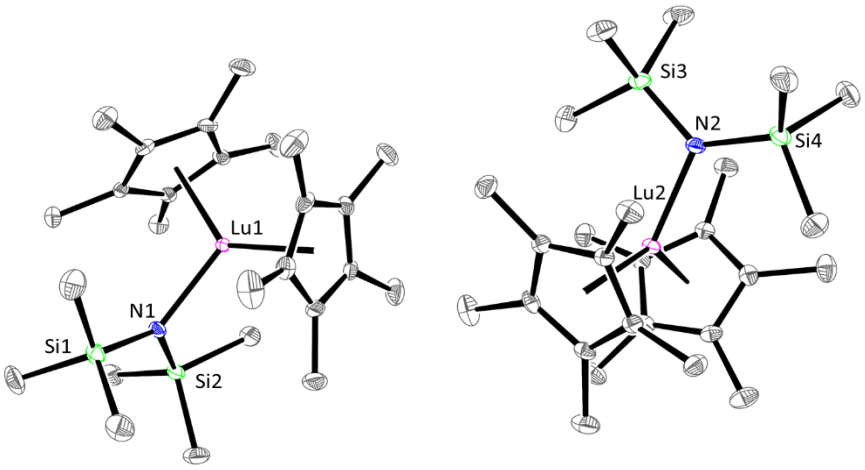

Figure B.3. Displacement ellipsoid plot of $[(C_5Me_5)_2LuN(SiMe_3)_2]$, with ellipsoids drawn at the 50% probability level. Two molecules crystallized in the unit cell. Hydrogen atoms and the $[K(crypt)]^{1+}$ counter-cation were omitted for clarity.

Similar to the $Cp^X_2Y(NR_2)$ complexes, treatment of – 35 °C THF solutions of $Cp^X_2Ln(NR_2)$ in the presence of crypt and KC_8 generated dark blue solutions, ($Cp^X = C_5Me_5$, Ln = Ce, **3**; Nd, **4**; Lu, **5**; $Cp^X = C_5Me_4H$, Ln = Sm, **6**) consistent with Ln(II) formation. For **3**, **4**, and **6**, UV-visible spectra were collected and for **6**, crystallographic-characterization was achieved. Unfortunately, **5** was thermally unstable at – 35 °C and – 78 °C and decomposed to a colorless solution within minutes. The UV-visible spectra of **3**, **4**, and **6** are presented along with $[(C_5Me_5)_2Y(NR_2)]^{1-}$ for comparison in Figure B.4. All three solutions feature similar absorptions to those above for **2**.

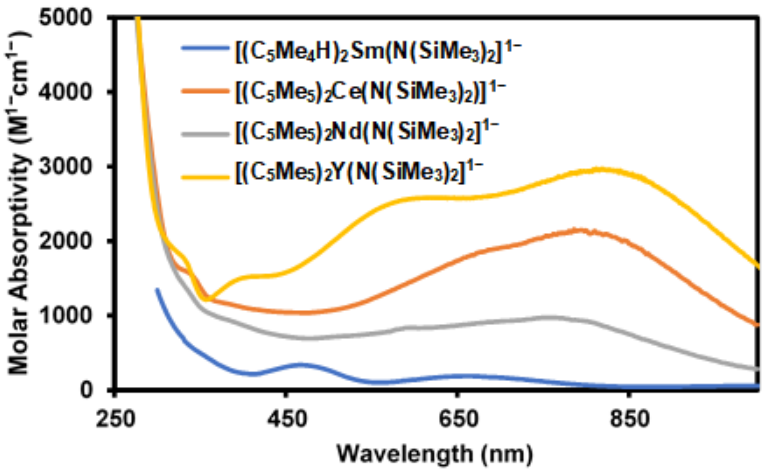

Figure B.4. UV-visible spectra of solutions, **3**, and **4**, generated upon reducing $(C_5Me_5)_2Ln(NR_2)$ for Ln = Ce, Nd, respectively, and $[(C_5Me_4H)_2Sm(NR_2)]^{1-}$, **6**, plotted with $[(C_5Me_5)_2Y(NR_2)]^{1-}$ for comparison.

Similar to the decomposition studies performed for the $[Cp^X_2Y(NR_2)]^{1-}$ complex, the thermal stability of **3** was studied. The absorption spectra for **3** as a function of time are shown in Figure B.5, left. The observation of an isosbestic point indicates that decomposition proceeds cleanly for **3**, similar to the $[Cp^X_2Y(NR_2)]^{1-}$ system. The concentration of Ln(II) in **3** was tracked at λ_{max} = 515 nm. The decomposition was best modeled with first-order kinetics as shown in the plot of $\log_e$[Y(II)] versus time in Figure B.5, right.

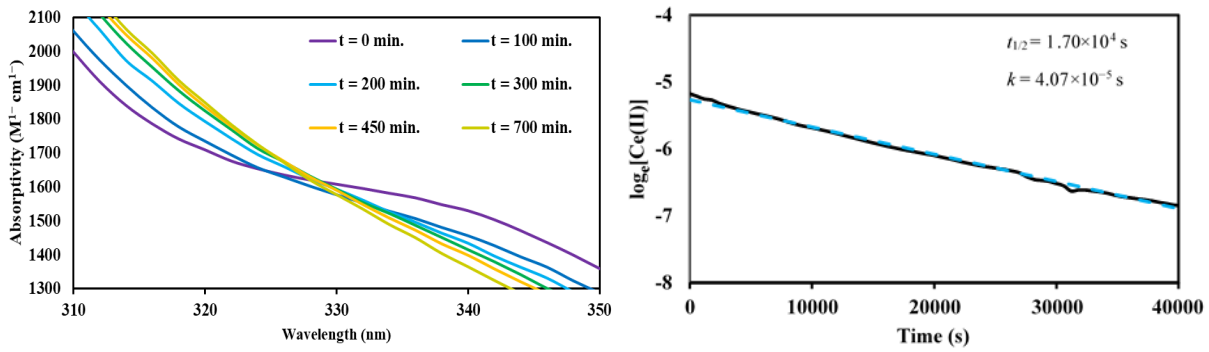

Figure B.5. (left) Overlay of UV-visible spectra of **2** during decomposition. The absorbance remains constant near λ = 328 nm. (right) Absorption of **3** collected at 9.0 mM concentration in THF at room temperature. Absorptions were measured at λ_{max} = 515 nm every 10 min.

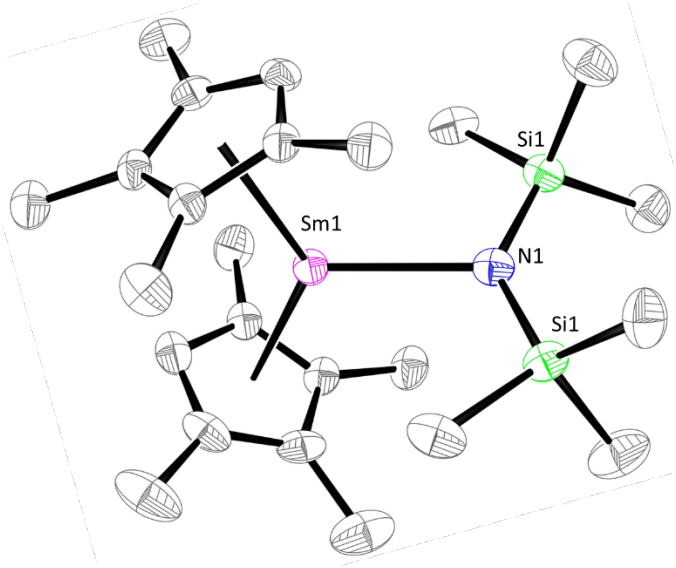

Figure B.6. Displacement ellipsoid plot of [K(crypt)][$(C_5Me_4H)_2SmN(SiMe_3)_2$], with ellipsoids drawn at the 50% probability level. Hydrogen atoms and the $[K(crypt)]^{1+}$ counter-cation were omitted for clarity.

The Sm(II) complex, [K(crypt)][$(C_5Me_4H)_2Sm(NR_2)$] was isolated from a chilled THF/Et_2O solution after sitting in the – 35 °C freezer overnight, Figure B.6. Although the Sm(III) precursor was not crystallographically-characterized, the data collected on the heteroleptic Sm^{II} complex are compared to the previously reported complexes, $(C_5Me_5)_2Sm^{III}(NR_2)$ and $[(C_5Me_5)Sm^{II}(NR_2)(\mu\text{-}C_5Me_5)K(THF)_2]_\infty$, in Table B.1.[8, 9] The Sm^{II} anionic complex, $[(C_5Me_4H)_2Sm(NR_2)]^{1-}$, has a Sm–N distance of 2.473(2) Å which is indistinguishable from the Sm–N distance reported for $[(C_5Me_5)Sm^{II}(NR_2)(\mu\text{-}C_5Me_5)K(THF)_2]_\infty$, which is 2.49(1) Å. These distances are ~ 0.20 Å longer than the Sm–N distance in the Sm^{III} complex, $(C_5Me_5)_2Sm^{III}(NR_2)$, of 2.301 Å, which is consistent with Sm^{II} formation upon reduction of the Sm^{III} complex.[4] Similar Sm…C($SiMe_3$) distances and Sm–N–Si angles are observed as well. The most notable difference between the Sm^{II} complexes are the Sm–ring centroid distances. For the C_5Me_4H complex, the Sm–ring centroid distances are 2.556 Å and 2.573 Å, while for the C_5Me_5 complex, the distances are farther apart, 2.560 Å and 2.708 Å. However, the interaction of the $K(THF)_2$ unit in the C_5Me_5 complex may distort the structure and explain the anomalous centroid distance.

Table B.1. Selected bond lengths and angles of [K(crypt)][$(C_5Me_4H)_2Sm(NR_2)$] and structurally related $(C_5Me_5)_2Sm^{III}(NR_2)$ and, $[(C_5Me_5)Sm^{II}(NR_2)(\mu\text{-}C_5Me_5)K(THF)_2]_\infty$.[8, 9]

	Sm–(ring centroid) Distances (Å)	Sm–N Distances (Å)	Sm…C($SiMe_3$) Distances (Å)	Sm–N–Si angles (°)
$[(C_5Me_4H)_2Sm^{II}\{N(SiMe_3)_2\}]^{1-}$	2.556, 2.573	2.473(2)	3.319(3), 3.401(3)	112.1(1), 116.2(1)
$[(C_5Me_5)Sm^{II}(NR_2)(\mu\text{-}C_5Me_5)K(THF)_2]_\infty$ [9]	2.569, 2.708	2.49(1)	3.37(3), 3.55(3)	114(1), 120(1)
$(C_5Me_5)_2Sm^{III}[N(SiMe_3)_2]$ [8]	2.470, 2.479	2.301(3)	3.282(5), 3.216(5)	115.0(2), 116.5(2)

Conclusion

The generality of heteroleptic yttrium complexes, $(C_5Me_5)_2Y(A)$, to form thermally stable Ln(II) ions has been investigated with A = BH_4 and $OAr^{tBu,tBu,Me}$. The BH_4 complex is unstable with respect to reduction and further characterization was not possible. The $OAr^{tBu,tBu,Me}$ complex was thermally stable enough to provide EPR and UV-visible spectroscopic information, but crystallographic-characterization was not possible. The generality of heteroleptic amide complexes, $Cp^X_2Ln(NR_2)$, was also investigated for $Cp^X = C_5Me_5$, Ln = Ce, Nd, Lu; $Cp^X = C_5Me_4H$, Ln = Sm. While only the Sm^{II} complex was crystallographically-characterized, the Ce and Nd complexes are thermally stable enough to collect UV-visible spectra of the Ln(II) ions.

Experimental Details

All manipulations and syntheses described below were conducted with the rigorous exclusion of air and water using standard Schlenk line and glovebox techniques under an argon or dinitrogen atmosphere. Solvents were sparged with UHP argon and dried by passage through columns containing Q-5 and molecular sieves prior to use. $(C_5Me_5)_2Y(NR_2)$, $(C_5Me_5)_2Ce(NR_2)$, KC_8, $Na(C_5Me_5)$, $KN(SiMe_3)_2$, and KC_5Me_4H were prepared as previously described.[10-14] 2.2.2-cryptand (crypt) (Aldrich) was dried under 10^{-5} Torr for 12 h before use. UV-Visible spectroscopy was performed using an Agilent Cary 60 Scan UV-visible spectrophotometer in a 1 mm quartz cuvette.

Synthesis of $(C_5Me_5)_2Y(OAr^{tBu,tBu,Me})$. $(C_5Me_5)_2Y(NR_2)$ (150 mg, 0.289 mmol) was charged into a vial and dissolved in 5 mL of hexane. $HOAr^{tBu,tBu,Me}$ (68 mg, 0.309 mmol) was added to the hexane solution and stirred overnight, the color became more yellow in color. The hexane solution was centrifuged to remove insoluble material, filtered, and the solvent was removed under vacuum to yield a light yellow solid, presumably, $(C_5Me_5)_2Y(OAr^{tBu,tBu,Me})$ (110 mg, 66%).

Synthesis of $(C_5Me_5)_2Nd(NR_2)$. $(C_5Me_5)_2Nd(\mu\text{-}Cl)_2K(THF)_2$ (189 mg, 0.283 mmol) was charged into a vial and stirred in 10 mL of THF. $KN(SiMe_3)$ (60 mg, 0.301 mmol) was stirred in 2 mL of THF. The $KN(SiMe_3)$ solution was added to the 10 mL THF solution and stirred overnight. The solution developed a deep blue color, and the THF was removed under vacuum. Toluene was added and stirred for 2 h, after which the solution was centrifuged to remove insoluble materials, filtered, and dried under vacuum to yield a blue powder, $(C_5Me_5)_2Nd(NR_2)$ (88 mg, 54%).

Synthesis of $(C_5Me_5)_2Lu(NR_2)$. $(C_5Me_5)_2Lu(\mu\text{-}Cl)_2K(THF)_2$ (189 mg, 0.283 mmol) was charged into a vial and stirred in 10 mL of THF. $KN(SiMe_3)$ (60 mg, 0.301 mmol) was stirred in

2 mL of THF. The $KN(SiMe_3)$ solution was added to the 10 mL THF solution and stirred overnight. The solution developed a yellow color, and the THF was removed under vacuum. Toluene was added and stirred for 2 h, after which the solution was centrifuged to remove insoluble materials, filtered, and layered under chilled hexane. Overnight, pale yellow crystals formed which were identified by X-ray crystallography to be $(C_5Me_5)_2Lu(NR_2)$ (88 mg, 54%).

Reduction of $(C_5Me_5)_2Y(OAr^{tBu,tBu,Me})$. $(C_5Me_5)_2Y(OAr^{tBu,tBu,Me})$ (90 mg, 0.17 mmol) and 2.2.2-cryptand (76 mg, 0.20 mmol) were charged into a vial and stirred in 5 mL of THF for 20 min. A vial was charged with KC_8 (40 mg, 0.30 mmol) and both vials were place in the freezer for 2 h. The yellow THF solution was added to the KC_8 and stirred for 5 min, turning dark blue. This solution was filtered and layered using chilled pentane. After placing in the freezer at −35°C, dark black/ purple solids were isolated upon drying (104 mg, 61 %). UV-vis (THF) λ_{max} nm (ε, $M^{1-}cm^{1-}$): 798 (1700), 603 (1400), 338 (5000).

Reduction of $(C_5Me_5)_2Y(BH_4)$. $(C_5Me_5)_2Y(BH_4)$ (45 mg, 0.17 mmol) and 2.2.2-cryptand (76 mg, 0.20 mmol) were charged into a vial and stirred in 5 mL of THF for 20 min. A vial was charged with KC_8 (40 mg, 0.30 mmol) and both vials were place in the freezer for 2 h. The yellow THF solution was added to the KC_8 and stirred for 1 min, turning dark blue. Before the solution could be filtered and layered using chilled pentane, the color dissipated.

Reduction of $(C_5Me_5)_2Ce(NR_2)$. $(C_5Me_5)_2CeNR_2$ (47 mg, 0.082 mmol) and 2.2.2-cryptand (28 mg, 0.074 mmol) were charged into a vial and stirred in 5 mL of THF for 20 min. A vial was charged with KC_8 (45 mg, 0.30 mmol) and both vials were place in the freezer for 2 h. The THF solution was added to the KC_8 and stirred for 5 min, turning dark blue. This solution was filtered and layered using chilled pentane. After placing in the freezer at −35°C, dark black/ purple

solids were isolated upon drying (24 mg, 30 %). UV-vis (THF) λ_{max} nm (ε, $M^{1-}cm^{1-}$): 792 (2100), 672 (1800), 332 (1600).

Reduction of $(C_5Me_5)_2Nd(NR_2)$. $(C_5Me_5)_2NdNR_2$ (38 mg, 0.066 mmol) and 2.2.2-cryptand (28 mg, 0.074 mmol) were charged into a vial and stirred in 5 mL of THF for 20 min. A vial was charged with KC_8 (40 mg, 0.30 mmol) and both vials were place in the freezer for 2 h. The yellow THF solution was added to the KC_8 and stirred for 5 min. This solution was filtered and layered using chilled pentane. After placing in the freezer at −35°C, dark black/ purple solids were isolated upon drying (18 mg, 26 %). UV-vis (THF) λ_{max} nm (ε, $M^{1-}cm^{1-}$): 767 (1000), 672 (900), 596 (800).

Reduction of $(C_5Me_4H)_2Sm(NR_2)$, 6. $(C_5Me_4H)_3Sm$ (60 mg, 0.12 mmol) and 2.2.2-cryptand (38 mg, 0.10 mmol) were charged into a vial and stirred in 5 mL of THF for 20 min, with a small amount of $KN(SiMe_3)_2$ present. A vial was charged with KC_8 (40 mg, 0.3 mmol) and both vials were place in the freezer for 2 h. The orange THF solution was added to the KC_8 and stirred for 5 min. This solution was filtered and layered using chilled pentane. After placing in the freezer at −35°C for 24 h, dark black/ purple crystals containing **6** were isolated (70 mg, 65 %). UV-vis (THF) λ_{max} nm (ε, $M^{1-}cm^{1-}$): 1018 (100), 686 (200), 468 (300).

Reduction of $(C_5Me_5)_2Lu(NR_2)$. $(C_5Me_5)_2LuNR_2$ (37 mg, 0.17 mmol) and 2.2.2-cryptand (76 mg, 0.20 mmol) were charged into a vial and stirred in 5 mL of THF for 20 min. A vial was charged with KC_8 (40 mg, 0.30 mmol) and both vials were place in the freezer for 2 h. The yellow THF solution was added to the KC_8 and stirred for 1 min, turning dark blue. Before the solution could be filtered and layered using chilled pentane, the color dissipated.

References

(1) Evans, W. J. *Inorg. Chem.* **2007,** *46*, 3435-3449.

(2) Corbey, J. F.; Woen, D. H.; Palumbo, C. T.; Fieser, M. E.; Ziller, J. W.; Furche, F.; Evans, W. J. *Organometallics* **2015,** *34*, 3909-3921.

(3) Palumbo, C. T.; Darago, L. E.; Windorff, C. J.; Ziller, J. W.; Evans, W. J. *Organometallics* **2018,** *37*, 900-905.

(4) Evans, W. J. *Organometallics* **2016,** *35*, 3088-3100.

(5) Ryan, A. J.; Ziller, J. W.; Evans, W. J. *Chem. Sci.* **2020,** *11*, 2006-2014.

(6) Moehring, S. A.; Miehlich, M.; Hoerger, C. J.; Meyer, K.; Ziller, J. W.; Evans, W. J. *Inorg. Chem.* **2020,** *59*, 3207-3214.

(7) MacDonald, M. R.; Ziller, J. W.; Evans, W. J. *J. Am. Chem. Soc.* **2011,** *133*, 15914-15917.

(8) Evans, W. J.; Keyer, R. A.; Ziller, J. W. *Organometallics* **1993,** *12*, 2618-2633.

(9) Hou, Z.; Zhang, Y.; Tezuka, H.; Xie, P.; Tardif, O.; Koizumi, T.-a.; Yamazaki, H.; Wakatsuki, Y. *J. Am. Chem. Soc.* **2000,** *122*, 10533-10543.

(10) Bergbreiter, D. E.; Killough, J. M. *J. Am. Chem. Soc.* **1978,** *100*, 2126-2134.

(11) Den Haan, K. H.; De Boer, J. L.; Teuben, J. H.; Spek, A. L.; Kojic-Prodic, B.; Hays, G. R.; Huis, R. *Organometallics* **1986,** *5*, 1726-1733.

(12) Den Haan, K. H.; Luinstra, G. A.; Meetsma, A.; Teuben, J. H. *Organometallics* **1987,** *6*, 1509-1515.

(13) Evans, W. J.; Kozimor, S. A.; Ziller, J. W.; Fagin, A. A.; Bochkarev, M. N. *Inorg. Chem.* **2005,** *44*, 3993-4000.

(14) Demir, S.; Siladke, N. A.; Ziller, J. W.; Evans, W. J. *Dalton Trans.* **2012,** *41*, 9659-9666.